Ph.D. thesis

Superconductivity in disordered systems

Břetislav Šopík

Faculty of Mathematics and Physics,

Charles University, Prague

Author: Mgr. Břetislav Šopík

Thesis advisor: doc. Pavel Lipavský, CSc.

Ph.D. thesis

Superconductivity in disordered systems

Abstract

We study some aspects of the superconductivity in disordered systems - namely the superconductivity in a boron-doped diamond. We also apply theoretical methods originally developed in the field of the disordered systems to the theory of superconductivity.

In the case of the boron-doped diamond we focus on the question of the dependence of the critical temperature T_c on boron doping. We discuss the impact of the boron distribution correlations on the T_c as well. First, we evaluate the density of states at the Fermi energy N_0 within the dynamical cluster approximation. We discuss the T_c as a function of N_0 within the BCS, the McMillan and the Belitz theory. In the case of 100 samples, the simplified Belitz theory gives the best agreement with experimental data. For 111 samples the McMillan theory is sufficient. We also show that the difference of 100 and 111 samples in the N_0 dependence of T_c can be explained as given by attractive correlations in the boron distribution.

Applying the concept of the coherent potential approximation, we remove a self-interaction from the Galitskii-Feynman T-matrix approximation. This correction has no effect in the normal state but makes the theory applicable to the superconducting state. Our correction does not violate the two-particle symmetry of the T-matrix, therefore the present theory is conserving in the Baym-Kadanoff sense. The theory is developed for retarded interactions leading to the Eliashberg theory in the approximation of a single pairing channel. We also show that contrary to the Kadanoff-Martin approximation this theory describes a condensate, which is stable against excitations of noncondensed Cooper pairs.

sopik@fzu.cz

Published work

As an outcome of last four years work several papers have been published. The Chapters 4.1, 5.1, 6.1, and 7.1 present work devoted to the study of a dependence of the critical temperature on boron doping that appeared in

> "Model for the boron-doping dependence of the critical temperature of superconducting boron-doped diamond", B. Šopík, New J. Phys. **11**, 103026 (2009).

The new T-matrix theory of superconductivity from the Chapter 10 was proposed in

> "Conserving T-matrix theory of superconductivity", B. Šopík, P. Lipavský, M. Männel, and K. Morawetz, submitted to New J. Phys., arXiv:0906.3677v2.

The study of the stability of the condensate against noncondensed Cooper pair excitations – also in Chapter 10 – was published in

> "Microscopic mechanism of symmetry breaking in superconductivity", P. Lipavský, B. Šopík, M. Männel, and K. Morawetz, submitted to New J. Phys.

Some work already presented in this thesis has not been published yet. This includes the study of the impact of the boron distribution correlations on the critical temperature – Chapters 4.2.3, 6.2, and 7.2 – extension of the DCA to Matsubara frequencies in Chapter 5.2, and the concept of higher order approximations of selfenergy in the DCA in Chapter 5.3.

Acknowledgments

In the first place I would like to thank to my family – to my parents Anna and Ladislav and to my sister Iveta. The simple fact that this thesis exists is a result of their neverending support and love.

I would also like to thank to my advisor Pavel Lipavský. The decision to become his Ph.D. student was one of the best in my life. He was for me a great inspiration not only as a physicist but as well as a person.

I should not forget to thank to all my friends and others that inspired and supported me in any way.

Dedicated to my parents

Anna and Ladislav.

Contents

Chapter 1

Foreword

The topic of this Ph.D. thesis is "Superconductivity in disordered systems". Later experience has shown that the name could be more precise, e.g., "Role of avoiding selfinteraction in theory of superconductivity in disordered systems". Indeed, the idea that avoiding of selfinteraction is physically very relevant and can provide significant improvement of a theory pops up in this thesis repeatedly.

In the first part of the thesis we study the superconductivity in a boron-doped diamond. This material is a disordered superconductor close to the metal-insulator transition. We focus on the question of a dependence of the critical temperature on the boron doping and also on the role of the boron distribution correlations. To calculate the density of states at the Fermi level, we employ the coherent potential approximation and also the dynamical cluster approximation.

It was the coherent potential approximation that in late sixties exceeded its predecessors, because it removed the selfinteraction from the description of disordered systems. In the disordered crystal the electron wavefunction is given by a superposition of an initial wave and contributions from all scattering centers. The observation that the wave acting on the scattering center should not contain the contribution from that center, caused important improvement of the theory.

In the second part of the thesis we study a many-body T-matrix approximation and its ability to describe the superconductivity. It is known fact that the so called Galitskii-Feynman approximation is very successful in the normal state but does not

describe the superconducting gap.

Here we observe that the Galitskii-Feynman approximation includes selfinteraction processes. In the normal state these processes form a negligible contribution, but when the superconducting condensate appears this contribution becomes singular. We conclude that it is right this contribution what blocks the formation of the superconducting gap.

On a basis of that we form a new T-matrix approximation which is free of this selfinteraction. These selfinteraction processes are removed in a way, which is similar to the coherent potential approximation. It turns out that this new T-matrix theory describes the superconducting state, which is stable not only against fermionic type of excitations but against excitations of noncondensed Cooper pair as well.

The idea that removing of selfinteraction could be responsible for important results is very old. Its application can be found, e.g., in a problem of an electric field in a cavity in dielectric medium from late 19th century. Here we show that this very physical idea is still of general importance.

Part I

Superconductivity in boron-doped diamond

Chapter 2

Introduction

The superconductivity is an outstanding example of a coherent quantum state of macroscopic size. The interest in new materials and the search for higher critical temperatures for a long time motivates the study of disordered superconductors. The idea that semiconductors doped beyond the metal-insulator transition point (MIT) could become superconducting was already being discussed in the 1960's. But, probably because of the low critical temperatures, the interest in superconducting doped semiconductors did not last until the recent discovery of superconductivity in boron-doped diamond triggered a renewed excitement especially about semiconductors based on group IV elements.

2.1   Boron-doped diamond

Diamond is an electrical insulator with band gap of ~ 5.5 eV well known for its exceptional physical properties – outstanding hardness and thermal conductivity. With these physical properties, it is very attractive for electronic applications. Of course, it is necessary to introduce charge carriers. One of very suitable dopants is a boron. It has one less electron than carbon and is relatively easily incorporated into dense diamond lattice due to its small atomic radius,

There has been a large experimental interest in the boron-doped diamond giving a good knowledge about its properties. Samples are prepared using High Pressure High

Temperature (HPHT) method as well as Microwave Plasma-assisted Chemical Vapour Deposition (MPCVD). It is known that boron dopes holes into a shallow acceptor level close to the top of the valence band. At low boron concentrations lower than ≈ 0.01 per cent material is a semiconductor with an activation energy of ~ 0.35 eV. Increasing the concentration gradually decreases the activation energy and for concentrations higher than ≈ 0.1 per cent the electrical conductivity reaches metallic-like behaviour near room temperature that signals a metal-insulator transition.

In 2004 Ekimov *et al* published in Nature their discovery of superconducting state in boron-doped diamond [ESB$^+$04]. The sample was prepared using HPHT and had $T_c = 2.3$ K at doping of 2.6 per cent. It was found that material is type-II superconductor with upper critical field estimated to $H_{c2}(0) = 3.4$ T at $T = 0$ K.

This discovery was a big surprise which immediately started a rich discussion especially about the possible band structure [YNM$^+$05] and superconductivity driving mechanism. Many ab-initio computations have been done using Virtual Crystal (VC) [LP04, BKA04, MTC$^+$05] or Super Cell (SC) [BAC04, XLY$^+$04, GYS$^+$07] method. Majority of theoreticians believe that electrons are mostly coupled by localized vibrational modes on the boron atoms in an optic spectra. However other theories based on possible presence of weak localisation were discussed as well [MNH$^+$07, MHNK07].

Experimental data on boron-doped diamond are controversial. Majority of samples have been prepared in thin layers and their properties strongly depend on crystallographic orientation of the surface. There are two widely studied types with 100 and 111 orientation, see Refs. [KAK$^+$07] and [TNT$^+$05], respectively. Both referred groups have used the MPCVD method though under different growth conditions. Their samples differ in many characteristics including the T_c. As can be seen in Figure 2.1, the 111 samples have higher T_c in general. The 100 samples reveal a T_c comparable with bulk samples prepared using the HPHT method.

There can be several reasons for the difference in T_c of samples. Mukuda *et al* [MTH$^+$07] made NMR study of various kinds of samples. From the spectra it was found that boron can form B+H molecules with hydrogen or occupy interstitial sites as well, thus effectively lowering the number of charge carriers. However such complexes are not the only possible boron passivating structure. Recently it was suggested that
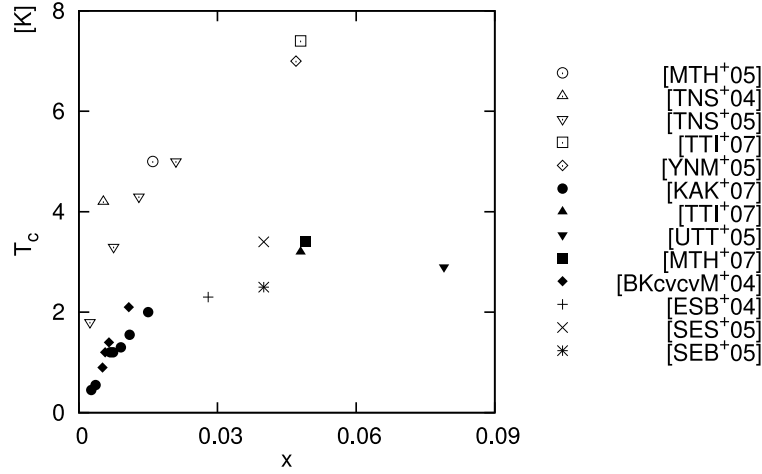
Figure 2.1: Figure shows the dependence of T_c on boron doping concentration x. Open symbols represent the 111 MPCVD data, full symbols the 100 MPCVD data and crosses the HPHT data. The 111 films in general present higher T_c than the 100 and HPHT samples.

boron atoms in boron-doped diamond form also correlated multi-boron complexes mostly dimers [BBA+06, LDG+08]. Stability of such boron clusters and its impact on T_c is still a matter of discussion.

With the discovery of superconductivity in boron-doped diamond, the attention was focused on a superconductivity of group IV elements [BBC+09]. The very activity of research on this field illustrate the discovery of superconductivity in doped sillicon [BMA+06] and recent discovery of superconductivity in boron-doped germanium [HHI+09].

2.2   Disordered superconductors

Since the boron-doped diamond is a superconductor close to the metal-insulator transition (MIT) point, theoretical description of its properties is very appealing. So far superconductors in this region are not fully understood and microscopical theory is still missing.

First theories based on the microscopical approach trying to describe the disor-

dered superconductors came right after the BCS and were focused mainly on super-conducting alloys. There is a strong experimental evidence that even small concentration of magnetic impurities destroys the superconductivity. The interest is therefore usually focused on the study of nonmagnetic ones. The basic illustration of these materials was nicely given in a book of Abrikosov, Gorkov and Dzyaloshinski [AGD63]:

> In an alloy, the electrons are scattered by the impurities, and since this scattering takes place randomly at arbitrary angles and the scattered electrons have very small wavelengths, the correlation between the electrons is very sensitive to the scattering processes. This means that impurity scattering must decrease the spatial coherence between the electrons.
>
> For very low concentrations, the role of the impurities is small, but an increase in the concentration leads to a decrease in the coherence distance of the electrons in the superconductor. For sufficiently high concentrations, the role of the coherence distance ξ_0 is taken over by the mean free path of the electron, and for such concentrations we have a right to expect new characteristic properties of the superconductor to appear.
>
> The point is that for large impurity concentrations, we are essentially dealing with a new substance, whose properties have nothing in common with the original superconductor.

The change of the coherence length affects mainly magnetic properties of the alloy, but it is obvious that we can expect change in T_c as well. Indeed, search for high T_c materials was one of the main motivations to study the disordered superconductors. It was found however that in the case of superconducting alloys, T_c is usually suppressed by the disorder. To explain this Anderson [And59] proposed theorem, which states that in the case of weak coupling BCS superconductors the nonmagnetic impurities influence the critical temperature T_c mainly through the change of the density of states on the Fermi energy level N_0.

In general to successfully describe the disorder in superconductor one has to combine the standard treatment of superconductivity with an adequate description of the disorder. It is therefore no surprise that next improvement in the theory of disordered superconductors followed after the development of the coherent potential approximation (CPA) in late sixties. The CPA was a milestone in studies of disordered systems and there was a lot of effort to combine the CPA with the BCS theory using a Nambu-Gorkov formalism afterwards [Lus73, KB74, WZ74, WZ75, BKK80, KKB81]. These
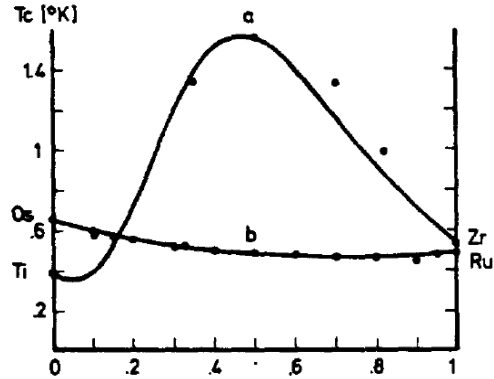
Figure 2.2: Figure illustrates achievements of the CPA and BCS combination [WZ74] in description of alloys of weak coupling superconductors. The solid line represents theory and dots experimental data.

theories managed to explain alloying of weak coupling superconductors that can significantly differ from simple interpolation between components as demonstrated in Figure 2.2.

Later the interest moved to strong coupling superconductors described by Eliashberg equations which distinguish electron-electron and electron-phonon coupling and their influence on the formation of the condensed state. The fusion of Eliashberg equations with the CPA was proposed by Wysokiński [WK83, Wys87]. For strong coupling materials Anderson theorem does not hold and impurities can have a big influence on electron-electron or electron-phonon coupling. There were even studied cases, for which influence of disorder on interactions was taken as the only relevant part of the problem [KS76, EWGW86]. Finally, based on the approach given by Keck and Schmid [KS76] Belitz has developed one of the most complex theories for disordered superconducting alloys [Bel87a, Bel87b, Bel87c], which was capable of successful description of the T_c suppression in strong coupling superconductors. This is illustrated in Figure 2.3.

Doped semiconductors are too distinct from metallic alloys, however. The first theory capable to explain properties of the disordered superconductors close to the
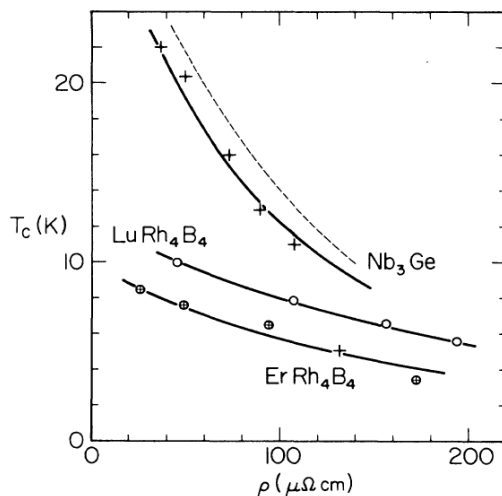
Figure 2.3: Figure shows suppression of T_c in strong coupling superconductors. The disorder is measured by resistivity ρ_{300K}. Dots are experimental data and solid lines represent the theory [Bel87b].

MIT appeared at the beginning of the new century [OSC+01, OSC+02]. Osofsky and his coworkers made the observation that close to the MIT doped superconductors often present strong enhancement of T_c as reveals Figure 2.4. By rescaling the parameters in the BCS they created a heuristical theory which describes this peculiar behaviour. Their scaling ideas were then put together with microscopic theories to get a more firm ground [SOC03]. Nevertheless, this theory has to be understood as a phenomenological description rather inspired by than based on microscopical approach.

It is important to stress that the boron-doped diamond differs from the materials studied by the group of Osofsky *et al.* They have studied materials superconducting in the clean limit, which were doped to reach the vicinity of the MIT. As was mentioned already, diamond itself is the insulator and all its superconducting properties are given by the boron doping. This makes any expansion around the clean limit solution inapplicable.

To summarize the discovery of superconductivity of boron-doped diamond was a big surprise and it became very intensively studied material [Bus06] with many promising properties. From theoretical point of view, it is very appealing as well,
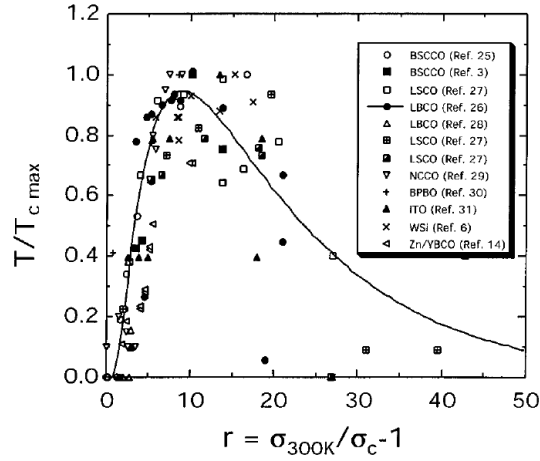
Figure 2.4: Figure shows the critical temperature $T/T_{c\,max}$ versus a parameter r describing the distance from MIT for many disordered superconductors, which were studied by Osofsky *et al* [OSC+01]. Solid line is a theoretical prediction for LBCO.

because it belongs to the group of superconductors close to MIT, which is still not fully understood.

A structure of this part is following. Chapter 3 gives introduction in two questions we have paid special attention to – namely a dependence of the critical temperature on boron doping and an impact of the boron distribution correlations on the critical temperature. Necessary theory is explained in Chapter 4 and several improvements of numerical methods is discussed in Chapter 5. Chapter 6 brings results and Chapter 7 final conclusion.

Chapter 3

Motivation

There are many questions connected with the study of the boron-doped diamond. In this chapter we would like to introduce two of them, which we have paid special attention to – namely explaining of the peculiar dependence of T_c on dopant concentration and possible influence of correlated boron clusters on T_c.

3.1 Dependence of the critical temperature on boron doping

As was said in the introduction, the experimental data on boron-doped diamond are controversial. When we compare 100 and bulk HTHP samples we realize that they reveal comparable T_c. [KAK+07] However 111 samples have significantly higher T_c than the others. [MTH+07] The dependence of T_c on doping for all samples reminds other superconducting materials close to the MIT, where the T_c is enhanced very steeply close to MIT and then further from MIT saturates and eventually falls down. This behaviour is successfully described by the heuristical theory of Osofsky *et al.*

On the other hand Shirakawa *et al* [SHOF07] have applied microscopical treatment and shown that the dependence of T_c measured in boron-doped diamond cannot be reproduced by the BCS theory in which the disorder is described on the level of the CPA [VKE68]. This conclusion clarifies the Figure 3.1. Since their theory yields too
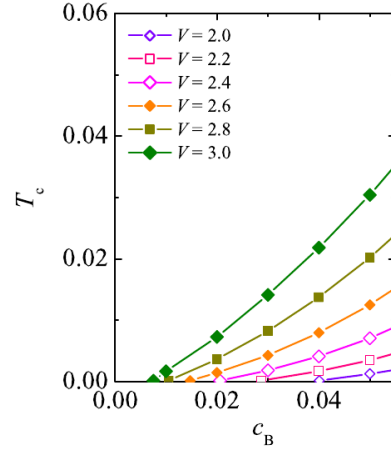
Figure 3.1: Figure shows T_c in Kelvins versus boron doping c_B for several strengths of BCS potential V obtained by Shirakawa *et al* [SHOF07]. One can observe that the predicted T_c values are too small and that the T_c trends do not match experimental results.

low values of T_c, they proposed that disorder effects beyond the CPA are responsible for this disagreement. We will show that corrections beyond the CPA do increase T_c, however in the extent which is not sufficient to cover discrepancies in question.

In the present work we compute the density of states at the Fermi energy level for boron-doped diamond within the dynamical cluster approximation (DCA) [JK01]. While the CPA assumes a single atom embed ed in the effective medium, the DCA generalises this idea by embedding a cluster. The cluster allows us to describe splitting of closely located impurity bound states which contributes to the shape of the impurity band. With respect to the superconductivity it is essential that the density of states at the Fermi level computed within the DCA is higher than the CPA value.

Apparently, the density of states at Fermi level is much lower in the impurity band than in ordinary metals. Since values of T_c are comparable, the boron-doped diamond belongs to the family of the strong coupling materials. One can expect large discrepancies from the BCS theory and we will show that this is indeed the case. Here we employ the Belitz theory [Bel87a], generalising the McMillan formula to disordered superconductors. We will simplify it so that it will depend on the density

of states exclusively. This simplified Belitz theory will be sufficient to reproduce the experimental T_c data.

3.2   Impact of the boron distribution correlations on the critical temperature

As we have mentioned already, recently it was suggested that boron atoms in boron-doped diamond form correlated multi-boron complexes mostly dimers [BBA+06]. These complexes together with B+H molecules or interstitial impurities reduce the possible density of charge carriers in material, which have an impact on a critical temperature. During the following discussions, three main questions appeared.

The first question is: (i) *Are these multi-boron complexes thermodynamically stable or not?* Ab initio investigation has shown that nearest neighbour dimer is energetically the most favourable of all two-boron configurations.[BBA+06] There is still some uncertainty, whether larger boron clusters are more favourable than separated dimers.[LDG+08, NZH+09]

The second question is: (ii) *What impact have these B-B dimers on the DOS near the Fermi energy level?* Again, ab initio investigations have shown that contrary to some suggestions, B-B dimers create deep inactive acceptor levels in the valence-conducting band gap.[GB06] This is in correspondence with widely accepted opinion that B-B dimer related states do not contribute to N_0. [BBA+06, BBC+09]

The last question is: (iii) *In what kind of samples do these correlations preferably appear?* This question is difficult to answer, because dimerisation of boron is not the only boron passivating structure. The SIMS measurement of boron content is not able to distinguish between active and passive fraction. Mukuda *et al* [MTH+07] made NMR study of various kinds of samples which can be seen in Figure 3.2. In the spectra, there was always found a sharp peak corresponding to single boron sites and broader spectra, which was identified with these lower symmetric B sites, such as B-H molecules, interstitial boron sites, B+B dimers, etc. Among those possible lower symmetric B sites the B+H complex was considered as the most likely. Another
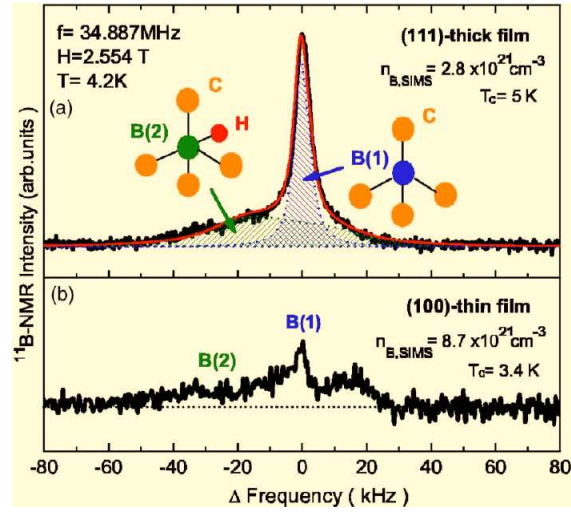
Figure 3.2:   The NMR spectrum of 111 and 100 boron-doped was obtained by Mukuda *et al* [MTH$^+$07]. Both spectra show sharp peak, which corresponds to single boron sites, and also a broader structure that is identified with lower symmetric boron sites, mainly B+H complexes. The SIMS measurement of the boron content is not able to distinguish between these two fractions.

experimental evidence is that among the samples prepared by the nonequilibrium MPCVD method those with 111 orientation have in general higher T_c than 100 films. As has been told the T_c of 100 films is comparable with quasi-equilibrium HTHP samples.

Here we will comment the questions (ii) and (iii). Using the DCA we will on a simple model show the difference in the density of states near the Fermi energy level when the boron correlations are present. With the help of the theory presented in Chapter 4 we will then compare the experimental T_c data and propose a possible explanation of preferable appearance of boron correlations.

Chapter 4

Theory

In this chapter we introduce theoretical concepts used in the following work. The chapter is divided into three parts. In first one we introduce the Belitz theory of disordered superconductors and its modification to the studied system. In the second part we explain some advanced methods of computing the electron band structure in disordered materials. These two theories will be used to construct the model of the critical temperature T_c dependence on the boron doping x. At the end of the chapter we explain the way we treat the correlated disorder. This method will be employed to study the effect of boron distribution correlations on the critical temperature.

4.1   Belitz theory

As was already mentioned the theory of Belitz is a very successful theory of superconducting alloys. It generalises the Eliashberg equations and the McMillan formula for T_c as well. Since our task is to describe the concentration dependence of the critical temperature, we introduce here only the Belitz formula for T_c and its modification to the studied system. Brief review of the Belitz theory can be found in the Appendix B.

4.1.1   Belitz formula

In the absence of currents, the Eliashberg selfenergy has three terms

$$\Sigma(\omega, \epsilon) = (1 - Z(\omega, \epsilon))\, \omega\, \tau_{\mathbf{0}} + Y(\omega, \epsilon)\, \tau_{\mathbf{3}} + W(\omega, \epsilon)\, \tau_{\mathbf{1}}\,, \tag{4.1}$$

where ϵ is the kinetic energy, ω is the Matsubara frequency and $\tau_{\mathbf{i}}$ Pauli matrices. For pure superconductors W renormalized by Z gives a gap function Δ. The dependence of Y on the kinetic energy can be omitted close to the Fermi energy. Thus Y is a scalar that only shifts the chemical potential having no effect on the critical temperature. In disordered superconductors the ϵ dependence of the Y parameter has to be kept, however. Belitz has shown that its energy derivative at Fermi energy

$$Y' = \frac{d}{d\,\epsilon} Y(\epsilon, \omega)\big|_{\epsilon=0}\,, \tag{4.2}$$

modifies the McMillan formula as

$$T_{\mathrm{c}} = \frac{\omega_{\mathrm{D}}}{1.45} \exp\left[-\frac{1.04\,(1 + \lambda + Y')}{\lambda - \mu^*\big(1 + 0.62\,\lambda/(1 + Y')\big)} \right]. \tag{4.3}$$

Here λ describes an electron-phonon coupling and

$$\mu^* = \mu \left[1 + \frac{\mu}{1 + Y'} \ln \frac{\omega_{\mathrm{C}}}{0.62\,\omega_{\mathrm{D}}} \right]^{-1} \tag{4.4}$$

is the screened pseudopotential, in which μ characterises a strength of the Coulomb interaction, ω_{C} is its effective range and ω_{D} is the Debye frequency. Setting $Y' = 0$ one recovers the McMillan formula.

4.1.2   Modification to boron-doped diamond

The Belitz theory was developed for systems that are in the clean limit good metals, where λ and μ^* is well defined. It is expected that impurities do not change the density of states at the Fermi level N_0 and the disorder corrections of the clean limit are present only in renormalisations of interaction vertex through the change of resistivity. Boron-doped diamond is in the clean limit an insulator, however. All the metal properties of the system are induced by the impurities and therefore the concept

of the disorder caused renormalisation of the clean limit values loses its meaning. Moreover since the system is close to the metal-insulator transition the density of states at the Fermi energy N_0 is expected to be strongly dependent on the disorder. We therefore drop the concept of clean limit renormalisations and express the λ, μ and Y' in a way that they are influenced by the disorder exclusively through N_0.

The pseudopotential μ reads [VIK82]

$$\mu = V_c N_0 \left[1 + \frac{V_c N_0}{1 + Y'} \ln \frac{E_{\mathrm{F}}}{\omega_{\mathrm{C}}}\right]^{-1}, \tag{4.5}$$

where V_c is the strength of the Coulomb interaction. Since we have found no measurement of V_c in the literature, we have to treat it as a parameter which is set from experimental data. Because in the boron-doped diamond the Fermi energy level is localised very close to the top of the valence band, the band edge is a natural cutoff for the Coulomb interaction. Thus we associate $E_{\mathrm{F}} \approx \omega_{\mathrm{C}}$. The equation (4.5) then has a simple form

$$\mu = V_c N_0. \tag{4.6}$$

We take λ from ab-initio computations. Since the published results cover only few concentrations – see Appendix A – we evaluate λ in the spirit of Morel and Anderson formula [MA62a]

$$\lambda = \frac{U N_0}{1 + Q N_0}. \tag{4.7}$$

Here U represents a phonon-electron coupling strength and $1 + Q N_0$ describes a screening.

The term Y' contains disorder induced contributions from both electron-phonon and electron-electron interaction. From (B.31) and (B.37) we for Y' write

$$Y' = 2\lambda - \mu. \tag{4.8}$$

Using equations (4.3), (4.4), (4.6), (4.7) and (4.8) we obtain T_c as a function of boron concentration x, having three interaction parameters V_c, U and Q.

4.2 Density of states

Now we establish the bare density of states at the Fermi energy N_0 as a function of the boron concentration x. This single particle quantity is not the physical density of states observed e.g. in the heat capacity, but a theoretical value independent of the electron-electron interaction, would it be the Coulomb repulsion or the phonon-mediated pairing potential. We thus want to evaluate the electron density of states given by a Hamiltonian

$$\hat{H} = \hat{H}_0 + \hat{V} , \tag{4.9}$$

with $\hat{H}_0$ being a Hamiltonian of the valence band in diamond and $\hat{V}$ a random potential of boron impurities

$$\hat{V} = \sum_i \eta_i \, \delta \, \hat{a}_i^\dagger \, \hat{a}_i . \tag{4.10}$$

Here $\eta_i = 1$ at impurity sites and zero elsewhere, and δ is the potential amplitude. We note that this single-site s-type potential does not cover the triple degeneracy of impurity state of boron. We adopt this Hamiltonian already studied by Shirakawa *et al* [SHOF07] to make a link between their and present results. As a model of $\hat{H}_0$ we take a tight-binding hamiltonian

$$\hat{H}_0 = \int \frac{d\mathbf{k}}{(2\pi)^3} \, \epsilon(\mathbf{k}) \, \hat{a}^\dagger(\mathbf{k}) \, \hat{a}(\mathbf{k}) =$$
$$= -t \int \frac{d\mathbf{k}}{(2\pi)^3} \, (\cos(k_x) + \cos(k_y) + \cos(k_z)) \, \hat{a}^\dagger(\mathbf{k}) \, \hat{a}(\mathbf{k}) , \tag{4.11}$$

parametrized by a bandwidth $W = 6t$.

The density of states is defined as the imaginary part of propagator local matrix element at energy slightly above the real axis

$$\rho(E) = -\frac{1}{\pi} \operatorname{Im} G_{ii}(E + i0) . \tag{4.12}$$

For the N_0 we thus write $N_0 = -\frac{1}{\pi} \operatorname{Im} G_{ii}(E_F + i0)$. The propagator is given by the expression

$$\hat{G}(z) = \left\langle \left[z\hat{I} - \hat{H}_0 - \hat{V} \right]^{-1} \right\rangle_{\text{av}} . \tag{4.13}$$

Here angle brackets mean an average over all possible realizations of the disorder $\hat{V}$.

Without the disorder the propagator (4.13) simplifies to

$$\hat{G}^0(z) = [z\hat{I} - \hat{H}_0]^{-1} .\tag{4.14}$$

This is diagonal in the momentum representation and we can write

$$G^0(z, \mathbf{k}) = \frac{1}{z - \epsilon(\mathbf{k})} .\tag{4.15}$$

The $G_{ii}^0(z)$ then has an explicit form

$$G_{ii}^0(z) = \int \frac{d\mathbf{k}}{(2\pi)^3} \frac{1}{z - \epsilon(\mathbf{k})} ,\tag{4.16}$$

and thus from (4.12) we have

$$\rho^0(E) = \int \frac{d\mathbf{k}}{(2\pi)^3} \delta(E - \epsilon(\mathbf{k})) .\tag{4.17}$$

We solve the disorder problem within the CPA and the DCA on a cluster of $2 \times 2 \times 2$ atoms on a cubic lattice. The CPA can be viewed as the DCA for a single site, i.e., the $1 \times 1 \times 1$ cluster. We only briefly introduce these two methods here, the reader can find all details about the CPA and DCA in references [Sov67, VKE68] and [JK01, MJPH05], respectively.

4.2.1   Coherent potential approximation

It is well known fact that in a perfect crystal lattice the electron wavefunction is periodical and electron propagation is non dissipative. If in the crystal impurities are present, they form scattering centers. The electron wavefunction is then a superposition of the initial wave and all the scattered ones.

The success of the CPA is given by the fact that it distinguishes the electron wavefunction from the wave acting on a scattering center. This is because the ongoing wave does not contain a contribution of the wave scattered on the center. Absence of a selfinteraction is a rather old idea and can be illustrated on example of electric field in a cavity.

Let us assume a crystal exposed to a light with an external electric field E_0. A total field inside the sample is microscopically given by a sum of contributions from

the propagating wave E_0 and scattered waves from all the crystal sites

$$E(\mathbf{r}) = E_0(\mathbf{r}) + \sum_j E_j(\mathbf{r}) = (1 + \chi)E_0 \,. \tag{4.18}$$

This would be seen by an ideal observer.

A different result is obtained, if we ask, what field acts on one particular atom on site i. Indeed the atom on site i is not influenced by its own electric field. Therefore the field that acts on this atom equals a sum of contributions from the external wave E_0 and scattered waves from all the sites except the site i,

$$E_{\text{atom}}(\mathbf{r}_i) = E_0(\mathbf{r}_i) + \sum_{j \neq i} E_j(\mathbf{r}_i) \,. \tag{4.19}$$

To calculate E_{atom}, Lorenz and Lorentz have introduced a similar problem of a cavity in dielectric medium. The field in the spherical cavity

$$E_{\text{cav}} = (1 + \frac{\chi}{3})E_0 \tag{4.20}$$

turned out to be the best among simple approximations of the field acting on single atom, $E_{\text{atom}} \approx E_{\text{cav}}$.

Important observation here is that the total field in the medium and electric field acting on a particular site are not the same. Field acting on the site is only partly selfconsistent.

In order to derive the CPA we will follow the original derivation of Soven [Sov67]. He obtained the CPA using rather different approach of variational coherent potential $\Sigma(z)$ forming an effective medium. The potential $\Sigma(z)$ is determined so that the quasiparticle propagating through the medium does not undergo any scatterings. After deriving of the CPA using the Soven's approach, we will show that it is equivalent to avoiding the selfinteraction.

The derivation proceeds as follows. At every site in the lattice we place an as yet unknown frequency dependent potential, which we denote by $\Sigma(z)$. The true potentials V_i at each site have values either δ or 0, see (4.10). Let $\hat{R}(z)$ be the formal Green's function for the lattice of potentials $\Sigma(z)$

$$\hat{R}(z) = \hat{G}_0(z) + \hat{G}_0(z)\,\Sigma(z)\hat{I}\,\hat{R}(z) \,. \tag{4.21}$$

The $\hat{R}(z)$ determines the propagation through the as yet undetermined medium.

Relative to the medium, the actual system consists of perturbing potentials $\delta - \Sigma(z)$ and $-\Sigma(z)$. The T-matrix $\hat{t}(z)$ describes scattering of an electron on these potentials and from the definition includes all possible sequences of collisions. For electron propagating according to $\hat{R}(z)$ and scattering on a single site on the perturbing potential $V_i - \Sigma(z)$ the local T-matrix element $t_i(z)$ is defined as

$$t_i(z) = (V_i - \Sigma(z)) + (V_i - \Sigma(z)) R_{ii}(z) t_i(z). \tag{4.22}$$

The equations (4.21) and (4.22) may be combined to yield an expression for the actual Green's function

$$\tilde{G}_{nm}(z) = R_{nm}(z) + \sum_i R_{ni}(z) t_i(z) R_{im}(z) +$$
$$+ \sum_i \sum_{j \neq i} R_{ni}(z) t_i(z) R_{ij}(z) t_j(z) R_{jm}(z) + \cdots . \tag{4.23}$$

This equation is exact rearrangement of the infinite series (4.13) for one realisation of disordered potentials $\hat{V} - \Sigma(z)\hat{I}$.

To obtain the required propagator $\hat{G}(z)$ which is averaged over all possible realisations of the disorder, we average the equation (4.23) and write

$$G_{nm}(z) = \langle \tilde{G}_{nm}(z) \rangle_{\mathrm{av}} = R_{nm}(z) + \sum_i R_{ni}(z) \langle t_i(z) \rangle_{\mathrm{av}} R_{im}(z) +$$
$$+ \sum_i \sum_{j \neq i} R_{ni}(z) \langle t_i(z) R_{ij}(z) t_j(z) \rangle_{\mathrm{av}} R_{jm}(z) + \cdots . \tag{4.24}$$

In equation (4.24) the $\Sigma(z)$ is an arbitrary parameter. Soven proposed to define it by the requirement that on the average there is no further scattering from the single-site perturbing potentials, i.e.,

$$\langle t_i(z) \rangle_{\mathrm{av}} = 0. \tag{4.25}$$

For the binary alloy with a concentration x for the potential δ and $1 - x$ for the zero potential using (4.22) we obtain

$$0 = x \frac{\delta - \Sigma(z)}{1 - (\delta - \Sigma(z)) R_{ii}(z)} + (1 - x) \frac{-\Sigma(z)}{1 + \Sigma(z) R_{ii}(z)}. \tag{4.26}$$

Figure 4.1: Figure illustrates the Soven's idea of effective medium in the case of a binary disorder with probabilities x and $1 - x$ for potentials $\delta - \Sigma(z)$ and $-\Sigma(z)$. For the selected site i embedded in the medium the propagator average of on site impurity scattering effects restores the medium value.

Neglecting correlations between higher order corrections to $\hat{R}(z)$ and decoupling averages of these higher orders to independent averages of t-matrices at individual sites in (4.24) we find the approximation

$$\hat{G}(z) \approx \hat{R}(z) \,. \tag{4.27}$$

The $\Sigma(z)$ is given by the equation (4.26). We need one more equation to determine the $G_{ii}(z)$. For this we use a formula for a local propagator element

$$G_{ii}(z) = \int \mathrm{d}E \, \frac{\rho^0(E)}{z - E - \Sigma(z)} \,, \tag{4.28}$$

where $\rho^0(E)$ is a density of states of a pure material. Equation (4.28) can be also written as

$$G_{ii}(z) = G_{ii}^0(z - \Sigma(z)) \,. \tag{4.29}$$

Equations (4.26) and (4.28) together form a set known as the Coherent potential approximation.

To illustrate the idea of avoiding the selfinteraction we first rewrite the equation (4.26) in a form

$$G_{ii}(z) = \left\langle \frac{1}{1/\mathcal{G}(z) - V_i} \right\rangle_{\mathrm{av}} \,, \tag{4.30}$$

where we define the curly propagator $\mathcal{G}(z)$ as

$$1/\mathcal{G}(z) = 1/G_{ii}(z) + \Sigma(z) \,. \tag{4.31}$$

The $G_{ii}(z)$ is evaluated as the average over amplitudes that describes a scattering on a one site potential V_i. To evaluate the amplitude properly, one has to subtract the
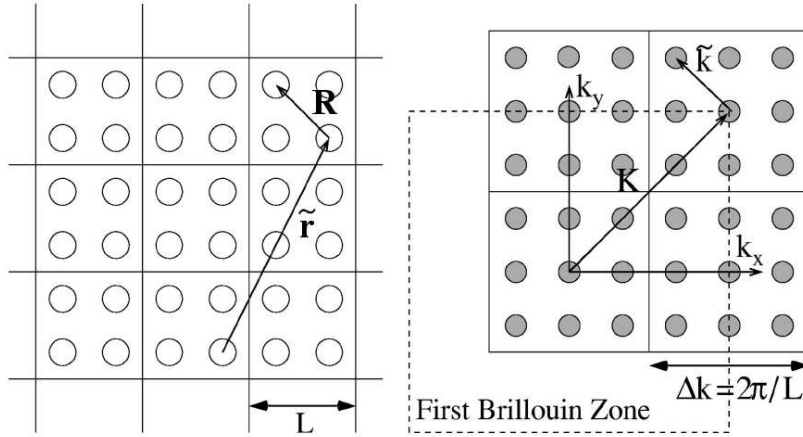
Figure 4.2: Figure from Ref. [AHJ03] illustrates the division of the Brillouin zone into subzones according to $\mathbf{K}$ and $\tilde{\mathbf{k}}$ on the easy example of a cubic lattice. The division of the Brillouin zone into subzones creates clusters in the lattice mapped by $\mathbf{R}$ with periodicity on a scale $\tilde{\mathbf{r}}$.

effect of this scattering from the wave acting on the site i. Thus the $\mathcal{G}(z)$ defined by (4.31) is used and so the selfinteraction is avoided. The Soven's idea of impurity embedded in the effective medium is illustrated in Figure 4.1.

4.2.2 Dynamical cluster approximation

There have been many attempts to formulate nonlocal corrections to the CPA. The main motivation for that was to include short-range correlations into the theory. Contrary to the CPA [MH73], however, these theories often turned out to be acausal [NB73].

One of the most sophisticated extensions is the travelling cluster approximation (TCA) [MR78, KLGD80]. It is designed to be causal. But it is nonsystematic in that the terms that are retained may be just as important as those dropped. Furthermore the TCA is very hard to implement numerically. So far, the best extension is arguably the dynamical cluster approximation. It is analytical, becomes exact in limit of large clusters and recovers the CPA for cluster of size 1.

The crucial problem of all previous cluster extensions of the CPA was in a fact that dividing into clusters violated initial translation invariance of the lattice, making thus the Brillouin zone much smaller. As a result it was not clear, what is a value of selfenergy matrix elements across cluster borders. At the end it was shown that breaking of the initial translation invariance of lattice leads to acausal selfenergy.

The DCA overcomes these difficulties approximating the selfenergy momentum dependence by a step function in the Brillouin zone. The selfenergy is then obtained solving the Soven equation on a small periodical cluster with a period of a cluster size. The Dyson equation is however solved on the initial lattice. The DCA thus can be seen as solving the Soven and Dyson equation on different lattices using convenient transformations between them.

To explain the DCA we first introduce a new mapping of space and momentum coordinates. As figure 4.2 reveals, we decompose the position of a site to intercluster part $\mathbf{R}$ and intracluster part $\tilde{\mathbf{r}}$. Since the vector $\mathbf{R}$ is on the cluster periodical, the Brillouin zone is according to lattice symmetries divided into subzones with base vectors $\mathbf{K}$ and $\tilde{\mathbf{k}}$. Naturally, the size of the cluster corresponds to the number of subzones as shown in figure 4.2.

To be able to generalize the Soven equation to the cluster of N_c atoms, we have to find some mapping of $G(z, \mathbf{k})$ to $G(z, \mathbf{K})$, respectively $G(z, \mathbf{R})$. A convenient transformation is the mean value

$$G(z, \mathbf{K}) = \frac{N_c}{N} \sum_{\tilde{\mathbf{k}}} G(z, \mathbf{K} + \tilde{\mathbf{k}}) \,. \tag{4.32}$$

The $G(z, \mathbf{R})$ is obtained by the discrete Fourier transformation.

Having the periodical $G(z, \mathbf{R})$ we can generalise the Soven equation (4.30) to a matrix equation in space coordinates

$$\bar{G}(z) = \left\langle \left[\bar{\mathcal{G}}^{-1}(z) - \bar{V} \right]^{-1} \right\rangle_{\text{av}} \,, \tag{4.33}$$

where

$$\bar{\mathcal{G}}^{-1}(z) = \bar{G}^{-1}(z) + \bar{\Sigma}(z) \,, \tag{4.34}$$

and the bar signals a matrix $N_c \times N_c$. In (4.33) the average is taken over all impurity realisations of $V(\mathbf{R})$ and is illustrated in figure 4.3. During the iteration, we first

Figure 4.3: Figure shows how the Soven's idea is in the DCA generalised to clusters embedded in the effective medium. In the matrix equation (4.33) the propagator is averaged over all possible configurations $\mathcal{I}$ of the potential $V(\mathcal{I})$ with a probability $p(\mathcal{I})$.

calculate (4.34) and (4.33). Then we substitute the new $\bar{G}(z)$ back to (4.34) to obtain a new $\bar{\Sigma}(z)$.

Now we come to a calculation of $G(z, \mathbf{k})$ from the Dyson equation. Therefore we need to construct $\Sigma(z, \mathbf{k})$ from $\Sigma(z, \mathbf{K})$. The original DCA uses the simplest approximation keeping $\Sigma(z, \mathbf{k})$ constant in each subzone

$$\Sigma(z, \mathbf{K} + \tilde{\mathbf{k}}) = \Sigma(z, \mathbf{K}) \,. \tag{4.35}$$

The Dyson equation thus reads

$$G(z, \mathbf{k}) = \frac{1}{z - \epsilon(\mathbf{K} + \tilde{\mathbf{k}}) - \Sigma(z, \mathbf{K})} \,. \tag{4.36}$$

Equations (4.32), (4.33), (4.34), (4.35) and (4.36) together form a closed set of equations. The local propagator element (4.12) is given by

$$G(z, \mathbf{0}) = \frac{1}{N_c} \sum_{\mathbf{K}} G(z, \mathbf{K}) \,. \tag{4.37}$$

The DCA can be viewed as a scheme that systematically restores the selfenergy momentum dependence. In the CPA the selfenergy has no momentum dependence at all. Closer look at the DCA iterative procedure can be found in the next Chapter 5.

4.2.3   Boron distribution correlations

Unlike the CPA the DCA can be employed to study the impact of impurity distribution correlations on the band structure. This can be seen from the equation (4.33)

where the summation runs over all realizations of the disorder on the cluster and each is weighted by its distribution function.

Although it is very likely that boron atoms are in the diamond correlated, exact form of the attractive "interaction" between them is still a matter of discussion. Since we study the band structure using the cubic lattice, we describe the attractive boron correlations using a simple model, which includes only nearest neighbours.

Let $\mathcal{I}$ be a realization of $n(\mathcal{I})$ boron atoms on N sites, then the Soven equation (4.33) reads

$$\bar{G}(z) = \sum_{\mathcal{I}} p(\mathcal{I}; x, \theta) \left[\bar{\mathcal{G}}^{-1}(z) - \bar{V}(\mathcal{I}) \right]^{-1} , \tag{4.38}$$

where $p(\mathcal{I}; x, \theta)$ is a probability of the configuration $V(\mathcal{I})$. For the probability $p(\mathcal{I}; x, \theta)$ we write

$$p(\mathcal{I}; x, \theta) = \frac{e^{-\beta \mathcal{H}(\mathcal{I}; x, \theta)}}{\sum_{\mathcal{I}} e^{-\beta \mathcal{H}(\mathcal{I}; x, \theta)}} , \tag{4.39}$$

where effective Hamiltonian $\beta \mathcal{H}$ is

$$\beta \mathcal{H}(\mathcal{I}; x, \theta) = n(\mathcal{I}) \ln \left(\frac{1}{x} \right) + (N - n(\mathcal{I})) \ln \left(\frac{1}{1-x} \right) - q \ln(1 + \theta) . \tag{4.40}$$

Here $x \in \langle 0, 1 \rangle$, $\theta \in \langle 0, \infty)$ are parameters of the distribution and q is a number of neighbour boron-boron pairs in configuration $\mathcal{I}$. Last term represents a binding energy of the dimer $\epsilon_\Delta / k_B T = -\ln(1 + \theta)$.

From (4.39) and (4.40) one can write the distribution

$$p(\mathcal{I}; x, \theta) = \frac{1}{Z(x, \theta)} x^{n(\mathcal{I})} (1 - x)^{N - n(\mathcal{I})} (1 + \theta)^q , \tag{4.41}$$

where $Z(x, \theta) = \sum_{\mathcal{I}} e^{-\beta \mathcal{H}(\mathcal{I}; x, \theta)}$ is a normalisation. We see that for $\theta \neq 0$ the parameter x does not play a role of the concentration anymore. Thus we have to calculate the boron density n_B from a definition

$$n_B = \sum_{\mathcal{I}} n(\mathcal{I}) p(\mathcal{I}; x, \theta) . \tag{4.42}$$

One can easily see that for $\theta = 0$ is $Z(x, \theta) = 1$ and $n_B = x$.

Chapter 5

Numerical methods

In this chapter we will discuss numerical methods and their improvements. A results oriented reader can skip this chapter and continue the reading from the next Chapter 6.

We will present here our results which improve and extend its applicability of the DCA. First we will discuss an effective implementation of the DCA scheme, which was already used in our numerics of density of states. Further we will study extension of the DCA to imaginary time – Matsubara frequencies. Finally we will propose higher order approximations of the selfenergy in the coarse graining step of the DCA scheme.

5.1   Effectivity of the DCA

The DCA method can be numerically very demanding even in the case of a cluster of $2 \times 2 \times 2$ sites. It is therefore appealing to search for an effective iteration scheme. The one we present here systematically approximates the density of states so that the summation over the Brillouin zone can be expressed in a simple analytical form.

The crystal lattice has infinite periodicity and is discrete, therefore its Fourier transform has a continuous Brillouin zone of a finite volume. It is then convenient to approximate a continuous selfenergy $\Sigma(\omega_n, \mathbf{k})$ by a step function in the momentum space $\Sigma(\omega_n, \mathbf{K} + \tilde{\mathbf{k}}) = \Sigma(\omega_n, \mathbf{K})$.

5.1.1 Iteration scheme

In the presence of Born-Karman periodic condition, which makes the original continuous Brillouin zone discrete, one may describe the standard DCA iterative procedure in this way:

1. Make some projection of the full lattice/Brillouin zone $G(\omega_n, \mathbf{k})$ to the simplified one $G(\omega_n, \mathbf{K})$ with smaller Born-Karman periodic condition. This can be done by averaging over the subzone

$$G(\omega_n, \mathbf{K}) = \frac{N_c}{N} \sum_{\tilde{\mathbf{k}} \in N_c} G(\omega_n, \mathbf{K} + \tilde{\mathbf{k}}). \tag{5.1}$$

2. Find a full solution of the manybody problem on the smaller periodic lattice or use some convenient approximation – FLEX, QMC, DMFT – to obtain a new selfenergy $\Sigma(\omega_n, \mathbf{K})$.

3. Use a backward construction to obtain $\Sigma(\omega_n, \mathbf{k})$. In our case we take

$$\Sigma(\omega_n, \mathbf{K} + \tilde{\mathbf{k}}) = \Sigma(\omega_n, \mathbf{K}). \tag{5.2}$$

4. Get a new $G(\omega_n, \mathbf{k})$ from the Dyson equation

$$G(\omega_n, \mathbf{k}) = \frac{1}{\mathrm{i}\,\omega_n - \xi(\mathbf{k}) - \Sigma(\omega_n, \mathbf{k})}. \tag{5.3}$$

This procedure is illustrated in Fig. 5.1.

5.1.2 Decomposition of the density of states

Let us observe at this point that since we solve the many-body problem on the small cluster, we can limit the periodicity of the original lattice to infinity, if we send $N \to \infty$ while the N_c is fixed. Summation over $\tilde{\mathbf{k}}$ momenta in (5.1) is then replaced by integration over the subzone density of states

$$G(\omega_n, \mathbf{K}) = N_c \int \frac{\rho_{\mathbf{K}}^0(E)}{\mathrm{i}\,\omega_n - E - \Sigma(\omega_n, \mathbf{K})}\, \mathrm{d}E, \tag{5.4}$$
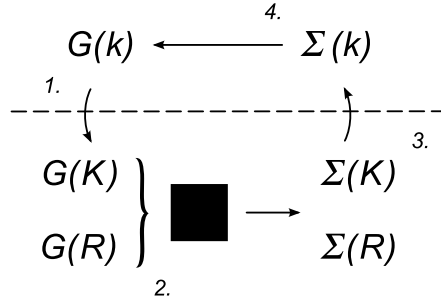
Figure 5.1: Figure illustrating the momentum DCA. Due to the step function character of the selfenergy in the momentum representation new smaller scale Born-Karman periodic conditions of $\Sigma(\mathbf{R})$ appear in the spatial dimension.

where the density of states is decomposed according to the subzones of the Brillouin zone

$$\rho^0(E) = \sum_{\mathbf{K}} \rho_{\mathbf{K}}^0(E) = \sum_{\mathbf{K}} \frac{1}{N} \sum_{\tilde{\mathbf{k}}} \delta(E - \epsilon(\mathbf{K} + \tilde{\mathbf{k}})) . \tag{5.5}$$

The density of states $\rho_{\mathbf{K}}^0(E)$ in each $\mathbf{K}$ subzone can be approximated by the semielliptical function

$$\rho_{\mathbf{K}}^{(0)}(E) = \frac{1}{N_{\mathrm{c}}} \frac{2}{\pi\, u_{\mathbf{K}}} \sqrt{1 - \left(\frac{E - v_{\mathbf{K}}}{u_{\mathbf{K}}}\right)^2} , \tag{5.6}$$

where

$$u_{\mathbf{K}} = \frac{1}{2}\left(E_{\mathbf{K}}^{\mathrm{max}} - E_{\mathbf{K}}^{\mathrm{min}}\right) , \tag{5.7}$$

$$v_{\mathbf{K}} = \frac{1}{2}\left(E_{\mathbf{K}}^{\mathrm{max}} + E_{\mathbf{K}}^{\mathrm{min}}\right) , \tag{5.8}$$

reproduce the maximum $E_{\mathbf{K}}^{\mathrm{max}}$ and minimum $E_{\mathbf{K}}^{\mathrm{min}}$ energy in the subzone $\mathbf{K}$.

With the density of states of such form the integral in (5.4) can be done analytically. The final expression for the propagator is

$$G(\omega_n, \mathbf{K}) = \frac{2}{u_{\mathbf{K}}} \left[\frac{\mathrm{i}\,\omega_n - \Sigma(\omega_n, \mathbf{K}) - v_{\mathbf{K}}}{u_{\mathbf{K}}} - \sqrt{\left(\frac{\mathrm{i}\,\omega_n - \Sigma(\omega_n, \mathbf{K}) - v_{\mathbf{K}}}{u_{\mathbf{K}}}\right)^2 - 1} \right] . \tag{5.9}$$

This formula significantly reduces numerical demands.

It's worth to mention here that the systematical decomposition and approximation of the subzone density of states $\rho_{\mathbf{K}}^0(E)$ by any reasonable analytical function approaches the original density of states $\rho^0(E)$ in the limit of high N_c.

The density of states (5.5) by definition maintains the width of the valence band. Accidentally, this approximation also yields a correct curvature at the edge, i.e., it correctly reproduces an effective mass of holes near the band edge. This feature is vital for a realistic description of the relatively shallow impurity state.

The number of subzones used to evaluate the density of states can be higher than the number of subzones given by a cluster size. Briefly, we can divide the cluster subzone into smaller subzones to obtain more realistic density of states. In this sense we employ the model valence band (5.5) in the CPA as well. Using the same density of states allows us to clearly identify features given by scattering on two or more impurities.

5.1.3 Selfenergy in space representation

Selfenergy projected on the smaller lattice is periodical and translationally invariant. Let us ask, how does the $\Sigma(\omega_n, \mathbf{r})$ look like. From the definition of the Fourier transform we directly obtain

$$\Sigma(\omega_n, \mathbf{r}) = \frac{1}{N} \sum_{\mathbf{k}} \Sigma(\omega_n, \mathbf{K}) \, e^{i\mathbf{k}\cdot\mathbf{r}} = \frac{1}{N_c} \sum_{\mathbf{K}} \Sigma(\omega_n, \mathbf{K}) \, e^{i\mathbf{K}\cdot\mathbf{r}} \frac{N_c}{N} \sum_{\tilde{\mathbf{k}}} e^{i\tilde{\mathbf{k}}\cdot\mathbf{r}} =$$
$$= \frac{1}{N_c} \sum_{\mathbf{K}} \Sigma(\omega_n, \mathbf{K}) \, e^{i\mathbf{K}\cdot(\mathbf{R}+\tilde{\mathbf{r}})} \frac{N_c}{N} \sum_{\tilde{\mathbf{k}}} e^{i\tilde{\mathbf{k}}\cdot(\mathbf{R}+\tilde{\mathbf{r}})} . \quad (5.10)$$

We observe that $\tilde{\mathbf{r}}$ is a periodicity vector for $\mathbf{K}$

$$e^{i\mathbf{K}\cdot\tilde{\mathbf{r}}} = 1 . \quad (5.11)$$

In a limit of infinite Born-Kamran periodic condition the summation over $\tilde{\mathbf{k}}$ becomes the integration

$$\Sigma(\omega_n, \mathbf{r}) = \frac{1}{N_c} \sum_{\mathbf{K}} \Sigma(\omega_n, \mathbf{K}) \, e^{i\mathbf{K}\cdot\mathbf{R}} \frac{N_c}{N} \sum_{\tilde{\mathbf{k}}} e^{i\tilde{\mathbf{k}}\cdot(\mathbf{R}+\tilde{\mathbf{r}})} \approx \Sigma(\omega_n, \mathbf{R}) \int_{-\frac{1}{2}\Delta\mathbf{K}}^{\frac{1}{2}\Delta\mathbf{K}} \frac{\mathrm{d}\tilde{k}}{2\pi} e^{i\tilde{\mathbf{k}}\cdot(\mathbf{R}+\tilde{\mathbf{r}})} ,$$
$$(5.12)$$

and one finally obtains

$$\Sigma(\omega_n, \mathbf{r}) = \Sigma(\omega_n, \mathbf{R}) \frac{\sin(\frac{1}{2}\Delta\mathbf{K}\cdot\mathbf{r})}{\frac{1}{2}\Delta\mathbf{K}\cdot\mathbf{r}} . \quad (5.13)$$

This expression has two limits. First, in a limit of clusters of a very large size

$$\Sigma(\omega_n, \mathbf{r}) = \Sigma(\omega_n, \mathbf{R}) \frac{\sin\left(\frac{1}{2}\Delta\mathbf{K} \cdot (\mathbf{R} + \tilde{\mathbf{r}})\right)}{\frac{1}{2}\Delta\mathbf{K} \cdot (\mathbf{R} + \tilde{\mathbf{r}})} \tag{5.14}$$

$$= \Sigma(\omega_n, \mathbf{R}); \quad \frac{N_c}{N} \to 1, \ \Delta\mathbf{K} \to 0, \tag{5.15}$$

one recovers the complete selfenergy. This limit cannot be achieved in practise, it merely shows that the DCA procedure is a systematical approximation. The opposite case is a limit of clusters with a size of one site. In this limit the sine in (5.14) equals zero and the selfenergy thus reads

$$\Sigma(\omega_n, \mathbf{r}) = \Sigma(\omega_n, \mathbf{0}) \, \delta(\tilde{\mathbf{r}}); \quad N_c = 1, \ \mathbf{R} \equiv 0. \tag{5.16}$$

This is the familiar mean-field solution or the CPA, if we solve the disorder problem.

5.2   DCA for imaginary time – Matsubara frequencies

The DCA is a very successful method suitable for solving of many-body problems. [MJPH05] Its basic idea how to link clusters in crystal lattice with coarse graining of continuous momenta seems to be quite general and applicable to various similar problems. Already Aryanpour *et al* discussed its application to Matsubara frequencies. [AHJ03] Their straightforward implementation however violated the analytical properties and thus causality. Here we modify the DCA for the Matsubara frequencies in a way which guarantees the causality. It allows us to form a unified DCA, which covers both momenta and frequencies.

The main idea of the DCA – which we would like to generalize here – is that it approximates the selfenergy by a step function on continuous intervals. This reduces a complexity of the problem to finite number of degrees of freedom. Selfenergy and propagator are then mapped to a simple Brillouin zone which makes the problem solvable.

We use this idea in the case of the imaginary time dimension. Here the symmetries are opposite to the situation of the momenta. Imaginary time axis is continuous and

has a finite periodicity. Its Fourier transform is discrete and range of Matsubara frequencies is infinite. Natural extension of the DCA to this dimension is therefore to approximate the continuous selfenergy $\Sigma(\tau, \mathbf{k})$ by the step function on the imaginary time axis

$$\Sigma(\tau, \mathbf{k}) = \Sigma(\mathcal{T} + \tilde{\tau}, \mathbf{k}) = \Sigma(\mathcal{T}, \mathbf{k}) \,. \tag{5.17}$$

A complication that emerges here is that the Dyson equation is convolutive in time and diagonal in frequencies. It is therefore convenient to work in the frequency representation.

5.2.1 Iteration scheme

In the Matsubara DCA scheme we iteratively solve two equations - equation for the selfenergy and the Dyson equation for the propagator. Each equation we however solve on a different set of Matsubara frequencies. The Dyson equation is solved on the unrestricted infinite set of frequencies. But the numerically unavoidable coarse graining of the imaginary time interval to finite set of points implies a periodicity of solution in Matsubara frequencies. The equation for selfenergy is thus solved on some finite set of frequency points. The Matsubara DCA scheme inherently includes transformations of functions between these two sets.

The iterative scheme of the Matsubara frequency DCA is similar to the standard case with slight differences given by Fourier transformations:

1. The full propagator $G(\tau, \mathbf{k})$ is projected to the time grid $G(\mathcal{T}, \mathbf{k})$. Contrary to the momentum DCA, where we project to the smaller grid via the average, the natural transformation in this case is simply a point projection of $G(\tau, \mathbf{k})$ in $\mathcal{T}$. Comparing with (5.1) we express this trivially using a δ-function

$$G(\mathcal{T}, \mathbf{k}) = \frac{1}{\Delta \mathcal{T}} \int_{\mathcal{T} - \frac{1}{2}\Delta \mathcal{T}}^{\mathcal{T} + \frac{1}{2}\Delta \mathcal{T}} G(\tau, \mathbf{k}) \, \delta(\tau - \mathcal{T}) \, \mathrm{d}\tau \,. \tag{5.18}$$

From the $G(\mathcal{T}, \mathbf{k})$ we get $G(\Omega_l, \mathbf{k})$ via the discrete Fourier transformation.

The projection of $G(\tau, \mathbf{k})$ to $G(\mathcal{T}, \mathbf{k})$ is equal to the projection of $G(\omega_n, \mathbf{k})$ from the infinite set of Matsubara frequencies to the finite periodical set of frequency points $G(\Omega_l, \mathbf{k})$.

2. On the finite set of frequencies the many-body problem is solved and the new periodical selfenergy $\Sigma(\Omega_l, \mathbf{k})$ resp. $\Sigma(\mathcal{T}, \mathbf{k})$ is found.

3. A new selfenergy $\Sigma(\tau, \mathbf{k})$ resp. $\Sigma(\omega_n, \mathbf{k})$ is constructed via inverse transformation of the periodical $\Sigma(\Omega_l, \mathbf{k})$ from the finite set of frequency points back to the frequencies on the imaginary axis.

4. A new propagator $G(\omega_n, \mathbf{k})$ is found using the Dyson equation. Propagator is transformed back to the imaginary time $G(\tau, \mathbf{k})$.

This procedure is illustrated in the Fig 5.2.

5.2.2   Frequency dependent selfenergy

As was noticed already, the coarse graining of the imaginary time interval implies the periodicity of the selfenergy $\Sigma(\Omega_l, \mathbf{k})$. The selfenergy should (except the constant Hartree field) decay with frequency as $\sim 1/\mathrm{i}\,\omega_n$. Here we show that the transformed $\Sigma(\omega_n, \mathbf{k})$ has the correct asymptotics for the large $\mathrm{i}\,\omega_n$.

From the definition we write

$$\Sigma(\omega_n, \mathbf{k}) = \int_0^\beta e^{\mathrm{i}\,\omega_n \tau}\, \Sigma(\tau, \mathbf{k})\, \mathrm{d}\tau = \sum_{\mathcal{T}} \Sigma(\mathcal{T}, \mathbf{k}) \int_{\mathcal{T}-\frac{1}{2}\Delta\mathcal{T}}^{\mathcal{T}+\frac{1}{2}\Delta\mathcal{T}} e^{\mathrm{i}\,\omega_n \tau}\, \mathrm{d}\tau =$$

$$= \sum_{\mathcal{T}} \Sigma(\mathcal{T}, \mathbf{k})\, e^{\mathrm{i}\,\omega_n \mathcal{T}}\, \frac{\mathrm{i}\sin(\frac{1}{2}\Delta\mathcal{T}\,\omega_n)}{\frac{1}{2}\,\mathrm{i}\,\omega_n}\,. \quad (5.19)$$

We parametrize frequencies as

$$\mathrm{i}\,\omega_n = \mathrm{i}\,\Omega_l + \mathrm{i}\,m\,\Delta\Omega\,, \quad m \in \mathcal{Z}\,, \quad (5.20)$$

where

$$\Delta\Omega_l = \frac{2\pi}{\beta} N_{\Omega_l}\,, \quad (5.21)$$

and for $\mathrm{i}\,\Omega_l$ we write

$$\mathrm{i}\,\Omega_l = \mathrm{i}\,\frac{\pi}{\beta}(2l+1)\,, \quad l \in [N_\Omega/2, \ldots, 0, \ldots, N_\Omega/2 - 1]\,. \quad (5.22)$$

$$\begin{array}{ccc}
G(\omega) & \xleftarrow{\quad 4. \quad} & \Sigma(\omega) \\
\downarrow & & \uparrow \\
\,G(\tau) & & \Sigma(\tau) \\
\end{array}$$
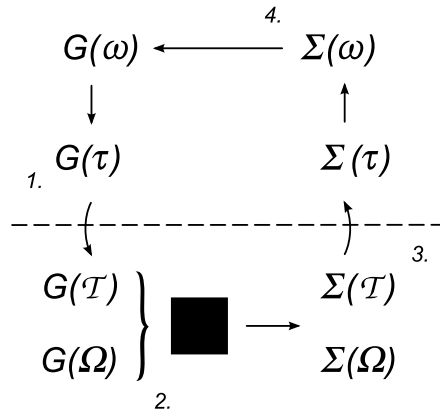
Figure 5.2: Figure illustrating the Matsubara frequency DCA scheme. The suitable representation for the selfenergy step function approximation is the imaginary time axis. The Dyson equation is solved on the infinite set of Matsubara frequencies on the complex plane. The selfenergy equation is solved on the finite set of frequencies. Other steps of the scheme are transformations of quantities between these two sets of Matsubara frequencies.

Observing $\Delta\mathcal{T} = \beta/N_\Omega$ and $e^{\mathrm{i}\, m\, \Delta\Omega\, \mathcal{T}} = 1$ we get the final form for $\Sigma(\omega_n, \mathbf{k})$

$$\Sigma(\omega_n, \mathbf{k}) = \frac{\beta}{N_\Omega} \sum_{\mathcal{T}} \Sigma(\mathcal{T}, \mathbf{k})\, e^{\mathrm{i}\Omega_l \mathcal{T}} \frac{\mathrm{i}\sin(\frac{1}{2}\Delta\mathcal{T}\,\omega_n)}{\mathrm{i}\,\frac{1}{2}\Delta\mathcal{T}\,\omega_n} = \Sigma(\Omega_l, \mathbf{k}) \frac{\sin(\frac{1}{2}\Delta\mathcal{T}\,\Omega_l)}{\frac{1}{2}\Delta\mathcal{T}\,\omega_n}\,, \quad (5.23)$$

which reminds (5.13). From this expression one easily sees that $\Sigma(\omega_n, \mathbf{k})$ naturally has $\sim 1/\mathrm{i}\,\omega_n$ asymptotic behaviour and is defined for all Matsubara frequencies.

5.2.3   Propagator formula

When applying the DCA to the many-body problem it is convenient to merge together all the steps following in the procedure from the new selfenergy estimate to the propagator (namely steps 3., 4. and 1.) as it is done in the momentum DCA in (5.9). Here one uses a new estimate of $\Sigma(\omega_n, \mathbf{K})$ and information about the environment $\rho_{\mathbf{K}}^0(E)$ to obtain the $G(\omega_n, \mathbf{K})$ in one integral equation. Similar compact expression is of course convenient in the frequency DCA as well.

Derivation of the formula

From a definition of the Fourier transform the projected propagator reads

$$G(\mathcal{T}, \mathbf{k}) = \frac{1}{\beta} \sum_{\omega_n} G(\omega_n, \mathbf{k}) \, e^{-\mathrm{i}\omega_n \mathcal{T}} . \tag{5.24}$$

Using the frequency parametrisation (5.20) we can decompose the summation over Matsubara frequencies,

$$G(\mathcal{T}, \mathbf{k}) = \frac{1}{\beta} \sum_{\Omega_l} \sum_m \frac{e^{-\mathrm{i}\Omega_l \mathcal{T}}}{G_0^{-1}(\Omega_l + m\,\Delta\Omega, \mathbf{k}) - \Sigma(\Omega_l, \mathbf{k}) \frac{\sin(\frac{1}{2}\Delta\mathcal{T}\,\Omega_l)}{\frac{1}{2}\Delta\mathcal{T}\,(\Omega_l + m\,\Delta\Omega)}} . \tag{5.25}$$

For $G(\mathcal{T}, \mathbf{k})$ we can write

$$G(\mathcal{T}, \mathbf{k}) = \frac{1}{\beta} \sum_{\Omega_l} G(\Omega_l, \mathbf{k}) \, e^{-\mathrm{i}\Omega_l \mathcal{T}} . \tag{5.26}$$

From (5.25) and (5.26) it follows

$$G(\Omega_l, \mathbf{k}) = \sum_m G(\Omega_l + m\,\Delta\Omega, \mathbf{k}) =$$

$$= \sum_m \frac{1}{G_0^{-1}(\Omega_l + m\,\Delta\Omega, \mathbf{k}) - \Sigma(\Omega_l, \mathbf{k}) \frac{\sin(\frac{1}{2}\Delta\mathcal{T}\,\Omega_l)}{\frac{1}{2}\Delta\mathcal{T}\,(\Omega_l + m\,\Delta\Omega)}} , \tag{5.27}$$

which is the searched expression for $G(\Omega_l, \mathbf{k})$.

Summation over frequencies

The summation in (5.27) is infinite. Since it is very difficult to find any analytical expression for it, it is problematic to evaluate this summation numerically. We should therefore look for some approximation. It could be convenient to replace in the summation from some point $M/2$ the full propagator by a bare one. The summation then reads

$$G(\Omega_l, \mathbf{k}) = \sum_{m'=-M/2}^{M/2} G(\Omega_l + m'\,\Delta\Omega, \mathbf{k}) - G^0(\Omega_l + m'\,\Delta\Omega, \mathbf{k}) +$$

$$+ \sum_m G^0(\Omega_l + m\,\Delta\Omega, \mathbf{k}) . \tag{5.28}$$

Our task is now to evaluate

$$G^0(\Omega_l, \mathbf{k}) = \sum_m G^0(\Omega_l + m\,\Delta\Omega, \mathbf{k}) = \sum_m \frac{1}{\mathrm{i}\,\Omega_l + m\,\mathrm{i}\,\Delta\Omega - \xi(\mathbf{k})}\,. \tag{5.29}$$

We will do this using the standard procedure of integration in the complex plane

$$\oint \frac{g(z)}{z - \xi(\mathbf{k})}\,\mathrm{d}z = 0\,, \tag{5.30}$$

where function $g(z)$ reads

$$g(z) = \frac{1}{1 + e^{-\beta z}} = 1 - \mathrm{f}(\beta z)\,. \tag{5.31}$$

To have the poles of $g(z)$ in the correct Matsubara frequencies, we introduce the phase shift $\mathrm{i}\,\phi(\Omega_l)$

$$\frac{\beta}{N_\Omega}(\mathrm{i}\,\tilde{\omega}_n + \mathrm{i}\,\phi(\Omega_l)) = \mathrm{i}\,\pi(1 + 2m)\,, \quad m \in \mathcal{Z}\,, \tag{5.32}$$

$$\mathrm{i}\,\phi(\Omega_l) = \mathrm{i}\,\frac{\pi}{\beta}N_\Omega - \mathrm{i}\,\Omega_l\,. \tag{5.33}$$

After the summation over the poles we obtain

$$0 = \frac{N_\Omega}{\beta} \sum_m \frac{1}{\mathrm{i}\,\Omega_l + m\,\mathrm{i}\,\Delta\Omega - \xi(\mathbf{k})} + 1 - \mathrm{f}\left(\frac{\beta}{N_\Omega}\left(\xi(\mathbf{k}) + \mathrm{i}\,\phi(\Omega_l)\right)\right)\,, \tag{5.34}$$

so we finally for the bare propagator write

$$G^0(\Omega_l, \mathbf{k}) = -\frac{\beta}{N_\Omega}\left[1 - \mathrm{f}\left(\frac{\beta}{N_\Omega}\left(\xi(\mathbf{k}) + \mathrm{i}\,\phi(\Omega_l)\right)\right)\right]\,. \tag{5.35}$$

The equation (5.28) thus reads

$$G(\Omega_l, \mathbf{k}) = \sum_{m'=-M/2}^{M/2} G(\Omega_l + m'\,\Delta\Omega, \mathbf{k}) - G^0(\Omega_l + m'\,\Delta\Omega, \mathbf{k}) +$$
$$- \frac{\beta}{N_\Omega}\left[1 - \mathrm{f}\left(\frac{\beta}{N_\Omega}\left(\xi(\mathbf{k}) + \mathrm{i}\,\phi(\Omega_l)\right)\right)\right]\,, \tag{5.36}$$

which is the searched approximation of the propagator formula (5.27).
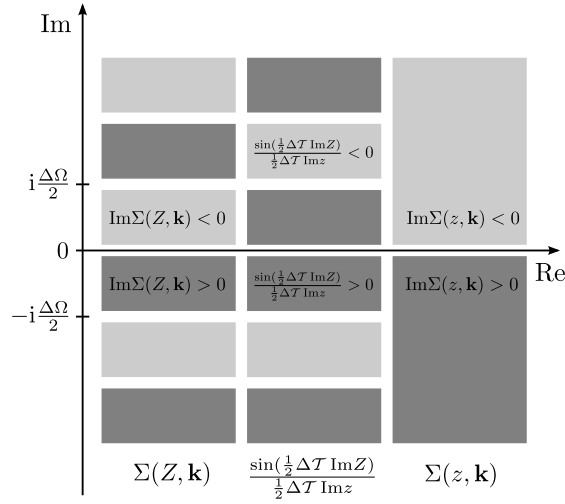
Figure 5.3:   Figure illustrates analytical properties of $\Sigma(Z,\mathbf{k})$ and $\Sigma(z,\mathbf{k})$. The $\Sigma(Z,\mathbf{k})$ is a periodical function along the imaginary axis and a sign of $\mathrm{Im}\,\Sigma(Z,\mathbf{k})$ changes as shown. The $\Sigma(z,\mathbf{k})$ is defined by (5.39) and due to the convenient sign properties of $\sin(\frac{1}{2}\Delta\mathcal{T}\,\mathrm{Im}\,Z)/(\frac{1}{2}\Delta\mathcal{T}\,\mathrm{Im}\,z)$ the imaginary part $\mathrm{Im}\,\Sigma(z,\mathbf{k})$ has the correct sign in upper and lower half-plane.

5.2.4   Causality

Here we discuss the causality of the Matsubara DCA. The iteration scheme consists of four steps (see Fig. 5.2) which we will comment step by step. We find it convenient to start from the step two:

2. We assume that the selfenergy approximation is causal, i.e., it produces causal $\Sigma(\Omega_l,\mathbf{k})$ if the input $G(\Omega_l,\mathbf{k})$ is causal as well. The solution is periodical in the Matsubara frequencies with a period $\Delta\Omega$. By causality we mean here that the analytically continued $\Sigma(Z,\mathbf{k})$ has a property

$$\mathrm{Im}\,\Sigma(Z,\mathbf{k}) < 0, \quad \mathrm{Im}\,Z \in (0, \mathrm{i}\tfrac{\Delta\Omega}{2}) + m\,\mathrm{i}\,\Delta\Omega, \quad m \in \mathcal{Z}, \qquad (5.37)$$

$$\mathrm{Im}\,\Sigma(Z,\mathbf{k}) > 0, \quad \mathrm{Im}\,Z \in (-\mathrm{i}\tfrac{\Delta\Omega}{2}, 0) + m\,\mathrm{i}\,\Delta\Omega, \quad m \in \mathcal{Z}, \qquad (5.38)$$

which reveals Fig. 5.3.

3. The periodical selfenergy $\Sigma(\Omega_l,\mathbf{k})$ is transformed from the finite set of Matsubara frequencies to the $\Sigma(\omega_n,\mathbf{k})$ on the imaginary axis using the formula (5.23).

This is equivalent to the continuation of the selfenergy $\Sigma(\mathcal{T}_i, \mathbf{k})$ from the discrete points to its $\Delta\mathcal{T}$ neighborhood. For the analytical continuation we write

$$\Sigma(z, \mathbf{k}) = \Sigma(Z, \mathbf{k}) \frac{\sin(\frac{1}{2}\Delta\mathcal{T} \operatorname{Im} Z)}{\frac{1}{2}\Delta\mathcal{T} \operatorname{Im} z} . \tag{5.39}$$

Here we demand $\operatorname{Im}\Sigma(z) \gtrless 0$ for $\operatorname{Im} z \lessgtr 0$. This is trivially fulfilled, because the sign of $\sin(\frac{1}{2}\Delta\mathcal{T} \operatorname{Im} Z)/(\frac{1}{2}\Delta\mathcal{T} \operatorname{Im} z)$ periodically changes together with $\operatorname{Im}\Sigma(Z, \mathbf{k})$, so the sign of a product keeps correct as is illustrated in Fig. 5.3.

4. This step is the Dyson equation solved on infinite set of Matsubara frequencies in the complex plane. There is no violation of the causality from the definition.

1. In this step we project $G(\omega_n, \mathbf{k})$ back to the finite set of the Matsubara frequencies $G(\Omega_l, \mathbf{k})$ using the formula (5.18). At this point we demand a periodical property

$$\operatorname{Im} G(Z, \mathbf{k}) < 0, \quad \operatorname{Im} Z \in (0, i\tfrac{\Delta\Omega}{2}) + m\, i\,\Delta\Omega, \quad m \in \mathcal{Z}, \tag{5.40}$$

$$\operatorname{Im} G(Z, \mathbf{k}) > 0, \quad \operatorname{Im} Z \in (-i\tfrac{\Delta\Omega}{2}, 0) + m\, i\,\Delta\Omega, \quad m \in \mathcal{Z}. \tag{5.41}$$

Let us show this for a bare propagator first. For $G^0(Z, \mathbf{k})$ we can write

$$G^0(Z, \mathbf{k}) = \sum_m \frac{1}{i\frac{\Delta\Omega}{2} 2m - (\epsilon(\mathbf{k}) - \operatorname{Re} Z - i\operatorname{Im} Z)} . \tag{5.42}$$

Performing the summation over frequencies $i\frac{\Delta\Omega}{2} 2m$ as in equation (5.35) we come to the expression

$$G^0(Z, \mathbf{k}) = \frac{\beta}{N_\Omega} \Big[\exp\Big(-\tfrac{\beta}{N_\Omega}(\epsilon(\mathbf{k}) - \operatorname{Re} Z)\Big) \cos(\tfrac{\beta}{N_\Omega} \operatorname{Im} Z) - 1 +$$
$$+ i\exp\Big(-\tfrac{\beta}{N_\Omega}(\epsilon(\mathbf{k}) - \operatorname{Re} Z)\Big) \sin(\tfrac{\beta}{N_\Omega} \operatorname{Im} Z)\Big]^{-1}. \tag{5.43}$$

As one can see $G^0(Z, \mathbf{k})$ has the desired property. Along the imaginary axis the sign of the imaginary part is changing in proper way with zero values at $\operatorname{Im} Z = 0$ and $\Delta\Omega/2$.

For the full propagator we have

$$G(Z, \mathbf{k}) = \sum_m \frac{1}{i\frac{\Delta\Omega}{2} 2m + Z - \epsilon(\mathbf{k}) - \Sigma(Z) \frac{\sin(\frac{1}{2}\Delta\mathcal{T} \operatorname{Im} Z)}{\frac{1}{2}\Delta\mathcal{T} \operatorname{Im} z}} . \tag{5.44}$$

Closer observation confirms the former properties of $G^0(Z, \mathbf{k})$ without the exact calculation. The imaginary part $\operatorname{Im}\Sigma(z, \mathbf{k})$ supports the $\operatorname{Im} z$ for $\forall Z$ and $\sin(\frac{1}{2}\Delta\mathcal{T}\operatorname{Im} Z)/(\frac{1}{2}\Delta\mathcal{T}\operatorname{Im} z)$ vanishes at $\operatorname{Im} z = 0$ and $\Delta\Omega/2$.

With this we finish the discussion and conclude that the Matsubara DCA does not violate causality in any step of the iteration scheme.

5.2.5   Unified DCA

By a unified DCA we mean a many-body problem solving procedure, which is a union of the proposed momentum and frequency DCA procedures. Making a combination of expressions (5.9) and (5.27) we get the resulting set of equations for estimating a new $G(\Omega_l, \mathbf{K})$ from $\Sigma(\Omega_l, \mathbf{K})$ using parameters temperature β and density of states $\rho^0_{\mathbf{K}}(E)$.

The resulting set of equations is very simple and reads

$$\Sigma(\Omega_l + m\,\Delta\Omega, \mathbf{K} + \tilde{\mathbf{k}}) = \Sigma(\Omega_l, \mathbf{K})\,\frac{\sin(\frac{1}{2}\Delta\mathcal{T}\,\Omega_l)}{\frac{1}{2}\Delta\mathcal{T}\,(\Omega_l + m\,\Delta\Omega)}\,, \tag{5.45}$$

$$G(\Omega_l + m\,\Delta\Omega, \mathbf{K}) = \frac{2}{u_{\mathbf{K}}}\left[\frac{\xi - v_{\mathbf{K}}}{u_{\mathbf{K}}} - \sqrt{\left(\frac{\xi - v_{\mathbf{K}}}{u_{\mathbf{K}}}\right)^2 - 1}\,\right]\,, \tag{5.46}$$

where we for ξ write

$$\xi = \mathrm{i}(\Omega_l + m\,\Delta\Omega) - \Sigma(\Omega_l + m\,\Delta\Omega, \mathbf{K} + \tilde{\mathbf{k}})\,. \tag{5.47}$$

Finally the propagator is

$$G(\Omega_l, \mathbf{K}) = \sum_m G(\Omega_l + m\,\Delta\Omega, \mathbf{K})\,, \tag{5.48}$$

which can be approximated in a similar way as (5.36).

5.3 Higher order approximations of the selfenergy in the DCA

The DCA is based on the idea of approximating the selfenergy by a step function on a continuous interval. Apparently, this is the first of a whole series of approximations based on the difference expansion. Here we propose a method, how to use higher order difference expansions on subintervals to approximate the selfenergy in the DCA. This could be a convenient improvement of the scheme.

The section is organised in a following way. First we will introduce the basic ideas and illustrate them on the example of the momentum DCA. Then we will discusses the case of a frequency DCA. Finally application of this concept to a unified DCA will be proposed.

5.3.1 Momentum DCA

In the standard momentum DCA, the selfenergy is in the Brillouin zone approximated by a constant function on subintervals labeled by $\mathbf{K}$. The momentum $\mathbf{k}$ is then decomposed as $\mathbf{k} = \mathbf{K} + \tilde{\mathbf{k}}$ and the selfenergy reads

$$\Sigma(\omega_n, \mathbf{k}) = \Sigma(\omega_n, \mathbf{K} + \tilde{\mathbf{k}}) = \Sigma(\omega_n, \mathbf{K}) \,. \tag{5.49}$$

The most important observation here is that the approximation (5.49) can be interpreted as a zeroth order difference selfenergy expansion in momentum. First order expansion is then

$$\Sigma(\omega_n, \mathbf{k}) = \Sigma(\omega_n, \mathbf{K}) + \mathbf{\Sigma}'(\omega_n, \mathbf{K}) \cdot \tilde{\mathbf{k}} \,, \tag{5.50}$$

where matrix elements of the vector $\mathbf{\Sigma}'$ are defined as the difference

$$\Sigma_i'(\omega_n, \mathbf{K}) = \frac{\Sigma(\omega_n, \mathbf{K} + \Delta\mathbf{K}_i) - \Sigma(\omega_n, \mathbf{K} - \Delta\mathbf{K}_i)}{2|\Delta\mathbf{K}|} \,. \tag{5.51}$$

If the system is isotropic it is of course convenient to use an energetical representation. Let ϵ_K be a set of $\epsilon(\mathbf{K})$ energies ordered according to its value. One can to the first order write

$$\Sigma(\omega_n, E) = \Sigma(\omega_n, \epsilon_K) + \Sigma'(\omega_n, \epsilon_K)(E - \epsilon_K) \,, \tag{5.52}$$

with scalar coefficients

$$\Sigma'(\omega_n, \epsilon_K) = \frac{\Sigma(\omega_n, \epsilon_{K+1}) - \Sigma(\omega_n, \epsilon_{K-1})}{\epsilon_{K+1} - \epsilon_{K-1}} \ . \tag{5.53}$$

This approximation of the selfenergy is used to construct a new $G(\omega_n, \mathbf{K})$. Let us show now that for a semielliptical density of states the integration can be done analytically even when we use the first order approximation of the selfenergy. We start from the definition

$$G(\omega_n, \mathbf{K}) = N_c \int \frac{\rho^0_{\mathbf{K}}(E) \, \mathrm{d}E}{\mathrm{i}\,\omega_n - E - \Sigma(\omega_n, \epsilon_K) - \Sigma'(\omega_n, \epsilon_K)(E - \epsilon_K)} \ . \tag{5.54}$$

After the rearrangement

$$G(\omega_n, \mathbf{K}) = \frac{N_c}{1 + \Sigma'(\omega_n, \epsilon_K)} \int \frac{\rho^0_{\mathbf{K}}(E)}{\frac{\mathrm{i}\,\omega_n - \Sigma(\omega_n, \epsilon_K) + \Sigma'(\omega_n, \epsilon_K)\epsilon_K}{1 + \Sigma'(\omega_n, \epsilon_K)} - E} \, \mathrm{d}E \ , \tag{5.55}$$

which we can write in a general form

$$G(\omega_n, \mathbf{K}) = \frac{1}{1 + \Sigma'(\omega_n, \epsilon_K)} \, G^0(\alpha(\omega_n, \mathbf{K}), \mathbf{K}) \ . \tag{5.56}$$

Here

$$\alpha(\omega_n, \mathbf{K}) = \frac{\mathrm{i}\,\omega_n - \Sigma(\omega_n, \epsilon_K) + \Sigma'(\omega_n, \epsilon_K)\epsilon_K}{1 + \Sigma'(\omega_n, \epsilon_K)} \ . \tag{5.57}$$

We can readily use the semielliptical density of states (5.6) to get the final expression for the propagator

$$G(\omega_n, \mathbf{K}) = \frac{1}{1 + \Sigma'(\omega_n, \epsilon_K)} \frac{2}{u(\mathbf{K})} \left[\frac{\alpha(\omega_n, \mathbf{K}) - v(\mathbf{K})}{u(\mathbf{K})} + \right.$$
$$\left. - \sqrt{\left(\frac{\alpha(\omega_n, \mathbf{K}) - v(\mathbf{K})}{u(\mathbf{K})}\right)^2 - 1} \right] \ . \tag{5.58}$$

In general it can be quite difficult to find analytical formula for the propagator, when using higher order approximations. On the other hand there is no dramatical enhancement of complexity of the numerical integration if the higher order approximation is used.

5.3.2 Frequency DCA

In the case of the frequency DCA the selfenergy can be to the second order in time subinterval approximated in a similar way

$$\Sigma(\tau, \mathbf{k}) = \Sigma(\mathcal{T}, \mathbf{k}) + \Sigma'(\mathcal{T}, \mathbf{k})(\tau - \mathcal{T}) + \frac{1}{2}\Sigma''(\mathcal{T}, \mathbf{k})(\tau - \mathcal{T})^2 \,, \tag{5.59}$$

with coefficients

$$\Sigma'(\mathcal{T}, \mathbf{k}) = \frac{\Sigma(\mathcal{T} + \Delta\mathcal{T}, \mathbf{k}) - \Sigma(\mathcal{T} - \Delta\mathcal{T}, \mathbf{k})}{2\Delta\mathcal{T}} \,, \tag{5.60}$$

and

$$\Sigma''(\mathcal{T}, \mathbf{k}) = \frac{1}{\Delta\mathcal{T}^2}\big(\Sigma(\mathcal{T} + \Delta\mathcal{T}, \mathbf{k}) - 2\Sigma(\mathcal{T}, \mathbf{k}) + \Sigma(\mathcal{T} - \Delta\mathcal{T}, \mathbf{k})\big) \,. \tag{5.61}$$

The Fourier transform of the selfenergy is

$$\Sigma(\omega_n) = \Delta\mathcal{T}\sum_{\mathcal{T}}\int_{\mathcal{T} - \frac{1}{2}\Delta\mathcal{T}}^{\mathcal{T} + \frac{1}{2}\Delta\mathcal{T}} \Sigma(\tau)\, e^{\mathrm{i}\omega_n\tau}\, \mathrm{d}\tau \,. \tag{5.62}$$

Transforming (5.59) we obtain

$$\Sigma(\omega_n, \mathbf{k}) = \Delta\mathcal{T}\sum_{\mathcal{T}}\Sigma(\mathcal{T}, \mathbf{k})\, e^{\mathrm{i}\omega_n\mathcal{T}}\, \frac{1}{\Delta\mathcal{T}}\int_{-\frac{1}{2}\Delta\mathcal{T}}^{+\frac{1}{2}\Delta\mathcal{T}} e^{\mathrm{i}\omega_n\tau}\, \mathrm{d}\tau +$$

$$+ \Delta\mathcal{T}\sum_{\mathcal{T}}\Sigma'(\mathcal{T}, \mathbf{k})\, e^{\mathrm{i}\omega_n\mathcal{T}}\, \frac{1}{\Delta\mathcal{T}}\int_{-\frac{1}{2}\Delta\mathcal{T}}^{+\frac{1}{2}\Delta\mathcal{T}} \tau\, e^{\mathrm{i}\omega_n\tau}\, \mathrm{d}\tau +$$

$$+ \frac{1}{2}\Delta\mathcal{T}\sum_{\mathcal{T}}\Sigma''(\mathcal{T}, \mathbf{k})\, e^{\mathrm{i}\omega_n\mathcal{T}}\, \frac{1}{\Delta\mathcal{T}}\int_{-\frac{1}{2}\Delta\mathcal{T}}^{+\frac{1}{2}\Delta\mathcal{T}} \tau^2\, e^{\mathrm{i}\omega_n\tau}\, \mathrm{d}\tau \,. \tag{5.63}$$

The integrals equal to

$$\frac{1}{\Delta\mathcal{T}}\int_{-\frac{1}{2}\Delta\mathcal{T}}^{+\frac{1}{2}\Delta\mathcal{T}} e^{\mathrm{i}\omega_n\tau}\, \mathrm{d}\tau = \frac{\sin(\frac{1}{2}\Delta\mathcal{T}\omega_n)}{\frac{1}{2}\Delta\mathcal{T}\omega_n} = W\left(\tfrac{1}{2}\Delta\mathcal{T}\omega_n\right) \,, \tag{5.64}$$

$$\frac{1}{\Delta\mathcal{T}}\int_{-\frac{1}{2}\Delta\mathcal{T}}^{+\frac{1}{2}\Delta\mathcal{T}} \tau\, e^{\mathrm{i}\omega_n\tau}\, \mathrm{d}\tau = \frac{\mathrm{i}}{\omega_n}\left(W(\tfrac{1}{2}\Delta\mathcal{T}\omega_n) - \cos(\tfrac{1}{2}\Delta\mathcal{T}\omega_n)\right) = \frac{\mathrm{i}}{\omega_n}Y\left(\tfrac{1}{2}\Delta\mathcal{T}\omega_n\right) \,,$$

$$\tag{5.65}$$

and

$$\frac{1}{\Delta \mathcal{T}} \int_{-\frac{1}{2}\Delta \mathcal{T}}^{+\frac{1}{2}\Delta \mathcal{T}} \tau^2 \, e^{\mathrm{i}\omega_n \tau} \, \mathrm{d}\tau = \frac{2}{\omega_n^2} \, Y(\tfrac{1}{2}\Delta \mathcal{T} \omega_n) - (\tfrac{1}{2}\Delta \mathcal{T})^2 \, W(\tfrac{1}{2}\Delta \mathcal{T} \omega_n) \,. \tag{5.66}$$

One can observe that $W(\tfrac{1}{2}\Delta \mathcal{T} \omega_n)$ and $Y(\tfrac{1}{2}\Delta \mathcal{T} \omega_n)$ have correct limits

$$W(\tfrac{1}{2}\Delta \mathcal{T} \omega_n) \to 1, \quad Y(\tfrac{1}{2}\Delta \mathcal{T} \omega_n) \to 0, \text{ for } \quad \Delta \mathcal{T} \to 0 \,. \tag{5.67}$$

For Fourier transform of differences we write

$$\Delta \mathcal{T} \sum_{\mathcal{T}} \Sigma^{(m)}(\mathcal{T}, \mathbf{k}) \, e^{\mathrm{i}\Omega_l \mathcal{T}} = (-\mathrm{i}\,\Omega_l)^m \, \Sigma(\Omega_l, \mathbf{k}) \,. \tag{5.68}$$

Using these results the final form for selfenergy to the second order reads

$$\Sigma(\omega_n, \mathbf{k}) = \Sigma(\Omega_l, \mathbf{k}) \left\{ W(\tfrac{1}{2}\Delta \mathcal{T} \omega_n) + \tfrac{\Omega_l}{\omega_n} \, Y(\tfrac{1}{2}\Delta \mathcal{T} \omega_n) + \right.$$
$$\left. - \tfrac{1}{2}\Omega_l^2 \left(\tfrac{2}{\omega_n^2} \, Y(\tfrac{1}{2}\Delta \mathcal{T} \omega_n) - (\tfrac{1}{2}\Delta \mathcal{T})^2 \, W(\tfrac{1}{2}\Delta \mathcal{T} \omega_n) \right) \right\} \,, \tag{5.69}$$

where we have used the decomposition $\mathrm{i}\,\omega_n = \mathrm{i}\,\Omega_l + m \, \mathrm{i}\,\Delta\Omega$.

In this chapter we have proposed theoretical improvements of the DCA concept. Some of them were used in our numerics. In the next chapter we will discuss results of the study of the boron-doped diamond.

Chapter 6

Results

In this chapter we are going to present our results of the study of the two proposed topics. In the first part of the chapter the dependence of the T_c on the boron doping is discussed. Its conclusions are then used in the second part, where we pay attention to the impact of the boron distribution correlations on the T_c

6.1   Dependence of the critical temperature on boron doping

Since we focus ourselves only on the impact of the disorder on the T_c through the change of the N_0, we can divide the studied problem into two. First we will pay attention to the computation of the band structure, mainly the N_0 as a function of the boron concentration x. Then we will use the obtained $N_0(x)$ to reproduce the experimental data of the superconducting transition.

6.1.1   Density of states

Now we establish the density of states at the Fermi energy N_0 as a function of the boron concentration x. The process of metallization in the boron-doped diamond was in the literature already discussed both experimentally and theoretically. [YNM+05, PL05] Pogorelov and Loktev [PL05] have focused on the fact that the diamond band

structure is at the top of the valence band triply degenerate. They have studied the possible changes of the impurity band if the boron was hybridized only to one or to all three valence bands. Despite to these effects given by the triple degeneracy of the top of the valence band, we employ here the proposed one-band tight-binding Hamiltonian (4.9), since we believe it reflects the basic physical properties of the studied system.

The parameters of the hamiltonian (4.9) are fitted according to the facts that the valence band is $22\,\text{eV}$ wide and the single impurity bound state appears at energy $0.37\,\text{eV}$ above the valence one. Using the local Green function corresponding to the density of states (5.5), we come to $\delta = 8.91$ eV.

We determine the Fermi energy level from a condition for a local averaged density of electrons at zero temperature $n_\sigma = \int_\mu^\infty \rho(E)\, dE = x/2$. We are aware that a measured number of charge carriers can differ significantly from a number deduced from the concentration of boron atoms in the sample. As has recently been pointed out by Mukuda *et al* [MTH$^+$07] quite a large fraction of boron atoms can form the neutral B-H complexes, reducing the concentration of charge carriers. On the other hand Klein *et al* [KAK$^+$07] found that the effective number of carriers deduced from Hall-effect measurements was much larger than the number of boron atoms in samples. Since the charge carrier concentrations for all samples are not accessible we assume for simplicity the films to be doped ideally.

We have evaluated N_0 within the DCA for clusters of $2 \times 2 \times 2$ atoms on a cubic lattice. Compared to the CPA density of states employed by Shirakawa *et al* , our cluster density of states includes nontrivial corrections given by bonding and anti-bonding states at neighbour impurity sites. Difference between the CPA and DCA density of states in the impurity band is illustrated in figure 6.1 for 5% of boron doping.

Within the CPA (dashed line) the impurity band yields rather featureless density of states having a slightly skewed semielliptic shape. The valence band starts approximately at an energy of -1.5 eV and ends at -23 eV. We focus on the impurity band because the Fermi energy, $E = 0$, lies there. Since boron is an acceptor, its bound states have higher energy than extended states in a valence band.
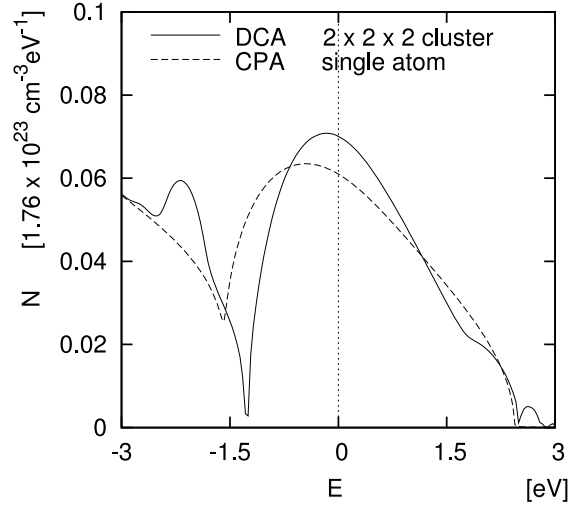
Figure 6.1: Impurity band of the density of states N as a function of energy E computed at $x = 0.05$ doping using the CPA and the DCA on the cluster of $2 \times 2 \times 2$ atoms.
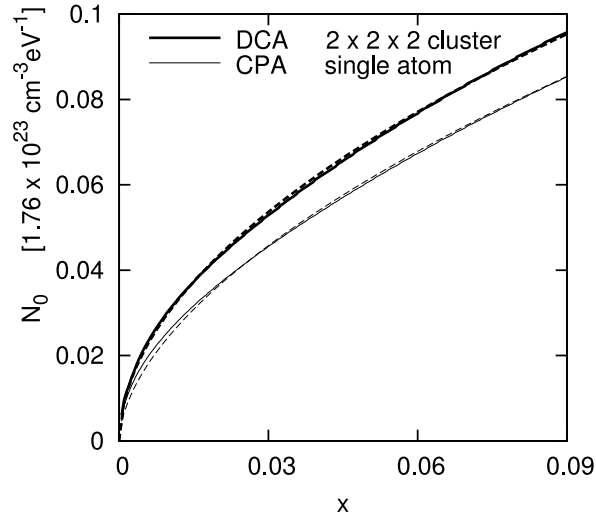
Figure 6.2: Density of states at the Fermi energy N_0 as a function of boron concentration x computed using the CPA method and the DCA on the cluster of $2 \times 2 \times 2$ atoms. The figure includes dashed curves $N_0^{\mathrm{CPA}} \approx 0.59\, x^{0.568} \times 10^{23}\,\mathrm{cm}^{-3}\mathrm{eV}^{-1}$ approximating CPA and $N_0^{\mathrm{DCA}} \approx 0.59\, x^{0.523} \times 10^{23}\,\mathrm{cm}^{-3}\mathrm{eV}^{-1}$ for DCA. In most regions approximations are indistinguishable from computed results within the linewidths.

In the DCA (solid line) one can distinguish additional contributions of two and three boron clusters. Clusters of four to eight borons are also included, but their contributions are invisible for the given concentration. The main part of the impurity band density of states is formed by a bound state on a single boron. A shoulder on the right side of the impurity band results from a symmetric bound state of two neighbouring borons. The nonsymmetric state is not bounded but forms a resonant state visible in the valence band. The tree boron bound state is splited off at an energy 2.8 eV. Higher states of the three boron clusters make a negligible contribution.

With respect to superconductivity the Fermi energy region is the most important. As one can see the density of states at $E = 0$ is dominated by the single boron states. This is a reason why the CPA and DCA give comparable N_0.

The resulting density of states at the Fermi level N_0 is presented in figure 6.2. For comparison we also show the CPA result. One can see that the DCA density of states is higher than the CPA value at all impurity concentrations. Both resulting densities with a good accuracy obey power-law, $N_0^{\mathrm{DCA}} \approx 0.59\, x^{0.568} \times 10^{23}\, \mathrm{cm}^{-3} \mathrm{eV}^{-1}$ and $N_0^{\mathrm{CPA}} \approx 0.59\, x^{0.523} \times 10^{23}\, \mathrm{cm}^{-3} \mathrm{eV}^{-1}$. A very good approximation by power-law also holds for the distance of the Fermi level from the top of the impurity band, $\omega_{\mathrm{C}} \approx 45.5\, N_0^{1.18}\, \mathrm{eV}$ for the DCA.

6.1.2   Critical temperature

In this subsection we discuss the concentration dependence of the critical temperature T_c. Since there are significant differences in T_c between type 111 and 100 samples (see Figure 2.1) we discuss them separately. Let us first focus on the 100 together with HPHT samples.

To be able to implement the Belitz theory we need the coupling strength λ and the pseudopotential μ as functions of N_0. The coupling strength λ we deduce from *ab initio* computations. In literature one finds the studies within the virtual crystal approximation and the supercell method. These data are summarized in the Table A.1 in Appendix A. In figure 4.3 we show fit of *ab initio* results by formula (4.7). We found that parameters $U = 13.61 \times 10^{-23}\, \mathrm{cm}^3\mathrm{eV}$ and $Q = 17.58 \times 10^{-23}\, \mathrm{cm}^3\mathrm{eV}$
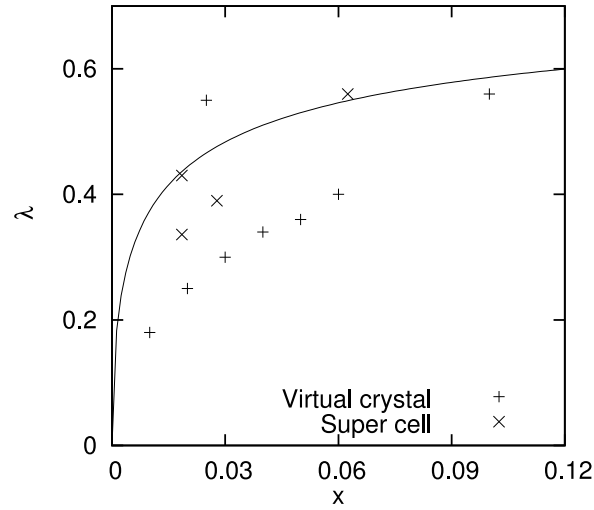
Figure 6.3: Electron-phonon coupling λ as a function of boron concentration x. The ploted data represent results of *ab initio* computations using super cell method [BAC04, GYS⁺07, XLY⁺04] and virtual crystal computations [BKA04, LP04, MTC⁺05]. Solid line is the Morel-Anderson formula (4.7) with $U = 13.61 \times 10^{-23}\,\mathrm{cm^3 eV}$ and $Q = 17.58 \times 10^{-23}\,\mathrm{cm^3 eV}$. Densities of states have been associated to individual computations via DCA results shown in figure 6.1.

yield a reasonable fit of rather scattered computed values. In the fit we have ignored the virtual crystal approximation values which are less accurate than the supercell results.

It remains to establish the pseudopotential μ. According to formula (4.6) we have to find a single parameter V_c, which determines μ for all concentrations. Dots in figure 6.4 show values of μ deduced from the Belitz theory and experimental values of T_c. One can see that all dots stay close to a line given by formula (4.6) with $V_c = 0.83 \times 10^{-23}\mathrm{cm^3 eV}$. The parameter V_c holds for all concentrations and it is the only material parameter fitted to experimental values of T_c in the present theory.

Now all relations and parameters are ready for predictions of the critical temperature. The concentration dependence of T_c of 100 and HPHT samples given by the Belitz formula (4.3) and power-law approximation of the DCA value of N_0 is shown in figure 6.5. As one can see, the theory describes a steep increase of T_c with doping at the region of small concentrations. At higher concentrations the critical temperature
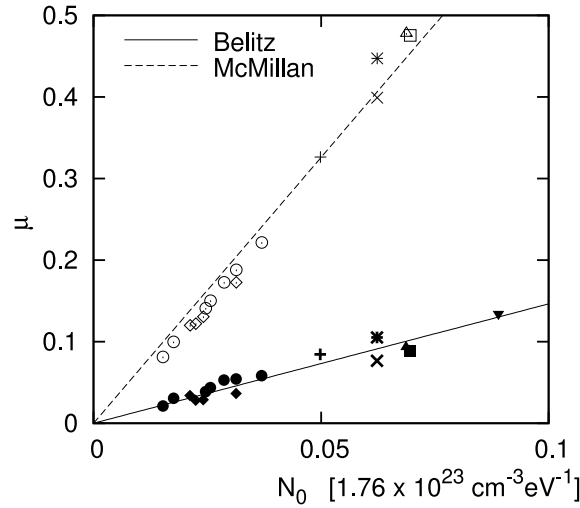
Figure 6.4: Coulomb pseudopotential μ as a function of density of states N_0 of boron-doped diamond. Full (empty) symbols are values of μ deduced by Belitz (McMillan) formula from 100 and HPHT experimental data – see the figure 2.1. The full symbols fall close to the solid line of the theoretical pseudopotential (4.6) with the Coulomb strength $V_c = 0.83 \times 10^{-23}\,\mathrm{cm^3eV}$ and the empty symbols are well reproduced with $V_c = 3.85 \times 10^{-23}\,\mathrm{cm^3eV}$.

saturates at about 3 K. This saturation reminds trends described by the theory of Osofsky *et al* [OSC$^+$01] based on a heuristic rescaling of the BCS parameters.

For comparison we also show the value predicted by the Belitz theory for the CPA density of states. As one expects from the lower density of states, the CPA leads to lower values of T_c, namely in the region of small concentrations. Our results thus confirm a trend predicted by Shirakawa *et al* that corrections beyond the CPA will lead to higher T_c.

We would like to emphasis that the disorder corrections by Belitz are necessary for a good agreement between experimental data and theory. It can be seen from attempt to the fit T_c with the McMillan formula as shown in figure 6.5. In the comparison we have not used the pseudopotential μ fitted within the Belitz theory, but made a separate fit directly from the McMillan formula, see figure 6.4.

Finally we show that the boron-doped diamond has to be treated as a strong coupling superconductor. In figure 6.6 we show 100 experimental T_c data and its
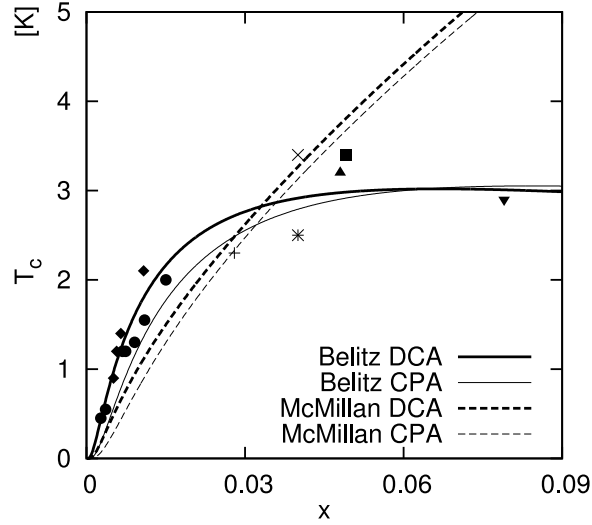
Figure 6.5: Critical temperature T_c of 100 and HPHT samples as a function of boron concentration x. Symbols are data as in figure 2.1. Thick (thin) solid line is a result given by the Belitz theory using the DCA (CPA) density of states. Results of the McMillan theory are in dashed lines.

description with the BCS formula $T_c = 1.14 \exp\left(-1/N_0 V_{\text{BCS}}\right)$, where $V_{\text{BCS}} = 1.30 \times 10^{-23}\,\text{cm}^3\text{eV}$ is the BCS interaction. Apparently, the BCS theory yields an incorrect concentration dependence. It is noteworthy how much the corrections beyond the CPA increase T_c within the BCS theory. In the strong coupling theory these corrections are smaller by an order of magnitude.

In the case of 111 samples we fit the λ as $U = 14.5 \times 10^{-23}\,\text{cm}^3\text{eV}$ and $Q = 23.15 \times 10^{-23}\,\text{cm}^3\text{eV}$. We obtain $V_c = -0.25 \times 10^{-23}\,\text{cm}^3\text{eV}$ for the Belitz formula, respectively $V_c = 1.99 \times 10^{-23}\,\text{cm}^3\text{eV}$ for the formula of McMillan. As one can see, in the case of 111 samples the Belitz theory fails, giving negative V_c, and the McMillan formula produces quite high V_c with $\mu^* = 0.15$ at $x = 0.1$. Reason for the failure of the Belitz theory is a too big strength of the correction Y'. This shows difficulties of the extension of the theory for alloys to doped semiconductors. As was said already, all the superconducting properties of the material are given by the disorder. Therefore it turns out to be problematic to calculate the correct magnitude of the Y' term, since it originally represents only corrections to the clean limit.

If we according to Morel and Anderson [MA62b] estimate the value of $\mu^\star$ in the
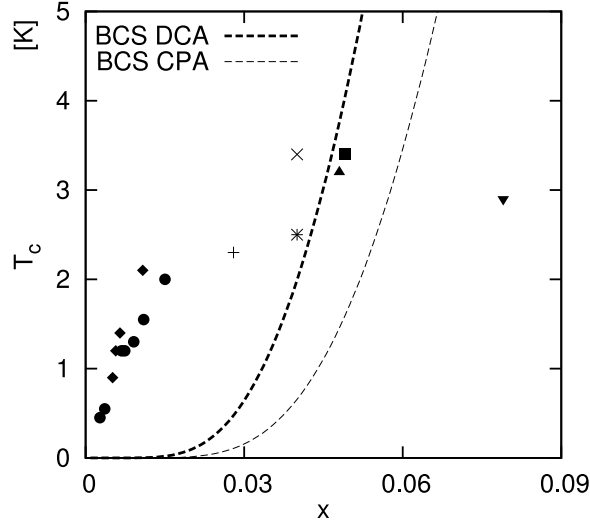
Figure 6.6:   Failure of the BCS approach to the boron-doped diamond. While experimental data (symbols) show decreasing slope of T_c as a function of boron concentration x, the BCS theory (dashed lines) predicts steeply increasing slope. The parameter $V_{\mathrm{BCS}} = 1.30 \times 10^{-23}\,\mathrm{cm^3 eV}$ was fitted within the DCA N_0 computations. Thick (thin) line is given by the DCA (CPA) N_0 results.

limit of well developed band at $x = 0.1$ to be $\mu^\star = 0.12$, we can set the strength of the Y' as a free parameter α

$$Y' = \alpha(2\lambda - \mu)\,. \tag{6.1}$$

Using the equation (6.1) we then obtain $V_c = 1.59 \times 10^{-23}\,\mathrm{cm^3 eV}$ and $\alpha = 0.14$. The comparison of these results with the McMillan formula reveals figure 6.7.

6.2   Impact of the boron distribution correlations on the critical temperature

At the beginning of the discussion we specify the used model. We take T_c to be dependent on the disorder via N_0 in the λ and μ. Therefore the correlations of boron distribution influence the T_c as well only through the changes in the band structure. For the description of boron correlations we use the distribution function (4.41) that has two parameters x and θ. The parameter $\theta \in \langle 0, \infty)$ increases the probability of
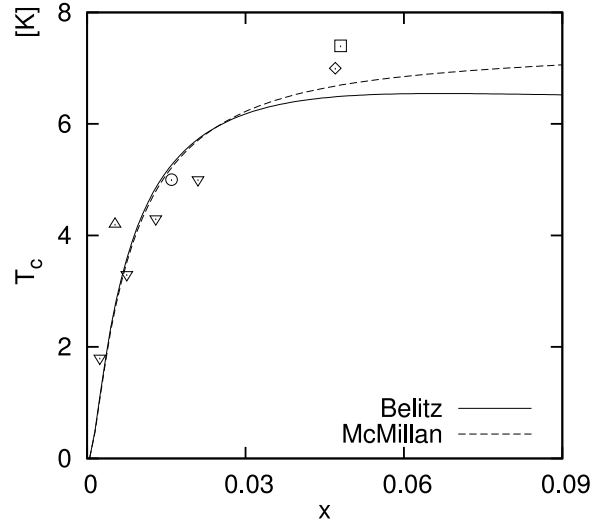
Figure 6.7: Figure shows the T_c concentration dependence of 111 samples. Solid line reproduces the data using the Belitz formula with Y' corrected according to (6.1) and $\mu^\star$ asymptotically set to $\mu^\star = 0.12$. Using $U = 14.5 \times 10^{-23}\,\text{cm}^3\text{eV}$ and $Q = 23.15 \times 10^{-23}\,\text{cm}^3\text{eV}$ we obtain $V_c = 1.59 \times 10^{-23}\,\text{cm}^3\text{eV}$ with $\alpha = 0.14$. For comparison we plot the McMillan formula represented by the dashed line where $V_c = 1.99 \times 10^{-23}\,\text{cm}^3\text{eV}$.

boron dimers, which are in the literature considered as a stable configuration.

Figures 6.8 a) and b) illustrate the impact of boron correlations on the band structure. In both cases we have $n_B = 0.05$ and we have employed the DCA on the cluster of $2 \times 2 \times 2$ sites. The figure 6.8 a) reveals the DOS of weakly correlated boron distribution with $\theta = 4$. The lower figure 6.8 b) shows the impurity band structure of strongly correlated distribution for $\theta = 34$. In both cases the thick line represents the density of states and thin lines its decomposition into contributions according to number of boron atoms in cluster configurations. The noncorrelated distribution density of states was discussed in the figure 6.1 already. Thus we pay attention only to changes caused by the attractive boron correlation here.

Comparison of the weakly correlated DOS and the non-correlated one shows that increasing of the boron correlation enhances number of states associated with bonding and antibonding states on boron dimers. Since the main part of the impurity band density of states is formed by a bound state on a single boron, with enhancing of

attractive correlations the N_0 decreases. For strong correlations larger clusters become the most frequent boron configuration, see figure 6.8 b), and the N_0 trends can get more complicated. The N_0 as a function of x for some values of θ reveals figure 6.9.

Having obtained the $N_0(x)$ for correlated distributions with arbitrary θ we can study the impact on the T_c. Let us first clarify the model again. From the NMR study of boron-doped diamond films it follows that 111 films tend to have smaller fraction of passive boron complexes than 100. [MTH$^+$07] From *ab initio* computations it seems to be very likely that at least boron dimers are energetically more favourable than single borons and sample prepared by an equilibrium method should contain a large fraction of them. Noting this, we can in simple first-step model divide the present T_c experimental data into two groups – 111 films and 100 + quasi-equilibrium HPHT samples – approximating the 111 films as the case with noncorrelated boron sites and 100 + HPHT samples as containing correlated boron complexes.

As noted already we assume parameters U, Q, V_c in λ and μ to be correlation independent. Thus we can reproduce the trends of the concentration dependence of T_c of 111 and 100 + HPHT data for one set of parameters obtaining the $N_0(x)$ dependence in noncorrelated and correlated ($\theta = 34$) case. To obtain the T_c we use the McMillan formula. The figure 6.7 reveals that the McMillan formula is sufficient for the description of the 111 samples and absence of the disorder corrections allows to study just the impact of correlations. Results are shown in figure 6.10, where $U = 21.6$, $Q = 53.9$ and $V_c = 1.0$. From the figure one can see that for small boron densities the model reproduces the experimental T_c data well and thus suggests that the presence of the correlations in boron distribution could be the important parameter responsible for different T_c of distinct types of samples.
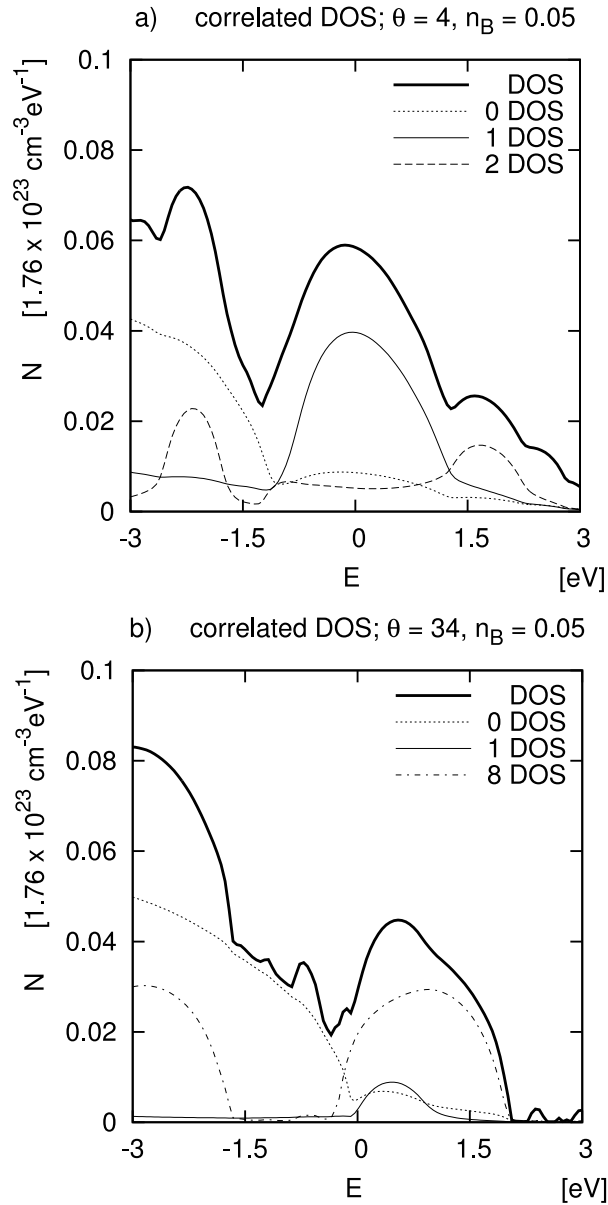
Figure 6.8: The density of states for correlated boron distribution with $n_B = 0.05$ and $\theta = 4$, respectively $\theta = 34$ in figure a), respectively b). The thick line represents the DOS and thin lines its decomposition into contributions according to number of boron atoms in cluster configurations. In the case of weakly correlated distribution the most frequent boron configurations are single-boron and boron dimer configuration. In the case of strongly correlated distribution it is the configuration with single-boron and eight-boron cluster.
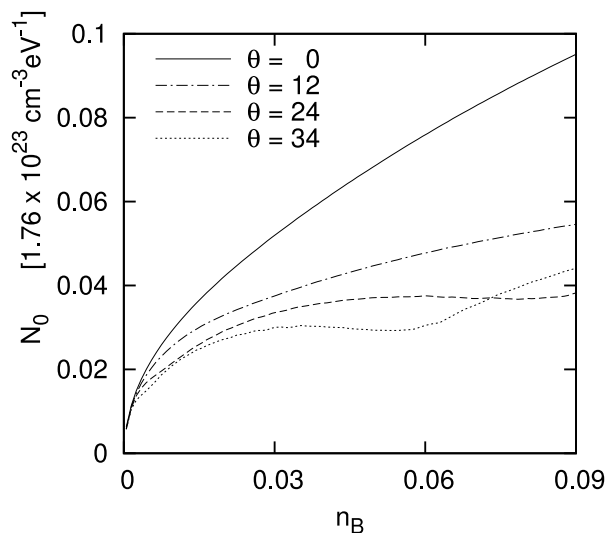
Figure 6.9: The N_0 as a function of boron concentration n_B for several correlation strengths θ. For weak correlations the presence of states associated with boron dimers always lowers the N_0. In the strongly correlated cases larger clusters of boron atoms become frequent and the N_0 dependence can get more complicated.
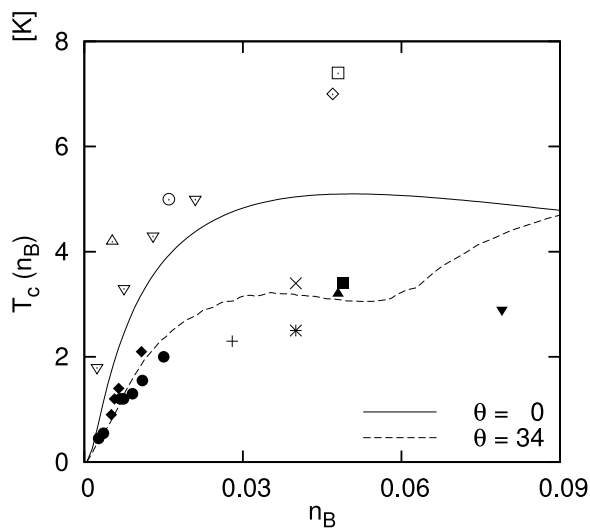
Figure 6.10: Figure illustrates the impact of boron distribution correlations on the T_c. The solid line is the McMillan formula with $U = 21.6$, $Q = 53.9$ and $V_c = 1.0$ using a noncorrelated N_0. The dashed line was obtained using the same parameters but correlated N_0 with $\theta = 34$. As one can see, for small boron concentrations the trends follow the experimental data, suggesting that the boron distribution correlations could be the reason for the difference of the T_c in distinct types of samples.

Chapter 7

Conclusion

In this chapter we make the final conclusions. We divide them into two sections according to the studied problem. First we conclude the study of the dependence of the T_c on boron doping and then the study of the impact of the boron distribution correlations on the T_c.

7.1 Dependence of the critical temperature on boron doping

We have discussed corrections beyond the CPA to the density of states in diamond doped with boron. From numerical studies of the DCA with cluster of $2 \times 2 \times 2$ atoms, it follows that these corrections increase the density of states at the Fermi level, see figure 6.2. This causes an increase of the critical temperature as predicted by Shirakawa *et al* [SHOF07], however in the extent, which is not sufficient to reproduce the experimental data. This shows figure 6.6.

Comparing different approximations we have shown that the strong coupling theory is necessary to predict the realistic critical temperature. It is shown that the disorder corrections of Belitz improve agreement with 100 and HPHT experimental data – see figure 6.5 – reproducing trends observed by Osofsky *et al* [OSC$^+$01]. In the case of the 111 samples the Belitz corrections calculated by the proposed method

turn out to be too strong and the McMillan formula is found to be sufficient for reproducing the experimental data as is shown in figure 6.7.

7.2   Impact of the boron distribution correlations on the critical temperature

We have studied, how boron distribution correlations influence the density of states of boron-doped diamond. For the numerical studies we have again used the DCA with cluster of $2 \times 2 \times 2$ atoms. From the results shown in figure 6.8 it follows that the weak attractive boron correlations lower the N_0. This is in agreement with the *ab initio* studies, claiming that the boron dimers create inactive levels that do not contribute to N_0. For stronger correlations larger boron complexes become frequent and states associated with them can influence the N_0 as well. This reveals figure 6.9.

Figure 6.10 shows that using the McMillan formula, we can for one set of interaction parameters reproduce the T_c trends of both 111 and 100 + HPHT samples using N_0 of noncorrelated and correlated density of states. This suggests that the boron distribution correlations could be the explanation for the difference of the T_c in distinct types of samples.

Part II

Conserving T-matrix theory of superconductivity

Chapter 8

Introduction

Many problems of contemporary condensed-matter physics are so complex that it is believed, their full solution cannot be found. Among such problems one counts systems with multiple collisions would they be with impurities in disordered material of a particles in many-body systems. In these cases one looks for some approximative theory capable of a sufficient description. Frequently used and successful concept is a T-matrix approximation.

In a case of alloys the basic question concerns propagation of a particle through a disordered medium. The T-matrix is defined as an amplitude containing a sum of all possible successive interactions of a wave with some impurity atom. Interaction of the wave with the whole crystal is then described by T-matrix elements from all impurities. Many successful theories were based on the analysis of the T-matrix faithfully describing properties of alloys [VKE68].

The problem of many-body interacting systems exceeds by its complexity the problem of impurity scattering in alloys, nevertheless the concept of T-matrix can be employed also to the case of two-particle interaction. In this field a formalism of many-body Green's functions is widely used and T-matrix plays a role of an object describing the two-particle correlations [BK61]. This approximation is justified for dilute systems, but it is used for dense systems too.

In literature one finds various approximations based on the T-matrix. They differ in the Pauli blocking, in the relation between the T-matrix and the single-particle

spectrum and the level of selfconsistency. The approach we have in mind is known as the Galitskii-Feynman (GF) approximation. The Galitskii-Feynman theory is widely used in a nuclear physics for both equilibrium [KM93, Bdz99] and non-equilibrium [LMŠ01] problems, in the theory of dilute gases, liquid ^{3}He [GBS76], and in studies of electron-electron correlations in molecules and solids [Tou70, GKSB99].

In spite of many achievements in other fields the Galitskii-Feynman approximation isn't able to describe the superconducting phase. Although it becomes unstable at the critical temperature [BSI75] and the T-matrix diverges there, the GF selfenergy constructed from the T-matrix fails to describe the superconducting gap. For this purpose a simplified version of T-matrix approximation was proposed by Kadanoff and Martin [KM61]. In the Kadanoff-Martin (KM) approach the interacting particles of the pair in the T-matrix ladder are not described on the same footing. This in the Green's functions formalism means that one particle is treated selfconsistently and other non selfconsistently. Kadanoff-Martin approximation is used exclusively in the theory of superconductivity [JML97, MJL99, CCHL07]. In other fields its non-symmetry is viewed as unjustified and unacceptable.

The paradox that the worse approximation (KM) works well while the better one (GF) fails was first noticed by Prange [Pra60] and Wild [Wil60] prior to the work of Kadanoff and Martin. The origin of this paradox lies in the fact that the GF approximation includes processes which block a formation of the gap, while the KM is free of them. Apparently GF should be revised with respect to this observation.

We will show that processes which in the GF block the creation of the gap represent nonphysical processes inherently present in the theory. On the basis of this knowledge we will propose a new T-matrix approximation, which from the GF subtracts just these nonphysical processes. The nonphysical processes form a vanishingly small fraction in the normal phase. Therefore, in the normal state the present theory differs from the GF theory by negligible terms. When the condensate appears however, they play an important role and their subtraction enables formation of the superconducting gap in the selfenergy. The revised T-matrix approximation is therefore a unified theory describing both normal and superconducting phase, from which nontrivial conclusions about the nature of the superconducting state can be derived.

Like for the Bose-Einstein condensate a very important property of the superconducting condensate is its stability. According to Landau the stability demands blocking of a creation of fluctuations that would dissipate an energy. This is caused by specific dispersion relation of excitations above the condensate, which significantly differs from a general dependence quadratic in momenta.

In a case of the superconducting condensate there are two possible kinds of excitations. The well known and thoroughly studied are fermionic quasiparticles, which appear in pair and are associated with breaking of the Cooper pair. Much less is known about excitations of the Cooper pair out of the condensate.

The fermionic type of excitations is restricted by the energy gap Δ. The question is, what restricts the non-condensed Cooper pairs. The BCS theory gives no answer to this, because non-condensed pairs are not assumed at all. In the KM approximation the non-condensed pairs appear, but their excitation spectrum is parabolic like in non-interacting Bose gas. The KM approximation thus in fact does not describe the superconductivity since the condensate is unstable. [LCCH10]

We will show that contrary to the KM approximation the reformulated T-matrix theory not only describes the gap Δ but also produces another energy gap in the spectra of Cooper pairs. We can therefore conclude that the reformulated T-matrix theory describes a stable superconducting condensate.

In the following Chapter 9 we will introduce the Galitskii-Feynman and Kadanoff-Martin approximation. In Chapter 10 we discuss the nonphysical processes present in the GF and then propose a new T-matrix theory. Chapter 11 includes results and conclusion.

Chapter 9

Review of T-matrix theories

In this chapter we are going to review two T-matrix theories, namely the Galitskii-Feynman approximation and Kadanoff-Martin approximation. We will observe that both of them fail in description of the rigid superconducting condensate. To introduce the concept of T-matrix, first we will derive it as an approximate solution of equations of motion.

9.1   Equations of motion

Let us consider a many-particle system, which is governed by the hamiltonian

$$\hat{H}(\tau_1) = \frac{1}{\Omega} \sum_{\sigma=\uparrow,\downarrow} \sum_{\mathbf{k}_1} \frac{\mathbf{k}_1^2}{2m} \, \hat{a}_\sigma^\dagger(\tau_1, \mathbf{k}_1) \, \hat{a}_\sigma(\tau_1, \mathbf{k}_1) +$$

$$+ \frac{1}{\Omega^2} \sum_{\mathbf{k}_1, \mathbf{k}_2} \int_0^\beta \mathrm{d}\tau_2 \, \hat{a}_\uparrow^\dagger(\tau_1, \mathbf{k}_1) \, \hat{a}_\downarrow^\dagger(\tau_2, \mathbf{k}_2) \times$$

$$\times \, \mathcal{V}(|\tau_1 - \tau_2|, |\mathbf{k}_1 - \mathbf{k}_2|) \, \hat{a}_\downarrow(\tau_2, \mathbf{k}_2) \, \hat{a}_\uparrow(\tau_1, \mathbf{k}_1), \quad (9.1)$$

where potential $\mathcal{V}$ is translationally invariant in time and space and Ω is a quantized volume. We define the one-particle Green's function $G_\downarrow(\tau_1, \mathbf{k}_1; \tau_2, \mathbf{k}_2)$ as

$$G_\downarrow(\tau_1, \mathbf{k}_1; \tau_2, \mathbf{k}_2) = -\frac{\left\langle \mathcal{T}\{\hat{a}_\downarrow(\tau_1, \mathbf{k}_1) \, \hat{a}_\downarrow^\dagger(\tau_2, \mathbf{k}_2) \, \hat{\sigma}(\beta)\} \right\rangle}{\langle \hat{\sigma}(\beta) \rangle}, \quad (9.2)$$

Here $\langle \ldots \rangle$ is the symbol of grandcanonical averaging and $\hat{\sigma}(\beta)$ stands for the evolution operator – see (B.1) and (B.15) in Appendix B. By derivation of the one-particle Green's function with respect to τ_1 one obtains an equation of motion [KB62]

$$G_{\downarrow}^{0\,-1}(\tau_1, \mathbf{k}_1)\, G_{\downarrow}(\tau_1, \mathbf{k}_1; \tau_2, \mathbf{k}_2) = \delta(\tau_1 - \tau_2)\, \delta(\mathbf{k}_1 - \mathbf{k}_2) + $$
$$+ \frac{1}{\Omega} \sum_{\mathbf{k}_3} \int_0^{\beta} \mathrm{d}\tau_3\, \mathcal{V}(|\tau_1 - \tau_3|, |\mathbf{k}_1 - \mathbf{k}_3|)\, G_{2\downarrow\uparrow}(\tau_1, \mathbf{k}_1; \tau_3^-, \mathbf{k}_3; \tau_2, \mathbf{k}_2; \tau_3^+, \mathbf{k}_3)\,, \quad (9.3)$$

where for the free propagator G^0 is

$$G_{\downarrow}^{0\,-1}(\tau_1, \mathbf{k}_1) = \frac{\partial}{\partial \tau_1} - \frac{\mathbf{k}_1^2}{2m} + \mu\,, \quad (9.4)$$

and a two-particle propagator G_2 reads

$$G_{2\downarrow\uparrow}(\tau_1, \mathbf{k}_1; \tau_2, \mathbf{k}_2; \tau_3, \mathbf{k}_3; \tau_4, \mathbf{k}_4) = $$
$$= -\frac{\left\langle \mathcal{T}\{\hat{a}_{\downarrow}(\tau_1, \mathbf{k}_1)\, \hat{a}_{\uparrow}(\tau_2, \mathbf{k}_2)\, \hat{a}_{\downarrow}^{\dagger}(\tau_3, \mathbf{k}_3)\, \hat{a}_{\uparrow}^{\dagger}(\tau_4, \mathbf{k}_4)\, \hat{\sigma}(\beta)\} \right\rangle}{\langle \hat{\sigma}(\beta) \rangle}\,. \quad (9.5)$$

For the two-particle Green's function one can derive a similar equation of motion, where a three-particle propagator G_3 appears. Apparently (9.3) is a first of a whole infinite hierarchy of equations coupling higher and higher orders of propagators.

9.2 Galitskii-Feynman approximation

It is, in general, impossible to solve the hierarchy exactly. It is therefore usually cut at the second order [MS59, BK61] and the two-particle propagator G_2 is approximated by some simplified equation of motion.

9.2.1 Derivation of the GF theory

The two-particle propagator G_2 describes a propagation of two particles that may be correlated by collisions. To describe these correlations to an infinite order in

potential we approximate the G_2 by a solution of the Bethe-Goldstone equation

$$G_{2\downarrow\uparrow}(\tau_1, \mathbf{k}_1; \tau_2, \mathbf{k}_2; \tau_3, \mathbf{k}_3; \tau_4, \mathbf{k}_4) = G_\downarrow(\tau_1, \mathbf{k}_1; \tau_3, \mathbf{k}_3)\, G_\uparrow(\tau_2, \mathbf{k}_2; \tau_4, \mathbf{k}_4) +$$

$$+ \frac{1}{\Omega^2} \sum_{\mathbf{k}_5, \mathbf{k}_6} \int_0^\beta \mathrm{d}\tau_5\, \mathrm{d}\tau_6\, G_\downarrow(\tau_1, \mathbf{k}_1; \tau_5, \mathbf{k}_5)\, G_\uparrow(\tau_2, \mathbf{k}_2; \tau_6, \mathbf{k}_6) \times$$

$$\times\, \mathcal{V}(|\tau_5 - \tau_6|, |\mathbf{k}_5 - \mathbf{k}_6|)\, G_{2\downarrow\uparrow}(\tau_5, \mathbf{k}_5; \tau_6, \mathbf{k}_6; \tau_3, \mathbf{k}_3; \tau_4, \mathbf{k}_4)\,. \quad (9.6)$$

Here, the correlation between particles is given by the "ladder" of interactions.

Let us combine the equations (9.3) and (9.6). If we transform these equations from imaginary time to Matsubara frequencies, write $k = (\mathrm{i}\omega_n, \mathbf{k})$, and shorten the propagator notation, we arrive at the following set of equations, where the Dyson equation is

$$G_\uparrow(k) = G_\uparrow^0(k) + G_\uparrow^0(k)\, \Sigma_\uparrow(k)\, G_\uparrow(k) \qquad (9.7)$$

formula for the selfenergy is

$$\Sigma_\uparrow(k) = \frac{1}{\beta\Omega} \sum_q \mathcal{T}_{\uparrow\downarrow}(k, q - k; k, q - k)\, G_\downarrow(q - k)\,, \qquad (9.8)$$

and T-matrix reads

$$\mathcal{T}_{\uparrow\downarrow}(k, q - k; p, q - p) = \mathcal{V}(k, q - k; p, q - p) - \frac{1}{\beta\Omega} \sum_{k'} \mathcal{V}(k, q - k; k', q - k') \times$$

$$\times\, G_\uparrow(k')\, G_\downarrow(q - k')\, \mathcal{T}_{\uparrow\downarrow}(k', q - k'; p, q - p)\,. \quad (9.9)$$

We have used a translation symmetry due to which $G(k, k') = G(k)\, \delta(k - k')$ and similarly to the selfenergy. The equations (9.7)-(9.9) are in diagrammatic form shown in Fig 9.1.

As the interaction potential $\mathcal{V}(k, q - k; p, q - p)$ we use the BCS interaction

$$\mathcal{V}(k, q - k; p, q - p) = \mathcal{V}\, \theta(k)\, \theta(q - k)\, \theta(p)\, \theta(q - p)\,, \qquad (9.10)$$

where $\mathcal{V} < 0$ and $\theta(k)$ are cutoff factors,

$$\theta(k) = \begin{cases} 1 & \text{for} \quad |\epsilon(\mathbf{k}) - E_\mathrm{F}| < \omega_\mathrm{D}\,, \\ 0 & \text{for} \quad |\epsilon(\mathbf{k}) - E_\mathrm{F}| > \omega_\mathrm{D}\,. \end{cases} \qquad (9.11)$$
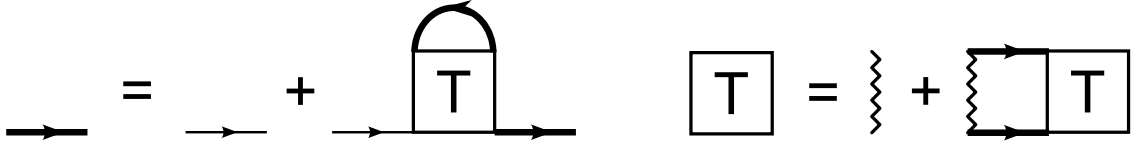
Figure 9.1: Diagrammatic reformulation of Galitskii-Feynman approximation. Thin (thick) line represents a bare (full) propagator. The GF approximation is thermodynamically conserving, however it does not describe the superconductivity.

The presence of cutoffs means that only electrons with energies in a narrow range of width $2\omega_\mathrm{D}$ near the Fermi surface ($\omega_\mathrm{D} \ll E_\mathrm{F}$) participate in the interaction.

The T-matrix then yields a form

$$\mathcal{T}_{\uparrow\downarrow}(k, q - k; p, q - p) = \mathcal{T}_{\uparrow\downarrow}(q)\,\theta(k)\,\theta(q - k)\,\theta(p)\,\theta(q - p)\,. \tag{9.12}$$

For simplicity we omit writing of the θ-functions in T-matrix and interaction potential. The equation (9.9) we then rewrite as

$$\mathcal{T}_{\uparrow\downarrow}(q) = \mathcal{V} - \frac{\mathcal{V}}{\beta\Omega}\sum_{k'}{}'\, G_{\uparrow}(k')\,G_{\downarrow}(q - k')\,\mathcal{T}_{\uparrow\downarrow}(q)\,. \tag{9.13}$$

Here the prime signals restriction of the summation by the cutoff.

9.2.2 Two-particle symmetry and conservation laws

A very desirable property of every many-body theory is conservation of particle number N, total momentum $\mathbf{P}$, angular momentum $\mathbf{L}$, and energy $\mathbf{E}$. Baym and Kadanoff [BK61, Bay62] studied methods, how to construct such conserving theories. They came with two conditions on G_2. The approximate G satisfies all conservation laws, if:

(A) the two-particle Green's function G_2 satisfies equation

$$\frac{1}{\Omega^2} \sum_{\mathbf{k}_2, \mathbf{k}_3} \int_0^\beta d\tau_2 \, d\tau_3 \, G(\tau_1, \mathbf{k}_1; \tau_2, \mathbf{k}_2) \, \mathcal{V}(|\tau_2 - \tau_3|, |\mathbf{k}_2 - \mathbf{k}_3|) \times$$

$$\times \, G_2(\tau_2, \mathbf{k}_2; \tau_3^-, \mathbf{k}_3; \tau_4, \mathbf{k}_4; \tau_3^+, \mathbf{k}_3) =$$

$$= \frac{1}{\Omega^2} \sum_{\mathbf{k}_2, \mathbf{k}_3} \int_0^\beta d\tau_2 \, d\tau_3 \, G_2(\tau_1, \mathbf{k}_1; \tau_3^-, \mathbf{k}_3; \tau_2, \mathbf{k}_2; \tau_3^+, \mathbf{k}_3) \times$$

$$\times \, \mathcal{V}(|\tau_3 - \tau_2|, |\mathbf{k}_3 - \mathbf{k}_2|) \, G(\tau_2, \mathbf{k}_2; \tau_4, \mathbf{k}_4) , \quad (9.14)$$

(B) the two-particle Green's function G_2 is symmetric with respect to interchange
of the upper and lower lines

$$G_2(\tau_1, \mathbf{k}_1; \tau_2, \mathbf{k}_2; \tau_3, \mathbf{k}_3; \tau_4, \mathbf{k}_4) = G_2(\tau_2, \mathbf{k}_2; \tau_1, \mathbf{k}_1; \tau_4, \mathbf{k}_4; \tau_3, \mathbf{k}_3) . \quad (9.15)$$

By inspection of the diagrammatic form of equations in Fig one can easily verify that the Galitskii-Feynman satisfies both conditions and therefore is a thermodynamically conserving theory.

9.2.3 Failure in description of the superconductivity

As was mentioned already, the GF approximation is not able to describe the superconductivity. Let us show this shortcoming.

The T-matrix (9.9) can be decomposed into channels according to the total four-momenta q of interacting pair of particles. Below the critical temperature particles form bound states of the Cooper pairs in one of these channels. In the absence of currents and in equilibrium it is the channel $q = (0, \mathbf{0})$. Its T-matrix $\mathcal{T}_{\uparrow\downarrow}(k, -k; p, -p)$ thus becomes singular being proportional to the volume Ω. This is because the T-matrix obeys a Bose statistics which is singular right at $q = 0$, giving finite occupation of the lowest state like in the Bose-Einstein condensation. For the T-matrix we thus write

$$-\frac{1}{\beta\Omega} \mathcal{T}_{\uparrow\downarrow}(k, -k; p, -p) = \Delta^2 . \quad (9.16)$$

Due to its singular character, the element $\mathcal{T}_{\uparrow\downarrow}(k, -k; k, -k)$ gives an important contribution to the selfenergy – for details see Appendix C. Neglecting the regular part of the selfenergy we obtain

$$\Sigma_{\uparrow}(k) \approx \frac{1}{\beta\Omega} \mathcal{T}_{\uparrow\downarrow}(k, -k; k, -k)\, G_{\downarrow}(-k) = -\Delta^2\, G_{\downarrow}(-k)\,. \qquad (9.17)$$

The full $G_{\uparrow}(k)$ propagator then reads

$$G_{\uparrow}(k) = \frac{1}{i\,\omega_n - \epsilon(\mathbf{k}) + \Delta^2\, G_{\downarrow}(-k)}\,, \qquad (9.18)$$

and together with a similar equation for $G_{\downarrow}(-k)$ leads to the quadratic equation with solution

$$G_{\uparrow}(k) = -\frac{-i\,\omega - \epsilon(\mathbf{k})}{2\Delta^2} \pm \frac{1}{\Delta} \sqrt{\frac{(-i\,\omega - \epsilon(-\mathbf{k}))^2}{4\Delta^2} + \frac{-i\,\omega - \epsilon(-\mathbf{k})}{i\,\omega - \epsilon(\mathbf{k})}}\,, \qquad (9.19)$$

Apparently, this propagator does not possess a pole in a form of the BCS dispersion. This observation was made by Prange [Pra60] and Wild [Wil60].

9.3 Kadanoff-Martin approximation

In his study of the GF approximation, Prange noticed that closing the loop in selfenergy by the bare propagator line arrives at the BCS gap. This construction is now known as the Kadanoff-Martin theory, since these authors analysed its properties in detail [KM61].

A structure of the KM theory is the same as of the GF approximation. The only difference is that in the KM approximation we construct the two-particle Green's function in nonsymmetric way and one of the propagator lines is made nonselfconsistent (or described on the level of the Hartree-Fock approximation).

As a result the Dyson equation reads

$$G_{\uparrow}(k) = G_{\uparrow}^0(k) + G_{\uparrow}^0(k)\, \Sigma_{\uparrow}(k)\, G_{\uparrow}(k)\,, \qquad (9.20)$$

$$\Sigma_{\uparrow}(k) = \frac{1}{\beta\,\Omega} \sum_q \mathcal{T}_{\uparrow\downarrow}(k, q - k; k, q - k)\, G_{\downarrow}^0(q - k)\,, \qquad (9.21)$$
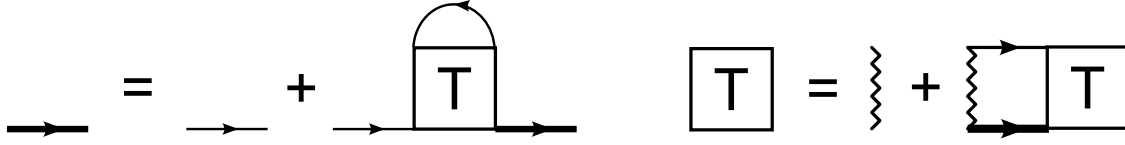
Figure 9.2: Diagrammatic reformulation of Kadanoff-Martin approximation. Thin (thick) line represents a bare (full) propagator. The KM theory is not thermodynamically conserving. It describes the superconducting gap, but the condensate is not rigid.

and for the T-matrix we write

$$\mathcal{T}_{\uparrow\downarrow}(k, q - k; p, q - p) = \mathcal{V} - \frac{\mathcal{V}}{\beta\Omega}\sideset{}{'}\sum_{k'} G_\uparrow(k')\, G_\downarrow^0(q - k') \times$$

$$\times\ \mathcal{T}_{\uparrow\downarrow}(k', q - k'; p, q - p)\,. \quad (9.22)$$

A diagrammatic reformulation of equations reveals Fig 9.2 One cas easily observe that in the case of KM approximation the conservation conditions (A) and (B) are not fulfilled.

9.3.1   Gap in the single-particle spectrum

Let us study a solution of equations (9.20)-(9.22) below the temperature of Cooper pair formation. First we show that the singular T-matrix develops a clear pole in the single-particle spectral function and that there is a gap in the energy spectrum. Then we derive the equation for the gap and discuss the rigidity of the condensate.

Propagator

Similarly as in the case of the GF (9.17) we approximate the selfenergy by the singular contribution

$$\Sigma_\uparrow(k) \approx -\Delta^2\, G_\downarrow^0(-k)\,. \quad (9.23)$$

In the KM approximation the Green's function closing the loop in the selfenergy is bare. Therefore from the Dyson equation we obtain a full propagator in a form

identical to the BCS theory

$$G_\uparrow(\mathrm{i}\,\omega_n, \mathbf{k}) = \frac{1}{\mathrm{i}\,\omega_n - \epsilon(\mathbf{k}) + \frac{\Delta^2}{-\mathrm{i}\,\omega_n - \epsilon(-\mathbf{k})}} = \frac{-\mathrm{i}\,\omega_n - \epsilon(-\mathbf{k})}{(\mathrm{i}\,\omega_n - \epsilon(\mathbf{k}))(-\mathrm{i}\,\omega_n - \epsilon(-\mathbf{k})) + \Delta^2}\,. \tag{9.24}$$

This propagator has two poles at energies $\pm E(\mathbf{k})$ given by

$$E(\mathbf{k}) = \sqrt{\epsilon^2(\mathbf{k}) + \Delta^2}\,. \tag{9.25}$$

The KM approach thus yields experimentally confirmed single-particle spectrum.

Gap equation

From (9.22) we can derive an equation for the gap. For the $\mathcal{T}_{\uparrow\downarrow}(k, q - k; k, q - k)$ we write

$$\frac{1}{\mathcal{T}_{\uparrow\downarrow}(q)} = \frac{1}{\mathcal{V}} + \frac{1}{\beta\,\Omega}\sum_{k'}{}' G_\uparrow(k')\,G_\downarrow^0(q - k')\,. \tag{9.26}$$

In the thermodynamical limit $\Omega \to \infty$, the T-matrix of the condensation mode diverges, i.e., $1/\mathcal{T}(q) \to 0$. Equation then simplifies to

$$0 = \frac{1}{\mathcal{V}} + \frac{1}{\beta\,\Omega}\sum_{k'}{}' G_\uparrow(k')\,G_\downarrow^0(q - k')\,, \tag{9.27}$$

which is for $q = 0$ easily rewritten in a form

$$\frac{1}{|\mathcal{V}|} = \frac{1}{\beta\,\Omega}\sum_{\mathrm{i}\,\omega_n', \mathbf{k}'}{}' \frac{1}{(\mathrm{i}\,\omega_n' - \epsilon(\mathbf{k}'))(-\mathrm{i}\,\omega_n' - \epsilon(-\mathbf{k}')) + \Delta^2}\,. \tag{9.28}$$

This is the familiar BCS gap equation.

9.3.2 Stability of the condensate with respect to noncondensed Cooper pairs

We have seen that within the KM theory one obtains the superconducting gap. Now we can ask, whether the condensate described by the KM is rigid.

Rigidity of the condensate follows from the dispersion relation of the excitations. [KCKL00] To stabilize the condensate the dispersion has to include restrictions which

prevent the system from the dissipation of energy through the excitations. In the superconducting condensate we distinguish two types of excitations - fermionic quasiparticles and noncondensed Cooper pairs.

Excitation of the fermion is connected with breaking of the Cooper pair and is restricted by the gap 2Δ in the one-particle spectrum. As we have seen above, this gap appears so that the condensate resulting from the KM approximation is stable in this point.

We thus focus on the dispersion of the Cooper pairs we obtain from the inversion of the T-matrix element (9.26). We will benefit from results of Gor'kov who analyzed the equation (9.27) close to the critical temperature T_c, where the gap is small. Keeping terms to the quadratic order in Δ he has shown that it leads to

$$0 = \frac{\mathbf{q}^2}{2m^*} - A + B|\Delta|^2 \,, \tag{9.29}$$

where m^* is a mass of the Cooper pair, $B = 3/(2E_F)$ and $A = 6\pi^2 k_B^2 T_c(T_c - T)/(7\zeta_{|3|}E_F)$.

The condensed Cooper pairs have four-momentum q. Now we assume a noncondensed mode $q' = (0, \mathbf{q}')$. Its inverse T-matrix can be written in a similar way

$$\frac{C}{\mathcal{T}(q')} = \frac{\mathbf{q}'^2}{2m^*} - A + B|\Delta|^2 \,, \tag{9.30}$$

with $C = 8\pi^2 k_B^2 T_c^2/(7\zeta_{|3|}n)$ and n being the electron density. The right hand side of equation (9.30) represents an energy of the noncondensed Cooper pair of momentum $\mathbf{q}'$. Combining (9.29) and (9.30) we obtain

$$\frac{C}{\mathcal{T}(q')} = \frac{\mathbf{q}'^2}{2m^*} - \frac{\mathbf{q}^2}{2m^*} \,. \tag{9.31}$$

In the frame moving with the condensate $\mathbf{q} = 0$ and one finds that noncondensed Cooper pairs obey a dispersion of free particles.

Apparently, in the KM approximation the condensate is not rigid, because condensation in competitive modes is not excluded and the gapless quadratic excitation energy allows for excitation of noncondensed Cooper pairs by any slow perturbation. From this we conclude that even the KM is not sufficient for the description of the superconductivity and one has to search for some more accurate theory.

Chapter 10

New T-matrix theory

As was already shown, both the GF and KM approximation at some level fail in description of the superconductivity. In this chapter we propose a new T-matrix theory, which is conserving in the Kadanoff-Baym sense and describes a rigid superconducting condensate.

10.1 Nonphysical processes in the Galitskii-Feynman approximation

We have observed a striking paradox that the worse (KM) approximation works quite well while the better one (GF) fails. Apparently, the GF approximation includes diagrams which block formation of the gap, while the KM approximation is free of them. One of such contributions is sketched in Fig 10.1. The diagram shows a nonphysical self-interaction which is enhanced when particles are bounded in the momentum space as it is in the case of Cooper pairs. This indirect self-interaction becomes crucial when the superconducting condensate appears.

Originally is the self-interaction in Feynman's diagrammatic expansion cancelled by corresponding exchange diagrams, which restore the antisymmetry of the propagating wave function. Such compensating exchange diagrams are beyond the T-matrix approximation and it is not clear how many and how complicated diagrams ought
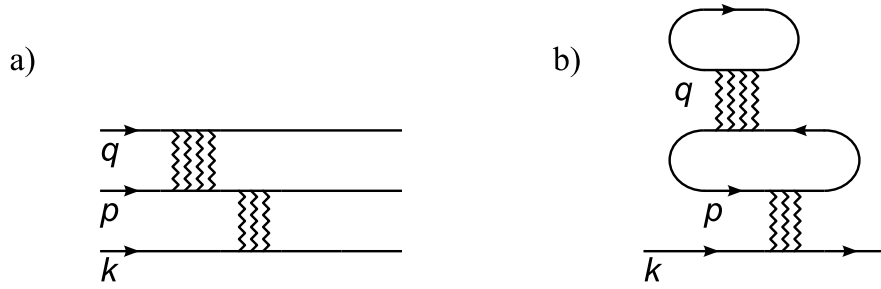
Figure 10.1:   a) Schematic picture of three interacting particles of initial quantum states $(k,\uparrow)$, $(p,\downarrow)$, $(q,\uparrow)$. Due to the Pauli principle all particles are in different states, so $q \neq k$. b) Corresponding Feynman diagrams for the Green function of the particle k, the other lines are closed into loops and momenta p, q are summed over with no restriction. For $q = k$ the diagram yields a self-interaction. In the superconducting state collisions are enhanced for $p = -k$. Similarly, the enhanced processes couple q with $p = -q$, which leads to $q = -p = k$. This indirect resonant self-interaction blocks the formation of the gap. The q-loop is included in the GF approximation while it is absent in the KM approximation.

to be included. The cancellation can be demonstrated on the simpler self-interaction present in the Hartree field. As one can see in Fig 10.2, this self-interaction is cancelled by the Fock selfenergy – one step more complicated theory. Apparently, the original simple problem is cured only on cost of an increase of complexity of theory.

One can eliminate the self-interaction by restriction of sums in the diagrams as well. Such correction is not equivalent to the inclusion of antisymmetrising diagrams, but it removes the biggest mistakes. This approach of sum restrictions we will follow here.

10.2   Derivation and properties

Let us on the basis of the former discussion propose a new T-matrix theory, which is free of the terms blocking the gap formation. To eliminate these terms we will restrict some of the sums over the frequency and momenta.
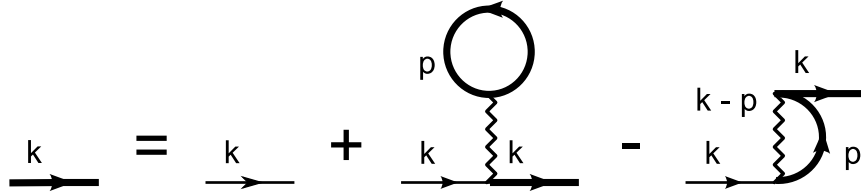
Figure 10.2: Diagrams of Hartree-Fock approximation with spin independent inter-action. In the Hartree term, a particle of four-momenta k collides with a particle p. Since p is summed over with no restriction, the diagram contains a self-interaction $p = k$ for parallel spins. This self-interaction is cancelled by the Fock term for $k - p = 0$. The Fock term is the only diagram needed to fully antisymmetrize the Hartree approximation. In contrast to cancel the self-interaction and restore the wave antisymmetry in the case of the T-matrix approximation, one would need to include infinite number of diagrams with exchanged lines.

10.2.1 Closed set of equations

When a pair of particles interact in stationary and homogeneous systems, its total frequency and momentum q conserve. Dressing of a particle $(k, \uparrow)$ of four-momentum k and spin $\uparrow$ is given by the selfenergy $\Sigma_\uparrow(k)$ which can be decomposed into a sum over interacting pairs

$$\Sigma_\uparrow(k) = \sum_q \sigma_{q\uparrow}(k). \tag{10.1}$$

In the spirit of the multiple scattering expansion [JQ74] we introduce a reduced propagator

$$G_{\slashed{q}\downarrow}(p) = G^0_\downarrow(p) + G^0_\downarrow(p) \sum_{q' \neq q} \sigma_{q'\downarrow}(p) \, G_{\slashed{q}\downarrow}(p). \tag{10.2}$$

The reduced propagator $G_{\slashed{q}\downarrow}(p)$ is dressed by all binary interactions except for the one in which the total four-momentum of the interacting pair equals q. By this we exclude the interaction of the particle $(q - p, \uparrow)$ with $(p, \downarrow)$.

The contribution of a collision of pair with four-momentum q to the selfenergy reads

$$\sigma_{q\uparrow}(k) = \frac{1}{\beta\Omega} \mathcal{T}_{\uparrow\downarrow}(k, q - k; k, q - k) \, G_{\slashed{q}\downarrow}(q - k). \tag{10.3}$$

We will call it a q-channel of selfenergy for brevity. The dressed propagator G is given

by the Dyson equation with the unrestricted sum over channels

$$G_\uparrow(k) = G_\uparrow^0(k) + G_\uparrow^0(k) \sum_q \sigma_{q\uparrow}(k)\, G_\uparrow(k)\,. \tag{10.4}$$

To avoid the self-interaction in (10.3) we use the reduced propagator $G_{\cancel{q}\downarrow}(q-k)$ to close the loop. To guarantee conservation laws, all propagators in the loop have to be in the same approximation. Accordingly, the T-matrix has to be constructed as

$$\mathcal{T}_{\uparrow\downarrow}(k, q-k; p, q-p) = \mathcal{V} - \frac{\mathcal{V}}{\beta\Omega}\sideset{}{'}\sum_{k'} G_\uparrow(k')\, G_{\cancel{q}\downarrow}(q-k') \times$$

$$\times\, \mathcal{T}_{\uparrow\downarrow}(k', q-k'; p, q-p)\,. \tag{10.5}$$

The set of equations (10.2)-(10.5) is closed. These equations do not have diagrammatic representation in the strict sense. It is because the Feynman diagrammatic rules are based on unrestricted sums over states.

10.2.2 Two particle symmetry

Now we show that the present theory is conserving in the Baym-Kadanoff sense, i.e., that it satisfies conditions (A) and (B) from Ref. [BK61]. For the present approximation the condition (A) is satisfied easily, since the T-matrix relates to the two-particle Green function G_2 as

$$G_{2\uparrow\downarrow}(k, q-k; p, q-p) = G_\uparrow(k)\, G_{\cancel{q}\downarrow}(q-k)\, \delta(k-p) +$$

$$-\, G_\uparrow(k)\, G_{\cancel{q}\downarrow}(q-k)\, \mathcal{T}_{\uparrow\downarrow}(k, q-k; p, q-p)\, G_\uparrow(p)\, G_{\cancel{q}\downarrow}(q-p)\,. \tag{10.6}$$

The condition (B), which demands that the two-particle Green function is symmetric with respect to interchange of the upper and lower line, is however from (10.6) not obvious.

First we show that the T-matrix (10.5) is symmetric with respect to the interchange of the upper and lower line

$$\mathcal{T}_{\uparrow\downarrow}(k, q-k; p, q-p) = \mathcal{T}_{\downarrow\uparrow}(p, q-p; k, q-k)\,, \tag{10.7}$$

in spite of the selfconsistency restricted only in the upper line. Apparently, symmetry (10.7) is satisfied for the lowest order $\mathcal{T} \approx \mathcal{V}$.

Now we assume that the T-matrix is symmetric in the n-th order and show that the symmetry of $(n+1)$-th order follows. For a general order obtained by iteration of equation (10.5) it is sufficient to show that

$$G_{\not{q}\uparrow}(k)\, G_{\downarrow}(q-k) = G_{\uparrow}(k)\, G_{\not{q}\downarrow}(q-k)\,. \tag{10.8}$$

In the iteration process we assume n-th order in the selfenergy of Green functions $G_{\not{q}}G$. From equation (10.3) we then have

$$
\begin{aligned}
\sigma_{q\uparrow}(k)\, G_{\not{q}\uparrow}(k) &= \mathcal{T}_{\uparrow\downarrow}(k, q-k; k, q-k)\, G_{\not{q}\downarrow}(q-k)\, G_{\not{q}\uparrow}(k) \\
&= \mathcal{T}_{\downarrow\uparrow}(q-k, k; q-k, k)\, G_{\not{q}\downarrow}(q-k)\, G_{\not{q}\uparrow}(k) \\
&= G_{\not{q}\downarrow}(q-k)\, \sigma_{q\downarrow}(k)\,, \tag{10.9}
\end{aligned}
$$

where we have used symmetry of the n-th order. Now we are ready to prove (10.8),

$$
\begin{aligned}
G_{\not{q}\uparrow}(k)\, G_{\downarrow}(q-k) &= G_{\uparrow}(k)\, (1 - \sigma_{q\uparrow}(k)\, G_{\not{q}\uparrow}(k)) \times \\
&\quad \times (1 + G_{\downarrow}(q-k)\, \sigma_{q\downarrow}(q-k))\, G_{\not{q}\downarrow}(q-k) \\
&= G_{\uparrow}(k)\, G_{\not{q}\downarrow}(q-k)\, (1 - \sigma_{q\downarrow}(q-k)\, G_{\not{q}\downarrow}(q-k)) \times \\
&\quad \times (1 + G_{\downarrow}(q-k)\, \sigma_{q\downarrow}(q-k))\,. \tag{10.10}
\end{aligned}
$$

In the first step we have used

$$G_{\downarrow}(q-k) = G_{\not{q}\downarrow}(q-k) + G_{\downarrow}(q-k)\, \sigma_{q\downarrow}(q-k)\, G_{\not{q}\downarrow}(q-k)\,, \tag{10.11}$$

which follows from (10.2) and (10.4), and a similar relation for $G_{\not{q}\uparrow}(k)$. In the second step we have substituted (10.9). From equation (10.11) it follows that the product of the two brackets in (10.10) equals to unity. Therefore, the relation (10.8) is proved and the symmetry (10.7) of the T-matrix is proved as well.

From the symmetry of the T-matrix (10.7) and relation (10.8) follows the symmetry of the two-particle Green function

$$G_{2\uparrow\downarrow}(k, q-k; p, q-p) = G_{2\downarrow\uparrow}(q-k, k; q-p, p)\,. \tag{10.12}$$

We can conclude that the present theory also satisfies the condition (B) and is conserving in the Baym-Kadanoff sense.

10.2.3   Multiple scattering approach

The nonphysical resonant self-interaction is naturally avoided in the Fadeev-Watson-Lovelace multiple scattering expansion [Wat53, GW64, Fad61, Lov64]. In Ref. [Lip08] the method of the multiple scattering theory was implemented to the theory of superconductivity following a rather different approach. It was argued that the GF approximation includes nonphysical contributions in which two particles interact again after they have accomplished a collision. Indeed, the T-matrix sums the interaction potential to the infinite order so that the next interaction is possible only with a next particle. When one eliminates such repeated collisions from the GF approximation, the resulting theory goes to the GF approximation in the normal state while it yields the gap in the superconducting state. Here we show that the present approach and the approach of Ref. [Lip08] modified to four-momentum yield identical results.

The nonphysical repeated collisions can be eliminated with the help of Soven's concept of effective medium modified for binary collisions. In this spirit one selects a q-channel which will be described explicitly while all other channels are described by the effective medium represented by the selfenergy. We thus eliminate the q-channel from the selfenergy of the particle $(k; \uparrow)$. This channel is included explicitly into the full propagator with a single collision being allowed,

$$G_\uparrow(k) = G_{\slashed{\sigma}\uparrow}(k) + G_{\slashed{\sigma}\uparrow}(k) \frac{1}{\beta\Omega} \mathcal{T}_{\uparrow\downarrow}(k, q-k; k, q-k) \, G_\downarrow(q-k) \, G_{\slashed{\sigma}\uparrow}(k) \,. \qquad (10.13)$$

Note that the loop is closed by the full Green function. This is because we have eliminated $\sigma_{q\uparrow}$ which does not enter $G_\downarrow$ in the loop.

The scattering equation (10.13) defines the selfenergy indirectly. Comparing (10.13) with $G_\uparrow(k) = G_{\slashed{\sigma}\uparrow}(k) + G_{\slashed{\sigma}\uparrow}(k) \, \sigma_{q\uparrow}(k) \, G_\uparrow(k)$ we find that q-channel selfenergy is given by

$$\frac{\sigma_{q\uparrow}(k)}{1 - \sigma_{q\uparrow}(k) \, G_{\slashed{\sigma}\uparrow}(k)} = \frac{1}{\beta\Omega} \mathcal{T}_{\uparrow\downarrow}(k, q-k; k, q-k) \, G_\downarrow(q-k) \,. \qquad (10.14)$$

This relation complicates a straightforward implementation of the theory obtained from Soven's scheme. Fortunately, it can be simplified to the set (10.2)-(10.5).

Using the symmetry (10.8) one can readily see that equation (10.13) is equivalent to the approximation introduced in this paper. Alternatively, one can multiply Eq. (10.14) by the denominator of the left hand side and use Eq. (10.9) to turn relation (10.14) into Eq. (10.3). Finally, we have to take into account that inside the T-matrix the reduced propagator appears for spin ↑, i.e., in the lower line. According to (10.7) this is equivalent to the T-matrix with the reduced upper line. The present derivation is thus equivalent to the application of Soven's scheme.

We note that here we identify the channel via frequency and momentum $q \equiv (\mathrm{i}\,\omega_n, \mathbf{q})$. In Ref. [Lip08] the channel was identified only via momentum $\mathbf{q}$ what applies only to non-retarded interactions and leads to slightly different results. In particular, the identification of a channel via momentum does not provide a two-particle Green function symmetric with respect to interchange of the upper and lower lines. The theory in Ref. [Lip08] thus does not satisfy the condition (B) and it is not conserving in the Baym-Kadanoff sense.

10.3   Description of the superconducting state

Here we will employ the new T-matrix approach to the superconducting phase and we will compare its ability to describe the rigid condensate with other T-matrix theories.

10.3.1   Gap equation

In the normal state, the single-channel contribution vanishes in the thermodynamic limit, $\sigma_{q\uparrow} \propto 1/\Omega \to 0$. The reduced propagator then equals to the dressed propagator, $G_{\not q\uparrow} \to G_\uparrow$, and the present theory is identical to the GF approximation.

As discussed earlier, in the well developed superconducting state a single T-matrix channel becomes singular and forms a major contribution to the selfenergy. In the absence of currents and in equilibrium, it is the zero frequency and zero momentum channel $q = (0, \mathbf{0})$. It is advantageous to split the singular part off the remaining

regular terms

$$\Sigma_\uparrow(k) = -\Delta^2 G_{\emptyset\downarrow}(-k) + \Sigma_{\emptyset\uparrow}(k) \,. \tag{10.15}$$

The reminder

$$\Sigma_{\emptyset\uparrow}(k) = \sum_{q\neq 0} \sigma_{q\uparrow}(k) \,, \tag{10.16}$$

covers normal processes in the background of superconductivity. From equations (10.2) and (9.16) one can see that Δ does not enter the reduced propagator

$$G_{\emptyset\uparrow}(k) = G^0(k) + G^0(k) \, \Sigma_{\emptyset\uparrow}(k) \, G_{\emptyset\uparrow}(k) \,. \tag{10.17}$$

The Green function $G_{\emptyset\uparrow}$ can be viewed as a propagator of the normal metal.

Using the selfenergy (10.15), the dressed Green function (10.4) can be expressed via the reduced propagator

$$G_\uparrow(k) = G_{\emptyset\uparrow}(k) - G_{\emptyset\uparrow}(k) \, \Delta^2 \, G_{\emptyset\downarrow}(-k) \, G_\uparrow(k) \,. \tag{10.18}$$

This equation shows that Δ equals to the energy and momentum independent anomalous selfenergy giving the superconducting gap in the Eliashberg theory [VIK82]. The anomalous selfenergy itself follows from the equation for the T-matrix (10.5) which we rewrite as

$$\frac{1}{\mathcal{T}(q)} = \frac{1}{\mathcal{V}} + \frac{1}{\beta\Omega} \sum_{k'} G_\uparrow(k) \, G_{\sslash\downarrow}(q - k) \,. \tag{10.19}$$

For the singular channel $q = 0$ we have $1/\mathcal{T}(q) \to 0$ and we finally obtain

$$\frac{1}{|\mathcal{V}|} = \frac{1}{\beta\Omega} \sum_{i\,\omega_n,\,\mathbf{k}'} \frac{1}{\left(G_\uparrow^{0\,-1}(k) - \Sigma_{\emptyset\uparrow}(k)\right) \left(G_\downarrow^{0\,-1}(-k) - \Sigma_{\emptyset\downarrow}(-k)\right) + \Delta^2} \,. \tag{10.20}$$

Apparently, in the well developed superconducting state the present theory asymptotically approaches the Eliashberg theory. There are some differences, however. In the present theory all processes, normal and pairing, are treated within the same T-matrix approximation. In the Eliashberg theory the normal processes are in the Migdal (or Born) approximation while the pairing covered by equations for anomalous functions is described by the approximation corresponding to the T-matrix.

10.3.2   Rigidity of the condensate

Let us now study the rigidity of the condensate as described by the proposed T-matrix theory. Below the critical temperature the proposed theory yields the gap Δ. Therefore the fermionic excitations obey the correct BCS-like dispersion and the condensate is with respect to these excitations stable.

Now we focus on the excited Cooper pairs. For the nonsingular channel q', the T-matrix $\mathcal{T}(q')$ is finite. From the equation (10.3) we see that $\sigma_{q'\uparrow} \to 0$ with $\Omega \to 0$ and also $G_{\bcancel{q}'\downarrow}(q' - k) \to G_{\downarrow}(q' - k)$. Accordingly we have

$$\frac{1}{\mathcal{T}(q')} = \frac{1}{\mathcal{V}} + \frac{1}{\beta\Omega} \sum_{k'} G_{\uparrow}(k) \, G_{\downarrow}(q' - k) \,. \tag{10.21}$$

Using again the results of Gor'kov we from (10.19) obtain equation identical with (9.29) except for values of A and B which are modified by the more elaborated self-energy. From (10.21) follows equation

$$\frac{C}{\mathcal{T}(q')} = \frac{\mathbf{q}'^2}{2m^*} - A + 2B|\Delta|^2 \,, \tag{10.22}$$

which differs from (9.30) by a factor of 2 in term $B|\Delta|^2$.

Combining equations (9.29) and (10.22) we obtain the T-matrix of the noncondensation mode

$$\frac{C}{\mathcal{T}(q')} = \frac{\mathbf{q}'^2}{2m^*} + A - \frac{\mathbf{q}^2}{m^*} \,. \tag{10.23}$$

First we will show that the right hand side of the equation cannot reach zero. Values of the pair momentum $\mathbf{q}$ are limited by the critical current, $\mathbf{q}^2 < \mathbf{q}_c^2$. The current is proportional to the square of the gap times the momentum, $\mathbf{j} \propto \mathbf{q}|\Delta|^2$. Using equation (9.29) one finds $\mathbf{j} \propto \mathbf{q}(A - \mathbf{q}^2/2m^*)$. The critical current is the maximum one, $\partial\mathbf{j}/\partial\mathbf{q}|_{\mathbf{q}_c} = 0$, which is achieved for $\mathbf{q}_c = 2m^*A/3$, see [Tin66]. Accordingly,

$$\frac{C}{\mathcal{T}(q')} > \frac{\mathbf{q}'^2}{2m^*} + A - \frac{\mathbf{q}_c^2}{m^*} = \frac{\mathbf{q}'^2}{2m^*} + \frac{A}{3} \,. \tag{10.24}$$

Inequality (10.24) implies that the mode of $q' \neq q$ cannot become singular once the condensate in the mode q emerges. Briefly, there is a single condensate, as it is tacitly assumed in the BCS theory.

The right hand side of equation (10.22) represents an energy of a noncondensed Cooper pair of four-momentum q'. In the frame moving with the condensate, $\mathbf{q} = 0$, a Cooper pair can be excited from the condensate into a noncondensed state with the minimal energy cost A. Let us estimate under which conditions Cooper pairs can be excited by an external perturbation. According to the Landau criterion [PS01] the external perturbation moving with velocity $\mathbf{v}$ can excite the Cooper pair of momentum $\mathbf{q}'$ if the Cherenkov condition

$$\mathbf{v}\mathbf{q}' = \frac{\mathbf{q}'^2}{2m^*} + A \tag{10.25}$$

is satisfied. This equation is solved by real $\mathbf{q}'$ for

$$|v| > \sqrt{\frac{2A}{m^*}}\,. \tag{10.26}$$

This velocity is higher than the critical velocity of pair breaking $v_c = \Delta/k_F$, where k_F is the Fermi momentum. Indeed from the equation (9.29) follows

$$\Delta = \sqrt{\frac{A}{B}} = \sqrt{\frac{A\,k_F^2}{3m}}\,, \tag{10.27}$$

where $m = m^*/2$ is the electronic mass, so that

$$|v| > \sqrt{3}\,v_c\,. \tag{10.28}$$

Briefly, it is easier to break a Cooper pair into two quasiparticles than to excite it from the condensate into a noncondensed Cooper pair.

As one could see, the new T-matrix theory is able to describe a condensate, which is stable against both fermionic and bosonic excitations. Moreover it explains, why there exists only one condensating channel. This demonstrates a superiority of this theory above the GF and KM approximation.

Chapter 11

Conclusion

Motivated by the fact that both GF and KM approximation fail in the description of the superconducting condensate, we have proposed a new T-matrix theory, which overcomes difficulties of its predecessors.

We have found out that the GF approximation is not able to describe the superconductivity, because it contains nonphysical processes, which block formation of the gap. We have removed these processes by restriction of summations over the frequencies and momenta. We have managed to do this restriction in a way, which contrary to the KM approximation preserves important Baym-Kadanoff symmetries. This implies that the theory conserves thermodynamical variables. The theory keeps the simple structure similar to the KM approximation, but is rooted in the many-body approach known as the multiple scattering approach.

This new T-matrix theory in normal phase recovers the GF approximation in the limit of infinite volume. Below the critical temperature it however describes the superconducting gap. Moreover the condensate obtained by this theory is stable not only against quasiparticle but also against Cooper pair excitations. An interesting implication of this rigidity is that the condensate can exist only in one of a pair four-momenta channels.

We have formulated this theory for the BCS interaction potential and therefore the obtained superconducting gap-function Δ is a simple frequency and momentum-independent scalar. The theory can be however easily reformulated for more compli-

cated retarded potentials, e.g., dependent on a transferred four-momentum $\mathcal{V}(p-k)$ between scattered in particle p and scattered out particle k. For the T-matrix in the singular channel $q = 0$ we then write

$$\mathcal{T}_{\uparrow\downarrow}(k, -k; p, -p) = -\frac{1}{\beta\Omega}\bar{\Delta}(k)\,\Delta(p)\,, \tag{11.1}$$

and Δ is a function of four-momenta. This shows that the theory can be applied to more realistic problems.

Bibliography

[AGD63]   A. A. Abrikosov, L. P. Gorkov, and I. E. Dzyaloshinski. *Methods of Quantum Field Theory in Statistical Physics*. Dover, New York, 1963.

[AHJ03]   K. Aryanpour, M. H. Hettler, and M. Jarrell. Dynamical cluster approximation employing the fluctuation exchange approximation as a cluster solver. *Phys. Rev. B*, 67(8):085101, Feb 2003.

[And59]   P. W. Anderson. Theory of dirty superconductors. *Journal of Physics and Chemistry of Solids*, 11:26 – 30, 1959.

[BAC04]   X. Blase, Ch. Adessi, and D. Connétable. Role of the dopant in the superconductivity of diamond. *Phys. Rev. Lett.*, 93(23):237004, Nov 2004.

[Bay62]   Gordon Baym. Self-consistent approximations in many-body systems. *Phys. Rev.*, 127(4):1391–1401, Aug 1962.

[BBA$^+$06]   E. Bourgeois, E. Bustarret, P. Achatz, F. Omnès, and X. Blase. Impurity dimers in superconducting B-doped diamond: Experiment and first-principles calculations. *Physical Review B (Condensed Matter and Materials Physics)*, 74(9):094509, 2006.

[BBC$^+$09]   X. Blase, E. Bustarret, C. Chapelier, T. Klein, and Ch. Marcenat. Superconducting group-IV semiconductors. *Nature materials*, 8:375–382, May 2009.

[Bdz99]   P. Bożek. Self-consistent solution of Galitskii-Feynman equations at finite temperature. *Phys. Rev. C*, 59(5):2619–2626, May 1999.

[Bel87a]   D. Belitz. Theory for dirty superconductors. I. Strong-coupling equations. *Phys. Rev. B*, 35(4):1636–1650, Feb 1987.

[Bel87b]   D. Belitz. Theory for dirty superconductors. II. McMillan solution and T_c degradation. *Phys. Rev. B*, 35(4):1651–1658, Feb 1987.

[Bel87c]   D. Belitz. Theory of disorder-induced increase and degradation of superconducting T_c. *Phys. Rev. B*, 36(1):47–53, Jul 1987.

[BK61]   Gordon Baym and Leo P. Kadanoff. Conservation laws and correlation functions. *Phys. Rev.*, 124(2):287–299, Oct 1961.

[BKA04]   Lilia Boeri, Jens Kortus, and O. K. Andersen. Three-dimensional MgB_2-type superconductivity in hole-doped diamond. *Phys. Rev. Lett.*, 93(23):237002, Nov 2004.

[BKcvcvM⁺04]   E. Bustarret, J. Kačmarčik, C. Marcenat, E. Gheeraert, C. Cytermann, J. Marcus, and T. Klein. Dependence of the superconducting transition temperature on the doping level in single-crystalline diamond films. *Phys. Rev. Lett.*, 93(23):237005, Dec 2004.

[BKK80]   A. Beckmann, E. Kolley, and W. Kolley. Off-diagonal CPA treatment of a dirty superconductor. *physica status solidi (b)*, 101(2):K107 – K110, 1980.

[BMA⁺06]   E. Bustarret, C. Marcenat, P. Achatz, J. Kacmarcik, F. Levy, A. Huxley, L. Ortega, E. Bourgeois, X. Blase, D. Debarre, and J. Boulmer. Superconductivity in doped cubic silicon. *Nature*, 444:465–468, 2006.

[BSI75]   R. F. Bishop, M. R. Strayer, and J. M. Irvine. Bound-state pairing singularities in the ^{3}He Galitskii-Feynman T-matrix: Temperature dependence. *Journal of Low Temperature Physics*, 20(5–6):573–584, 1975.

[Bus06]   E Bustarret. Superconducting diamond: an introduction. *physica status solidi (a)*, 205(5):997–1008, 2006.

[CCHL07]   Chih-Chun Chien, Qijin Chen, Yan He, and K. Levin. Superfluid phase diagrams of trapped Fermi gases with population imbalance. *Phys. Rev. Lett.*, 98(11):110404, Mar 2007.

[ESB⁺04]   E. A. Ekimov, V. A. Sidorov, E. D. Bauer, N. N. Mel'nik, N. J. Curro, J. D. Thompson, and S. M. Stishov. Superconductivity in diamond. *Nature*, 428:542–545, Apr 2004.

[EWGW86]   O. Entin-Wohlman, H. Gutfreund, and M. Weger. T_c degradation by the Coulomb interaction in anisotropic disordered superconductors. *Journal of Physics F: Metal Physics*, 16(10):1545 – 1553, 1986.

[Fad61]   L. D. Fadeev. *JETP*, 12:1014, 1961.

[GB06]   J. P. Goss and P. R. Briddon. Theory of boron aggregates in diamond: First-principles calculations. *Physical Review B (Condensed Matter and Materials Physics)*, 73(8):085204, 2006.

[GBS76]   H. B. Ghassib, R. F. Bishop, and M. R. Strayer. A study of the Galitskii-Feynman T-matrix for liquid ^{3}He. *Journal of Low Temperature Physics*, 23(3–4):393–410, 1976.

[GKSB99]   D. O. Gericke, S. Kosse, M. Schlanges, and M. Bonitz. T-matrix approach to equilibium and nonequilibrium carrier-carrier scattering in semiconductors. *Phys. Rev. B*, 59(16):10639–10650, Apr 1999.

[Gor58]   L. P. Gorkov. *JETP*, 34:735, 1958.

[GW64]   Marvin L. Goldberger and Kenneth M. Watson. *Collision theory.* Dover, New York, 1964.

[GYS+07]   Feliciano Giustino, Jonathan R. Yates, Ivo Souza, Marvin L. Cohen, and Steven G. Louie. Electron-phonon interaction via electronic and lattice Wannier functions: Superconductivity in boron-doped diamond reexamined. *Physical Review Letters*, 98(4):047005, 2007.

[HHI+09]   T. Herrmannsdörfer, V. Heera, O. Ignatchik, M. Uhlarz, A. Mücklich, M. Posselt, H. Reuther, B. Schmidt, K.-H. Heinig, W. Skorupa, M. Voelskow, C. Wündisch, R. Skrotzki, M. Helm, and J. Wosnitza. Superconducting state in a gallium-doped germanium layer at low temperatures. *Physical Review Letters*, 102(21):217003, 2009.

[JK01]   M. Jarrell and H. R. Krishnamurthy. Systematic and causal corrections to the coherent potential approximation. *Phys. Rev. B*, 63(12):125102, Mar 2001.

[JML97]   Boldizsár Jankó, Jiri Maly, and K. Levin. Pseudogap effects induced by resonant pair scattering. *Phys. Rev. B*, 56(18):R11407–R11410, Nov 1997.

[JQ74]   Charles J. Joachain and C. Quigg. Multiple scattering expansions in several particle dynamics. *Rev. Mod. Phys.*, 46(2):279–324, Apr 1974.

[KAK+07]   T. Klein, P. Achatz, J. Kacmarcik, C. Marcenat, F. Gustafsson, J. Marcus, E. Bustarret, J. Pernot, F. Omnes, Bo E. Sernelius, C. Persson, A. Ferreira da Silva, and C. Cytermann. Metal-insulator transition and superconductivity in boron-doped diamond. *Physical Review B (Condensed Matter and Materials Physics)*, 75(16):165313, 2007.

[KB62]   Leo P. Kadanoff and Gordon Baym. *Quantum Statistical Mechanics*.
            W. A. Benjamin, New York, 1962.

[KB74]   G. Kerker and K. H. Bennemann. Theory of superconductivity for
            transition-metal alloys. *Solid State Communications*, 14(5):399 – 401,
            1974.

[KCKL00]   Ioan Kosztin, Qijin Chen, Ying-Jer Kao, and K. Levin. Pair exci-
            tations, collective modes, and gauge invariance in the BCS – Bose-
            Einstein crossover scenario. *Phys. Rev. B*, 61(17):11662–11675, May
            2000.

[KKB81]   E. Kolley, W. Kolley, and A. Beckmann. Transition temperature of
            superconducting alloys with random transfer integrals. *physica status
            solidi (b)*, 103(2):775 – 781, 1981.

[KLGD80]   Theodore Kaplan, P. L. Leath, L. J. Gray, and H. W. Diehl. Self-
            consistent cluster theory for systems with off-diagonal disorder. *Phys.
            Rev. B*, 21(10):4230–4246, May 1980.

[KM61]   Leo P. Kadanoff and Paul C. Martin. Theory of many-particle sys-
            tems. II. Superconductivity. *Phys. Rev.*, 124(3):670–697, Nov 1961.

[KM93]   H. S. Köhler and Rudi Malfliet. Extended quasiparticle approxima-
            tion and Brueckner theory. *Phys. Rev. C*, 48(3):1034–1045, Sep 1993.

[KS76]   B. Keck and A. Schmid. Superconductivity and electron-phonon
            interaction in impure simple metals. *Journal of Low Temperature
            Physics*, 24(5):611 – 629, 1976.

[LCCH10]   Kathryn Levin, Qijin Chen, Chih-Chun Chien, and Yan He. Compari-
            son of different pairing fluctuation approaches to BCS-BEC crossover.
            Annals of Physics, 325(2):233 – 264, 2010.

[LDG+08]   Run Long, Ying Dai, Meng Guo, Lin Yu, Baibiao Huang, Ruiqin
            Zhang, and Wenjun Zhang. Effect of B-complexes on lattice structure
            and electronic properties in heavily boron-doped diamond. *Diamond
            and Related Materials*, 17(3):234 – 239, 2008.

[Lip08]   Pavel Lipavský. Multiple scattering corrections to the T-matrix ap-
            proximation: Unified theory of normal and superconducting states.
            Phys. Rev. B, 78(21):214506, Dec 2008.

[LMŠ01]   P. Lipavský, K Morawetz, and V. Špička. Kinetic equation for
            strongly interacting dense Fermi systems. *Annales de Physique*,
            26(1):1–254, 2001.

[Lov64]   C. Lovelace. Practical theory of three-particle states. I. Nonrelativistic. *Phys. Rev.*, 135(5B):B1225–B1249, Sep 1964.

[LP04]   K.-W. Lee and W. E. Pickett. Superconductivity in boron-doped diamond. *Phys. Rev. Lett.*, 93(23):237003, Nov 2004.

[Lus73]   H. Lustfeld. Coherent potential approximation for nonmagnetic weak-coupling superconducting alloys. *Journal of Low Temperature Physics*, 12:595 – 600, 1973.

[MA62a]   P. Morel and P. W. Anderson. Calculation of the superconducting state parameters with retarded electron-phonon interaction. *Phys. Rev.*, 125(4):1263–1271, Feb 1962.

[MA62b]   P. Morel and P. W. Anderson. Calculation of the superconducting state parameters with retarded electron-phonon interaction. *Phys. Rev.*, 125(4):1263–1271, Feb 1962.

[McM68]   W. L. McMillan. Transition temperature of strong-coupled superconductors. *Phys. Rev.*, 167(2):331–344, Mar 1968.

[MH73]   E. Müller-Hartmann. Analyticity of the coherent potential approximation. *Solid State Communications*, 12(12):1269 – 1270, 1973.

[MHNK07]   Jiří J. Mareš, Pavel Hubík, Milos Nesládek, and Jozef Kristofik. Boron-doped diamond – grained Mott's metal revealing superconductivity. *Diamond and Related Materials*, 16(4-7):921 – 925, 2007. Proceedings of Diamond 2006, the 17th European Conference on Diamond, Diamond-Like Materials, Carbon Nanotubes, Nitrides and Silicon Carbide - Diamond 2006.

[MJL99]   Jiri Maly, Boldizsár Jankó, and K. Levin. Superconductivity from a pseudogapped normal state: A mode-coupling approach to precursor superconductivity. *Phys. Rev. B*, 59(2):1354–1357, Jan 1999.

[MJPH05]   Thomas Maier, Mark Jarrell, Thomas Pruschke, and Matthias H. Hettler. Quantum cluster theories. *Rev. Mod. Phys.*, 77(3):1027–1080, Oct 2005.

[MNH+07]   J.J. Mareš, M. Nesládek, P. Hubík, D. Kindl, and J. Kristofik. On unconventional superconductivity in boron-doped diamond. *Diamond and Related Materials*, 16(1):1 – 5, 2007.

[MR78]   Robert Mills and Pisistha Ratanavararaksa. Analytic approximation for substitutional alloys. *Phys. Rev. B*, 18(10):5291–5308, Nov 1978.

[MS59]   Paul C. Martin and Julian Schwinger. Theory of many-particle sys-
            tems. I. *Phys. Rev.*, 115(6):1342–1373, Sep 1959.

[MTC$^+$05] Yanming Ma, John S. Tse, Tian Cui, Dennis D. Klug, Lijun Zhang,
            Yu Xie, Yingli Niu, and Guangtian Zou. First-principles study of
            electron-phonon coupling in hole- and electron-doped diamonds in
            the virtual crystal approximation. *Phys. Rev. B*, 72(1):014306, Jul
            2005.

[MTH$^+$07] H. Mukuda, T. Tsuchida, A. Harada, Y. Kitaoka, T. Takenouchi,
            Y. Takano, M. Nagao, I. Sakaguchi, T. Oguchi, and H. Kawarada.
            Microscopic evidence for evolution of superconductivity by effective
            carrier doping in boron-doped diamond: B-NMR study. *Physical
            Review B (Condensed Matter and Materials Physics)*, 75(3):033301,
            2007.

[Nam60]   Yoichiro Nambu. Quasi-particles and gauge invariance in the theory
            of superconductivity. *Phys. Rev.*, 117(3):648–663, Feb 1960.

[NB73]   Bernie G. Nickel and William H. Butler. Problems in strong-
            scattering binary alloys. *Phys. Rev. Lett.*, 30(9):373–377, Feb 1973.

[NZH$^+$09] Li Niu, Jia-Qi Zhu, Xiao Han, Man-Lin Tan, Wei Gao, and Shan-
            Yi Du. First principles study of structural, electronic and vibra-
            tional properties of heavily boron-doped diamond. *Physics Letters
            A*, 373(29):2494 – 2500, 2009.

[OSC$^+$01] M. S. Osofsky, R. J. Soulen, J. H. Claassen, G. Trotter, H. Kim, and
            J. S. Horwitz. New insight into enhanced superconductivity in metals
            near the metal-insulator transition. *Phys. Rev. Lett.*, 87(19):197004,
            Oct 2001.

[OSC$^+$02] M. S. Osofsky, R. J. Soulen, J. H. Claassen, G. Trotter, H. Kim, and
            J. Horwitz. Enhanced superconductivity in metallic oxides near the
            metal-insulator transition. *Phys. Rev. B*, 66(2):020502, Jul 2002.

[PL05]   Yu. G. Pogorelov and V. M. Loktev. Metallization in the boron-doped
            diamond CB_x. *Phys. Rev. B*, 72(7):075213, Aug 2005.

[Pra60]   R. E. Prange. *Proc. of Int. Spring School of Physics, Naples*, 1960.

[PS01]   C. J. Pethick and H. Smith. *Bose-Einstein Condensation in Dilute
            Gases*. Cambridge University Press, Oxford, 2001.

[SEB⁺05]   V.A. Sidorov, E.A. Ekimov, E.D. Bauer, N.N. Mel'nik, N.J. Curro, V. Fritsch, J.D. Thompson, S.M. Stishov, A.E. Alexenko, and B.V. Spitsyn. Superconductivity in boron-doped diamond. *Diamond and Related Materials*, 14(3-7):335 – 339, 2005. Proceedings of Diamond 2004, the 15th European Conference on Diamond, Diamond-Like Materials, Carbon Nanotubes, Nitrides and Silicon Carbide.

[SES⁺05]   V. A. Sidorov, E. A. Ekimov, S. M. Stishov, E. D. Bauer, and J. D. Thompson. Superconducting and normal-state properties of heavily hole-doped diamond. *Phys. Rev. B*, 71(6):060502, Feb 2005.

[SHOF07]   Tomonori Shirakawa, Satoshi Horiuchi, Yukinori Ohta, and Hidetoshi Fukuyama. Theoretical study on superconductivity in boron-doped diamond. *Journal of the Physical Society of Japan*, 76(1):014711, 2007.

[SOC03]   R. J. Soulen, M. S. Osofsky, and L. D. Cooley. Influence of screening on the superconductive transition temperature. *Phys. Rev. B*, 68(9):094505, Sep 2003.

[Sov67]   Paul Soven. Coherent-potential model of substitutional disordered alloys. *Phys. Rev.*, 156(3):809–813, Apr 1967.

[Tin66]   M. Tinkham. *Introduction to Superconductivity*. Mc-Graw Hill, New York, 1966.

[TNS⁺04]   Yoshihiko Takano, Masanori Nagao, Isao Sakaguchi, Minoru Tachiki, Takeshi Hatano, Kensaku Kobayashi, Hitoshi Umezawa, and Hiroshi Kawarada. Superconductivity in diamond thin films well above liquid helium temperature. *Applied Physics Letters*, 85(14):2851–2853, 2004.

[TNT⁺05]   Yoshihiko Takano, Masanori Nagao, Tomohiro Takenouchi, Hitoshi Umezawa, Isao Sakaguchi, Masashi Tachiki, and Hiroshi Kawarada. Superconductivity in polycrystalline diamond thin films. *Diamond and Related Materials*, 14(11-12):1936 – 1938, 2005. Proceedings of the 10th International Conference on New Diamond Science and Technology (ICNDST-10) - ICNDST-10 Special Issue.

[Tou70]   G. Toulouse. Infinite-*u* Anderson hamiltonian for dilute alloys. *Phys. Rev. B*, 2(2):270–277, Jul 1970.

[TTI⁺07]   Y. Takano, T. Takenouchi, S. Ishii, S. Ueda, T. Okutsu, I. Sakaguchi, H. Umezawa, H. Kawarada, and M. Tachiki. Superconducting properties of homoepitaxial CVD diamond. *Diamond and Related Materials*, 16(4-7):911 – 914, 2007. Proceedings of Diamond 2006, the 17th

European Conference on Diamond, Diamond-Like Materials, Carbon Nanotubes, Nitrides and Silicon Carbide - Diamond 2006.

[UTT$^+$05]   Hitoshi Umezawa, Tomohiro Takenouchi, Yoshihiko Takano, Kensaku Kobayashi, Masanori Nagao, Isao Sakaguchi, Minoru Tachiki, Takeshi Hatano, Guofang Zhong, Masashi Tachiki, and Hiroshi Kawarada. Advantage on superconductivity of heavily boron-doped (111) diamond films. 2005.

[VIK82]   S. V. Vonsovsky, Yu. A. Izyumov, and E. Z. Kurmaev. *Superconductivity of Transition Metals Their Alloys and Compounds*. Springer-Verlag, 1982.

[VKE68]   B. Velický, S. Kirkpatrick, and H. Ehrenreich. Single-site approximations in the electronic theory of simple binary alloys. *Phys. Rev.*, 175(3):747–766, Nov 1968.

[Wat53]   Kenneth M. Watson. Multiple scattering and the many-body problem – Applications to photomeson production in complex nuclei. *Phys. Rev.*, 89(3):575–587, Feb 1953.

[Wil60]   W. Wild. Zum Vielkörperproblem eines Fermionsystems. *Zeitschrift für Physik A*, 158(3):322–346, June 1960.

[WK83]   K. I. Wysokinski and A. L. Kuzemsky. The theory of strong coupling superconductivity in disordered transition metal alloys. *Journal of Low Temperature Physics*, 52(1):81–98, 1983.

[Wys87]   K. I. Wysokinski. On the T_c degradation in dirty transition metal superconductors. *Solid State Communications*, 63(3):205 – 208, 1987.

[WZ74]   A. Weinkauf and J. Zittartz. CPA treatment of superconducting alloys. *Solid State Communications*, 14(4):365 – 368, 1974.

[WZ75]   A. Weinkauf and J. Zittartz. Theory of superconducting alloys. *Journal of Low Temperature Physics*, 18(3):229 – 239, 1975.

[XLY$^+$04]   H. J. Xiang, Zhenyu Li, Jinlong Yang, J. G. Hou, and Qingshi Zhu. Electron-phonon coupling in a boron-doped diamond superconductor. *Phys. Rev. B*, 70(21):212504, Dec 2004.

[YNM$^+$05]   T. Yokoya, T. Nakamura, T. Matsushita, T. Muro, Y. Takano, M. Nagao, T. Takenouchi, H. Kawarada, and T. Oguchi. Origin of the metallic properties of heavily boron-doped superconducting diamond. *Nature*, 438:647–650, Dec 2005.

Appendix A

Experimental data

Table A.1: Results of boron doped diamond λ parameter *ab initio* computations

Method	Reference	Boron Concentration [%]	λ
Super Cell	Blase *et al* [BAC04]	1.85	0.43
	Giustino *et al* [GYS$^+$07]	1.85	0.34
	Xiang *et al* [XLY$^+$04]	6.25	0.56
Virtual Crystal	Boeri *et al* [BKA04]	3.0	0.3
		5.0	0.36
		10.0	0.56
	Lee *et al* [LP04]	2.5	0.55
	Ma *et al* [MTC$^+$05]	1.0	0.18
		2.0	0.25
		4.0	0.34
		6.0	0.40

Table A.2: Experimental T_c data of boron doped diamond

Method	Reference	Boron Concentration [%]	T_c [K]
111 MPCVD	Mukuda *et al* [MTH$^+$07]	1.6	5.0
	Takano *et al* [TNS$^+$04]	0.53	4.2
	Takano *et al* [TNT$^+$05]	0.24	1.8
		0.75	3.3
		1.3	4.3
		2.1	5.0
	Takano *et al* [TTI$^+$07]	4.8	7.4
	Yokoya *et al* [YNM$^+$05]	4.7	7.0
100 MPCVD	Bustarret *et al* [BKcvcvM$^+$04]	0.51	0.9
		0.57	1.2
		0.65	1.4
		1.08	2.1
	Klein *et al* [KAK$^+$07]	0.27	0.45
		0.36	0.55
		0.68	1.2
		0.74	1.2
		0.91	1.3
		1.1	1.55
		1.5	2.0
	Mukuda *et al* [MTH$^+$07]	4.9	3.4
	Takano *et al* [TTI$^+$07]	4.8	3.2
	Umezawa *et al* [UTT$^+$05]	7.9	2.9
HPHT	Ekimov *et al* [ESB$^+$04]	2.8	2.3
	Sidorov *et al* [SES$^+$05]	4.0	3.4
	Sidorov *et al* [SEB$^+$05]	4.0	2.5

Appendix B

Review of the Belitz theory

The Belitz theory belongs to approaches within which is the occurrence of a superconducting state in the electronic system of the metal associated with the presence of what is known as the anomalous averages $\langle \hat{a}_\downarrow(\mathbf{r}) \hat{a}_\uparrow(\mathbf{r}) \rangle$ and $\left\langle \hat{a}_\downarrow^\dagger(\mathbf{r}) \hat{a}_\uparrow^\dagger(\mathbf{r}) \right\rangle$ [VIK82]. Here $\hat{a}_\alpha^\dagger(\mathbf{r})$ and $\hat{a}_\alpha(\mathbf{r})$ stand for the operators of creation and annihilation of an electron at point $\mathbf{r}$ with spin α and $\langle \ldots \rangle$ is the symbol of grandcanonical averaging

$$\langle \ldots \rangle = \mathrm{Tr}\{\ldots e^{-\beta \hat{H}}\} / \mathrm{Tr}\{e^{-\beta \hat{H}}\} \, . \tag{B.1}$$

Our ability to evaluate these anomalous averages depends on complexity of the Hamiltonian.

B.0.3 Hamiltonian

We start our discussion from a very realistic hamiltonian that includes the electron-phonon interaction giving rise to an effective electron-electron attraction, the Coulomb repulsion and an interaction with static impurities. For Hamiltonian we therefore write

$$\hat{H} = \hat{H}_0 + \hat{V} + \hat{H}_{\mathrm{int}} \, , \tag{B.2}$$

$$\hat{H}_{\mathrm{int}} = \hat{H}_{\mathrm{e-e}} + \hat{H}_{\mathrm{e-ph}} \, . \tag{B.3}$$

As was pointed out by Nambu [Nam60] and independently by Gor'kov [Gor58], it is convenient to describe the superconductor with the aid of two-component field

operators

$$\hat{\Psi}(\mathbf{r}) = \begin{pmatrix} \hat{a}_\uparrow(\mathbf{r}) \\ \hat{a}_\downarrow^\dagger(\mathbf{r}) \end{pmatrix} , \quad \hat{\Psi}^\dagger(\mathbf{r}) = \left(\hat{a}_\uparrow^\dagger(\mathbf{r}), \, \hat{a}_\downarrow(\mathbf{r}) \right) . \tag{B.4}$$

This leads to the 2×2 matrix structure of the theory. It is thus convenient to write the Hamiltonian in terms of Pauli matrices

$$\tau_\mathbf{1} = \begin{pmatrix} 0 & 1 \\ 1 & 0 \end{pmatrix} , \quad \tau_\mathbf{2} = \begin{pmatrix} 0 & i \\ -i & 0 \end{pmatrix} , \quad \tau_\mathbf{3} = \begin{pmatrix} 1 & 0 \\ 0 & -1 \end{pmatrix} , \quad \tau_\mathbf{0} = \begin{pmatrix} 1 & 0 \\ 0 & 1 \end{pmatrix} , \tag{B.5}$$

which help to keep a clear structure of the perturbation theory. For free electrons and phonons we in momentum representation write

$$\hat{H}_0 = \sum_\mathbf{q} \epsilon(\mathbf{q}) \, \hat{\Psi}^\dagger(\mathbf{q}) \, \tau_\mathbf{3} \, \hat{\Psi}(\mathbf{q}) + \sum_l \sum_\mathbf{q} \omega_l(\mathbf{q}) \, \hat{b}_l^\dagger(\mathbf{q}) \, \hat{b}_l(\mathbf{q}) . \tag{B.6}$$

Here $\epsilon(\mathbf{q})$ is an electron kinetic energy with zero placed at the Fermi level and $\omega_l(\mathbf{q})$ energy of phonon modes. The interaction with the static disorder is described by

$$\hat{V} = \sum_\mathbf{r} V(\mathbf{r}) \, \hat{\Psi}^\dagger(\mathbf{r}) \, \tau_\mathbf{3} \, \hat{\Psi}(\mathbf{r}) , \tag{B.7}$$

where $V(\mathbf{r}_i)$ is the electron-impurity scattering potential specified in section about the electron density of states in Chapter 4. For the Coulomb repulsion we write

$$\hat{H}_{e-e} = \sum_{\mathbf{p_1}+\mathbf{p_2}=\mathbf{p_1'}+\mathbf{p_2'}=\mathbf{q}} V_c(\mathbf{q}) \left[\hat{\Psi}^\dagger(\mathbf{p_1}) \, \tau_\mathbf{3} \, \hat{\Psi}(\mathbf{p_1'}) \right] \left[\hat{\Psi}^\dagger(\mathbf{p_2}) \, \tau_\mathbf{3} \, \hat{\Psi}(\mathbf{p_2'}) \right] , \tag{B.8}$$

where $V_c(\mathbf{r} - \mathbf{r}')$ represents an effective Coulomb potential. The effective interaction between electrons and phonons is described by

$$\hat{H}_{e-\mathrm{ph}} = \frac{i}{m(\rho_i)^{1/2}} \sum_\mathbf{q} \frac{q}{\omega_\mathrm{L}(\mathbf{q})} \left[m \, \hat{t}_\mathrm{L}(\mathbf{q}) - \frac{1}{3} k_F^2 \, \hat{d}(\mathbf{q}) \right] \hat{\phi}_\mathrm{L}(\mathbf{q}) +$$

$$+ \frac{2\,i}{m(\rho_i)^{1/2}} \sum_\mathbf{q} \frac{q}{\omega_\mathrm{T}(\mathbf{q})} m \, \hat{t}_\mathrm{T}(\mathbf{q}) \, \hat{\phi}_\mathrm{T}(\mathbf{q}) . \tag{B.9}$$

Here the $t(\mathbf{q})$ are the longitudinal (L) and transverse (T) parts of the Fourier transforms of the electron stress operator

$$\hat{t}_{\alpha\beta}(\mathbf{q}) = -\frac{1}{4m} \sum_\mathbf{q} \mathbf{q}_\alpha \, \mathbf{q}_\beta \, \hat{\Psi}^\dagger(\mathbf{q}) \, \tau_\mathbf{3} \, \hat{\Psi}(2\mathbf{q}) , \tag{B.10}$$

and

$$\hat{d}(\mathbf{q}) = \sum_{\mathbf{r}} e^{\mathrm{i}\mathbf{q}\cdot\mathbf{r}} \, \hat{\Psi}^{\dagger}(\mathbf{r}) \, \tau_{\mathbf{3}} \, \hat{\Psi}(\mathbf{r}') \,, \tag{B.11}$$

is the Fourier transform of the electronic density operator. The phonon field operators $\phi_l(\mathbf{q})$ are defined as

$$\hat{\phi}_l(\mathbf{q}) = \left(\frac{\omega_l(\mathbf{q})}{2} \right)^{1/2} \left[\hat{b}_l(\mathbf{q}) + \hat{b}_l^{\dagger}(\mathbf{q}) \right] \,, \tag{B.12}$$

where $\omega_l(\mathbf{q})$ is the dispersion relation for polarization branch l and the $b^{\dagger}$, b are phonon creation and annihilation operators.

To compute the statistical average using such realistic Hamiltonian is very difficult task however. One therefore has to use some method capable of calculating these averages within controlled approximations.

B.0.4   Green's function formalism

The widely used method for calculating of the operator statistical averages is a Green's function formalism, which describes evolution of an excitation in the system. We define the Green's function of the noninteracting system with impurity disorder as

$$g^0(\tau - \tau', \mathbf{r} - \mathbf{r}') = - \left\langle \langle \mathcal{T}\{\hat{\Psi}(\tau, \mathbf{r})\hat{\Psi}^{\dagger}(\tau', \mathbf{r}')\}\rangle \right\rangle_{\mathrm{av}}. \tag{B.13}$$

Here $\mathcal{T}$ is the ordering operator for the imaginary time τ, $\langle\ldots\rangle$ means a thermodynamic average (B.1) with respect to hamiltonian $\hat{H}_0 + \hat{V}$, and $\langle\ldots\rangle_{\mathrm{av}}$ denotes the impurity average. The Green's function for interacting system is defined as

$$g(\tau - \tau', \mathbf{r} - \mathbf{r}') = - \left\langle \frac{\langle \mathcal{T}\{\hat{\Psi}(\tau, \mathbf{r})\hat{\Psi}^{\dagger}(\tau', \mathbf{r}')\hat{\sigma}(\beta)\}\rangle}{\langle\hat{\sigma}(\beta)\rangle} \right\rangle_{\mathrm{av}}, \tag{B.14}$$

with

$$\hat{\sigma}(\beta) = \sum_{n=0}^{\infty} \frac{(-1)^n}{n!} \int_0^{\beta} dt_1 \cdots \int_0^{\beta} dt_n \, \mathcal{T}\{\hat{H}_{\mathrm{int}}(t_1) \cdots \hat{H}_{\mathrm{int}}(t_n)\} \,. \tag{B.15}$$

We see that the calculation of Green's function for a superconductor reduces to a calculation of the averages of the $\mathcal{T}$ products of the field operators in the interaction representation.

It is effective for the perturbation theory to work in the momentum representation defined as

$$\hat{\Psi}(\tau, \mathbf{p}) = \frac{1}{\sqrt{\Omega}} \int d\mathbf{r}\, e^{i\,\mathbf{p}\cdot\mathbf{r}}\, \hat{\Psi}(\tau, \mathbf{r})\,, \tag{B.16}$$

where Ω is a quantisation volume. In disordered system momentum is not a good quantum number. It is thus useful to define energy dependent quantities instead. Let us assume that $\hat{H}_0 + \hat{V}$ has been diagonalised with a complete set of orthonormal eigenfunctions $\{\psi_n(\mathbf{r})\}$, and corresponding energies E_n. Then within the so-called exact eigenstate representation [And59, KS76] we for (B.13) write

$$g^0(i\,\omega_n) = \sum_n |E_n\rangle \frac{1}{i\,\omega_n\,\tau_0 - E_n\,\tau_3} \langle E_n|\,. \tag{B.17}$$

Using a method given by Keck and Schmid [KS76] we construct the energy-dependent averaged propagator of the noninteracting system as

$$g^0(i\,\omega_n, \epsilon) = \left\langle \frac{1}{N(\epsilon)} \sum_n \delta(\epsilon - E_n)\, \langle E_n|g^0(i\,\omega_n)|E_n\rangle \right\rangle_{\mathrm{av}}\,. \tag{B.18}$$

Here $N(\epsilon)$ is the density of states at the energy ϵ. To describe the interacting system we define the operator of selfenergy $\Sigma(\epsilon, i\,\omega_n)$ including all interaction effects. In absence of currents the selfenergy has in general three terms

$$\Sigma(i\,\omega_n, \epsilon) = [1 - Z(i\,\omega_n, \epsilon)]\,i\,\omega_n\,\tau_0 + Y(i\,\omega_n, \epsilon)\,\tau_3 + W(i\,\omega_n, \epsilon)\,\tau_1\,. \tag{B.19}$$

The Green's function of the interacting system equals

$$g^{-1}(i\,\omega_n, \epsilon) = g_0^{-1}(i\,\omega_n, \epsilon) - \Sigma(i\,\omega_n, \epsilon)\,, \tag{B.20}$$

with matrix elements of the form

$$g(i\,\omega_n, \epsilon) = \begin{bmatrix} G(i\,\omega_n, \epsilon) & F(i\,\omega_n, \epsilon) \\ F^\dagger(i\,\omega_n, \epsilon) & -G(-i\,\omega_n, \epsilon) \end{bmatrix}\,. \tag{B.21}$$

Inverting the matrix (B.21) with the selfenergy from (B.19) we obtain the diagonal element

$$G(i\,\omega_n, \epsilon) = \frac{i\,\omega_n\,Z(i\,\omega_n, \epsilon) + [\epsilon + Y(i\,\omega_n, \epsilon)]}{[i\,\omega_n\,Z(i\,\omega_n, \epsilon)]^2 - [\epsilon + Y(i\,\omega_n, \epsilon)]^2 - W(i\,\omega_n, \epsilon)^2}\,, \tag{B.22}$$
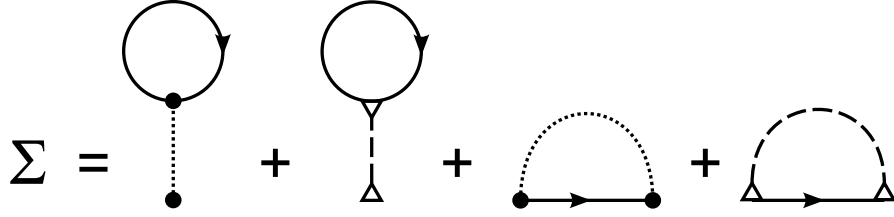
Figure B.1: Figure shows Feynman diagrams of Hartree-Fock approximation in which the selfenergy is calculated. Solid line with an arrow represents the full propagator, dotted line is the Coulomb potential, dashed line phonon propagator. Full circle represents Coulomb interaction vertex and triangle the phonon-electron coupling constant.

and anomalous one

$$F^{\dagger}(i\,\omega_n, \epsilon) = \frac{-W(i\,\omega_n, \epsilon)}{[i\,\omega_n\, Z(i\,\omega_n, \epsilon)]^2 - [\epsilon + Y(i\,\omega_n, \epsilon)]^2 - W(i\,\omega_n, \epsilon)^2} \,. \tag{B.23}$$

The anomalous propagator $F(i\,\omega_n, \epsilon)$ describes the anomalous average, which signalizes the occurrence of the superconducting state. Therefore we need within the averaged eigenstate representation to calculate the functions $Y(i\,\omega_n, \epsilon)$, $W(i\,\omega_n, \epsilon)$ and $Z(i\,\omega_n, \epsilon)$.

B.0.5 Strong coupling equations

From (B.14), (B.15) and (B.20) we find expression for $\Sigma(i\,\omega_n, \epsilon)$, according to perturbation theory, by summing a certain infinite sequence of terms. We calculate the selfenergy within an approximation called the Hartree-Fock approximation. This sequence of terms can be represented by the Feynman diagrams that are shown in the Figure B.1.

To illustrate the way, how the selfenergy $\Sigma(i\,\omega_n, \epsilon)$ is calculated and how the average over the disorder is performed, we write here the Fock term with the Coulomb

interaction

$$-\frac{1}{\beta}\sum_{i\omega_n}\sum_{\mathbf{q}}\int d\epsilon'\, R_c^F(\mathbf{q},\epsilon-\epsilon')\, V_c(\mathbf{q})\times$$

$$\times\,\frac{i\omega_n Z(i\omega_n,\epsilon')\tau_{\mathbf{0}}+[\epsilon'+Y(i\omega_n,\epsilon')]\tau_{\mathbf{3}}+W(i\omega_n,\epsilon')\tau_{\mathbf{1}}}{[i\omega_n Z(i\omega_n,\epsilon')]^2-[\epsilon'+Y(i\omega_n,\epsilon')]^2-W(i\omega_n,\epsilon')^2}\,. \quad \text{(B.24)}$$

The last term is the full propagator (B.21) and the first two terms are

$$R_c^F(\mathbf{q},\epsilon-\epsilon')\,V_c(\mathbf{q})=\left\langle\frac{1}{N(\epsilon)\,N(\epsilon')}\sum_{n,n'}\sum_{\mathbf{p_1}+\mathbf{p_2}=\mathbf{p'_1}+\mathbf{p'_2}=\mathbf{q}}\delta(\epsilon-E_n)\,\delta(\epsilon'-E_n')\times\right.$$

$$\left.\times\,\langle E_n|\mathbf{p_1}\rangle\,\langle E_n'|\mathbf{p_2}\rangle\,\langle\mathbf{p'}_1|E_n'\rangle\,\langle\mathbf{p'}_2|E_n\rangle\right\rangle_{\mathrm{av}}\langle\mathbf{p_1},\mathbf{p_2}|V_c(\mathbf{q})|\mathbf{p'}_1,\mathbf{p'}_2\rangle\,. \quad \text{(B.25)}$$

Here we for clarity write $V_c(\mathbf{q})=\langle\mathbf{p_1},\mathbf{p_2}|V_c(\mathbf{q})|\mathbf{p'}_1,\mathbf{p'}_2\rangle$. The vertex function $R_c^F(\mathbf{q},\epsilon-\epsilon')$ is a renormalization of interaction potential and represents its transformation from the momentum basis to the averaged basis of disordered system eigenstates. The following diagrams are evaluated in a similar manner.

For the superconducting transition is relevant the interaction of electrons for energies close to the Fermi level, we therefore focus on this region. For good metals one can in this region omit the energy dependence of $Z(\omega,\epsilon)$ and $W(\omega,\epsilon)$. In the case of clean systems the frequency independent term $Y(\epsilon)$ has very weak energy dependence as well and thus can be recast into a constant shift of the chemical potential. This is not true in the case of disordered systems however and the term $Y(\omega,\epsilon)$ has to be kept in the theory with its energy dependence. As a result one obtains a set of equations for functions $W(\omega)$, $Z(\omega)$, and $Y(\omega,\epsilon)$

$$W(\omega)=\int d\nu\,\alpha^2 F^F(\nu)\int\frac{dx}{\pi}\int d\epsilon'\,\mathrm{Im}\,F(x,\epsilon')\left[\frac{\mathrm{f}(x)}{x-\omega-\nu}+\frac{1-\mathrm{f}(x)}{x-\omega-\nu}\right]+$$

$$+\mu\int\frac{dx}{\pi}\,\mathrm{f}(x)\int d\epsilon'\,\mathrm{Im}\,F(x,\epsilon')\,, \quad \text{(B.26)}$$

$$\omega[1-Z(\omega)]=\int d\nu\,\alpha^2 F^F(x)\int\frac{dx}{\pi}\times$$

$$\times\int d\epsilon'\,\mathrm{Im}\,G(x,\epsilon')\omega\left[\frac{\mathrm{f}(x)}{(x-\nu)^2-\omega^2}+\frac{1-\mathrm{f}(x)}{(x+\nu)^2-\omega^2}\right]\,, \quad \text{(B.27)}$$

$$Y(\omega, \epsilon) = \int d\nu \int d\epsilon' \, \alpha^2 F^F(\nu, \epsilon - \epsilon') \int \frac{dx}{\pi} \times$$

$$\times \, \mathrm{Im}\, G(x, \epsilon') \left[\mathrm{f}(x) \frac{x - \nu}{(x - \nu)^2 - \omega^2} + [1 - \mathrm{f}(x)] \frac{x + \nu}{(x + \nu)^2 - \omega^2} \right] +$$

$$+ \int d\nu \int d\epsilon' \left[\frac{4}{\nu} \alpha^2 F^H(\nu, \epsilon - \epsilon') + \mu^Y(\epsilon - \epsilon') \, \delta(\nu) \right] \int \frac{dx}{\pi} \, \mathrm{f}(x) \, \mathrm{Im}\, G(x, \epsilon') \,.$$

$$\text{(B.28)}$$

The $\mathrm{f}(x)$ denotes the Fermi distribution function and the disorder dependent Eliashberg functions are defined as

$$\alpha^2 F^{F, H}(\nu, \epsilon) = \sum_{\mathbf{q}, l} R_l^{F, H}(\mathbf{q}, \epsilon) \, B_l(\nu, \mathbf{q}) \,, \tag{B.29}$$

where B_l is the phonon spectral function for polarization branch l. The Coulomb kernels are given by

$$\mu = \sum_{\mathbf{q}} R_c^F(0, \mathbf{q}) \, V_c(\mathbf{q}) \,, \tag{B.30}$$

and

$$\mu^Y(\epsilon) = \sum_{\mathbf{q}} [R_c^F(\mathbf{q}, \epsilon) - 2R_c^H(\mathbf{q}, \epsilon)] \, V_c(\mathbf{q}) \,. \tag{B.31}$$

The vertex functions $R_l^{F, H}(\mathbf{q}, \epsilon)$, $R_c^{F, H}(\mathbf{q}, \epsilon)$ are disorder induced renormalizations of interaction potentials.

Important new feature of the theory is the equation for the energy dependent $Y(\omega, \epsilon)$. The $Y(\omega, \epsilon)$ term is a diagonal part of $\Sigma(\omega, \epsilon)$ which is even in ϵ and in the disordered case also includes contributions from Fock terms. Since we use the representation of $\hat{H}_0 + \hat{V}$ exact eigenstates the set of equations (B.26), (B.27) and (B.28) has a structure of those of Eliashberg for pure metals, with angular degrees of freedom integrated away. One can naturally expect that the disorder induced changes of the theory have impact on the critical temperature.

B.0.6 Critical temperature formula

In order to derive the critical temperature formula we see that the main obstacle to solving (B.26) – (B.28) with the methods known from standard strong-coupling

theory is the energy dependence of $Y(\omega, \epsilon)$. To deal with this difficulty, we expand $Y(\omega, \epsilon)$ in a Taylor series with respect to ϵ

$$Y(\omega, \epsilon) = Y(\omega, 0) + Y' \epsilon, \tag{B.32}$$

where

$$Y' = \left. \frac{dY(\omega, \epsilon)}{d\epsilon} \right|_{\epsilon=0}. \tag{B.33}$$

It turns out that we can eliminate the first term $Y(\omega, 0)$, so we are in the theory left with Y', which is found to be independent of ω. Following the approach of McMillan [McM68] we come to the formula for T_c

$$T_c = \frac{\omega_D}{1.45} \exp\left[-\frac{1.04 \, (1 + \lambda + Y')}{\lambda - \mu^*(1 + 0.62 \, \lambda/(1 + Y'))} \right], \tag{B.34}$$

where

$$\lambda = 2 \int \frac{d\nu}{\nu} \alpha^2 F^F(\nu), \tag{B.35}$$

and

$$\mu^* = \mu \left[1 + \frac{\mu}{1 + Y'} \ln\left(\frac{\omega_C}{0.62 \, \omega_D} \right) \right]^{-1}. \tag{B.36}$$

The ω_C is the effective range of the Coulomb interaction. For the Y' we write

$$Y' = \delta\mu^Y + 4 \int \frac{d\nu}{\nu} \alpha^2 F^H(\nu), \tag{B.37}$$

where $\delta\mu = \mu - \mu^{(0)}$, $\mu^{(0)}$ is the contribution for zero disorder and $\alpha^2 F^H(\nu)$ is zero in the clean limit. Setting $Y' = 0$, one recovers the original McMillan formula.

Appendix C

Selfenergy contributions in the T-matrix theory

In this appendix we will show that the Cooper pair pole of T-matrix below the T_c forms a major contribution to the selfenergy.

Let us start from the selfenergy equation

$$\Sigma_\uparrow(k) = \frac{1}{\beta\,\Omega} \sum_q \mathcal{T}_{\uparrow\downarrow}(k, q-k; k, q-k)\, G_\downarrow(q-k)\,, \tag{C.1}$$

which can be with a help of Hilbert transformations of the T-matrix

$$\mathcal{T}_{\uparrow\downarrow}(\mathrm{i}\,\nu_m, \mathbf{q}) = -\frac{1}{\pi} \int \mathrm{d}z' \, \frac{\mathrm{Im}\,\mathcal{T}_{\uparrow\downarrow}(z', \mathbf{q})}{\mathrm{i}\,\nu_m - z'}\,, \tag{C.2}$$

and the full propagator

$$G_\downarrow(\mathrm{i}\,\nu_m - \mathrm{i}\,\omega_n, \mathbf{q} - \mathbf{k}) = -\frac{1}{\pi} \int \mathrm{d}z \, \frac{\mathrm{Im}\,G_\downarrow(z, \mathbf{q} - \mathbf{k})}{\mathrm{i}\,\nu_m - \mathrm{i}\,\omega_n - z}\,, \tag{C.3}$$

rewritten in a form

$$\Sigma_\uparrow(\mathrm{i}\,\omega_n, \mathbf{k}) = \frac{1}{\beta\,\Omega} \sum_{\mathrm{i}\,\nu_m, \mathbf{q}} \iint \frac{\mathrm{d}z}{\pi} \frac{\mathrm{d}z'}{\pi} \frac{\mathrm{Im}\,\mathcal{T}_{\uparrow\downarrow}(z', \mathbf{q})}{\mathrm{i}\,\nu_m - z'} \frac{\mathrm{Im}\,G_\downarrow(z, \mathbf{q} - \mathbf{k})}{\mathrm{i}\,\nu_m - \mathrm{i}\,\omega_n - z}\,. \tag{C.4}$$

The summation over Matsubara frequencies equals

$$\frac{1}{\beta} \sum_{\mathrm{i}\,\nu_m} \frac{1}{\mathrm{i}\,\nu_m - z'} \frac{1}{\mathrm{i}\,\nu_m - \mathrm{i}\,\omega_n - z} = -\frac{1}{2} \frac{\tanh(\frac{1}{2}\beta z) + \coth(\frac{1}{2}\beta z')}{\mathrm{i}\,\omega_n + z - z'}\,. \tag{C.5}$$

After the summation the selfenergy reads

$$\Sigma_\uparrow(i\,\omega_n,\mathbf{k}) = -\frac{1}{2\,\Omega} \sum_{\mathbf{q}} \iint \frac{\mathrm{d}z}{\pi} \frac{\mathrm{d}z'}{\pi} \operatorname{Im} \mathcal{T}_{\uparrow\downarrow}(z',\mathbf{q}) \times$$

$$\times \operatorname{Im} G_\downarrow(z,\mathbf{q}-\mathbf{k}) \frac{\tanh(\frac{1}{2}\beta z) + \coth(\frac{1}{2}\beta z')}{i\,\omega_n + z - z'} , \quad \text{(C.6)}$$

and consists of two contributions

$$\Sigma_\uparrow(i\,\omega_n,\mathbf{k}) = \Sigma_\uparrow^{\tanh}(i\,\omega_n,\mathbf{k}) + \Sigma_\uparrow^{\coth}(i\,\omega_n,\mathbf{k}) . \quad \text{(C.7)}$$

Below the critical temperature bound states of pairs develop in the system. For the T-matrix we thus write

$$\mathcal{T}(i\,\nu_m,\mathbf{q}) \approx \frac{a}{i\,\nu_m - \mathbf{q}^2/4m + \mu_{\mathrm{pair}}} , \quad \text{(C.8)}$$

where a is a constant, $\mathbf{q}^2/4m$ is a pair dispersion and μ_{pair} is an effective chemical potential of the pair. The imaginary part of the retarded T-matrix reads

$$\operatorname{Im} \mathcal{T}(z' + i\,0,\mathbf{q}) = -\pi a\,\delta(z' - \mathbf{q}^2/4m + \mu_{\mathrm{pair}}) . \quad \text{(C.9)}$$

Now the $\Sigma_\uparrow^{\tanh}(i\,\omega_n,\mathbf{k})$ term remains regular but due to the bosonic distribution a singular contribution develops in the $\Sigma_\uparrow^{\coth}(i\,\omega_n,\mathbf{k})$. After integration over z' one obtains

$$\Sigma_\uparrow^{\coth}(i\,\omega_n,\mathbf{k}) = \frac{a}{2\Omega} \sum_{\mathbf{q}} \int \frac{\mathrm{d}z}{\pi} \operatorname{Im} G_\downarrow(z,\mathbf{q}-\mathbf{k}) \frac{\coth\left(\frac{1}{2}\beta(\mathbf{q}^2/4m - \mu_{\mathrm{pair}})\right)}{i\,\omega_n + z} . \quad \text{(C.10)}$$

For the quantization cube of length $L = \Omega^{1/3}$ the first excitation energy of the pair is $\frac{\hbar^2}{4mL^2} = \frac{\hbar^2}{4m\Omega^{2/3}}$. This in the limit of the infinite volume vanishes slower than the chemical potential $\mu_{\mathrm{pair}} \sim -c/\Omega$, where c is a positive constant. From the summation over momenta $\mathbf{q}$ in (C.10) we therefore take only a singular contribution for zero momentum pair

$$\Sigma_\uparrow^{\coth}(i\,\omega_n,\mathbf{k}) = \frac{a}{2\Omega} \coth(-\tfrac{\beta}{2}\mu_{\mathrm{pair}}) \int \frac{\mathrm{d}z}{\pi} \frac{\operatorname{Im} G_\downarrow(z,-\mathbf{k})}{i\,\omega_n + z} . \quad \text{(C.11)}$$

Using expansion $\coth(x) \approx 1/x$ we come to the form

$$\Sigma_\uparrow(i\,\omega_n,\mathbf{k}) \approx -\frac{a}{2\Omega} \frac{2\Omega}{\beta c} G_\downarrow(-i\,\omega_n,-\mathbf{k}) = -\Delta^2\,G_\downarrow(-i\,\omega_n,-\mathbf{k}) , \quad \text{(C.12)}$$

where $\Delta^2 = a/\beta c$. This confirms the conclusion made in (9.17).